Chapter 2 Geophysical Prospecting

2-1 Electric Prospecting IP Method

2-1-1 Object

The object of the survey is to make clear the resistivity structure relating the mineralization and to extract IP anomaly zones by means of the IP survey for the potential zones found by the last year's airborne magnetic and electromagnetic survey.

2-1-2 Location and Perfored Survey

The survey area is situated about 15 kilometers southeast of Marrakech City. The area has been selected based on the last year's survey result. Figure II-2-1-1 shows the location of the survey area, and Figure II-2-1-2 shows the IP survey lines. The base coordinates for each district are shown in Table II-2-1-1. The spacing of each survey line is 200 meters, and the survey point interval is 100 meters except some 200 meters interval lines.

Table II-2-1-1 Coordinate of the Survey line

Area	Line Name	Direction	No. (Base)	UTM Coordinate	
				X	Y
MJTK-IP-1	A	N86°46' 3"E	0	586241	3490374
MJTK-IP-2	A	N87°26' 10"E	0	585020	3488168
MJTK-IP-3	C	N88°40' 59"E S 1°20' 2"E	5	586619	3487060
MJTK-IP-4	A	N46° 2' 29"E	3	585987	3495113
MJTK-IP-5	A	N87°59' 41"E	0	577082	3489164
MJTK-IP-6	C	N88°27' 58"E	10	579055	3494892
MJTK-IP-7	C	N87° 2' 47"E	15	582404	3483799
MJTK-IP-8	A	N66° 3' 35"E	0	585482	3482570

Table II-2-1-2 shows amounts of IP survey.

Table II-2-1-2 List of survey amount

Area	Number of lines	Total length	Number of points
MJTK-IP-1	2.0km×6 lines 1.6km×1 line	12.0km	460
MJTK-IP-2	2.0km×3 lines	6.0km	240
MJTK-IP-3	1.3km×2 lines 1.2km×2 lines	5.0km	170
MJTK-IP-4	1.0km×1 line	1.0km	30
MJTK-IP-5	1.0km×1 line	1.0km	30
MJTK-IP-6	1.0km×3 lines	3.0km	90
MJTK-IP-7	1.5km×3 lines [1.6km×1 line (a=200m)]	6.1km	185
MJTK-IP-8	1.2km×1 line	1.2km	30
Total	23lines	35.3km	1,235

Some rock samples have been taken from some outcrops and mine site, and measured their resistivity and chargeability in laboratory.

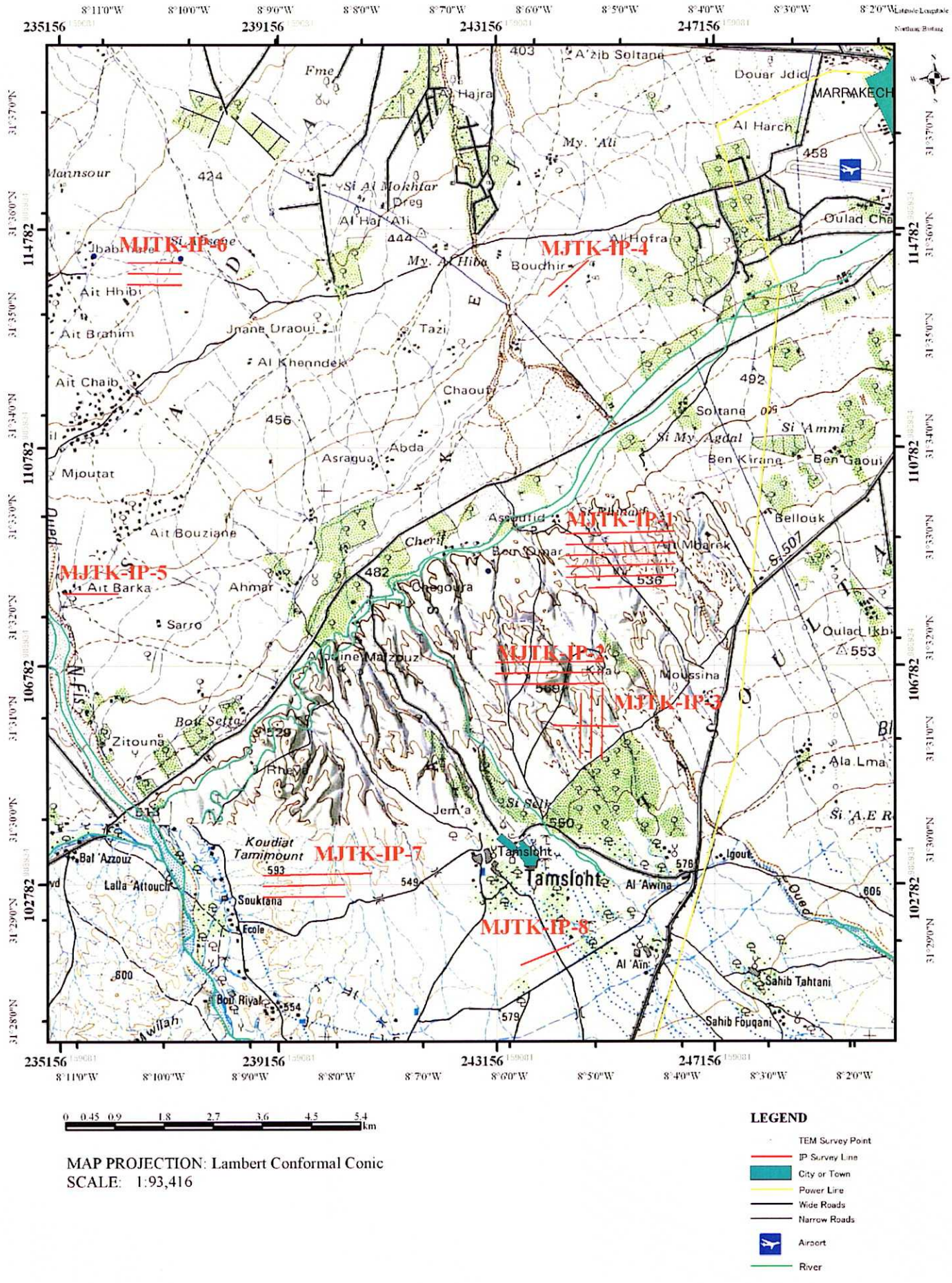

MAP PROJECTION: Lambert Conformal Conic
SCALE: 1:93,416

Fig.II-2-1-1 Survey location map of the Marrakech-Tekna area

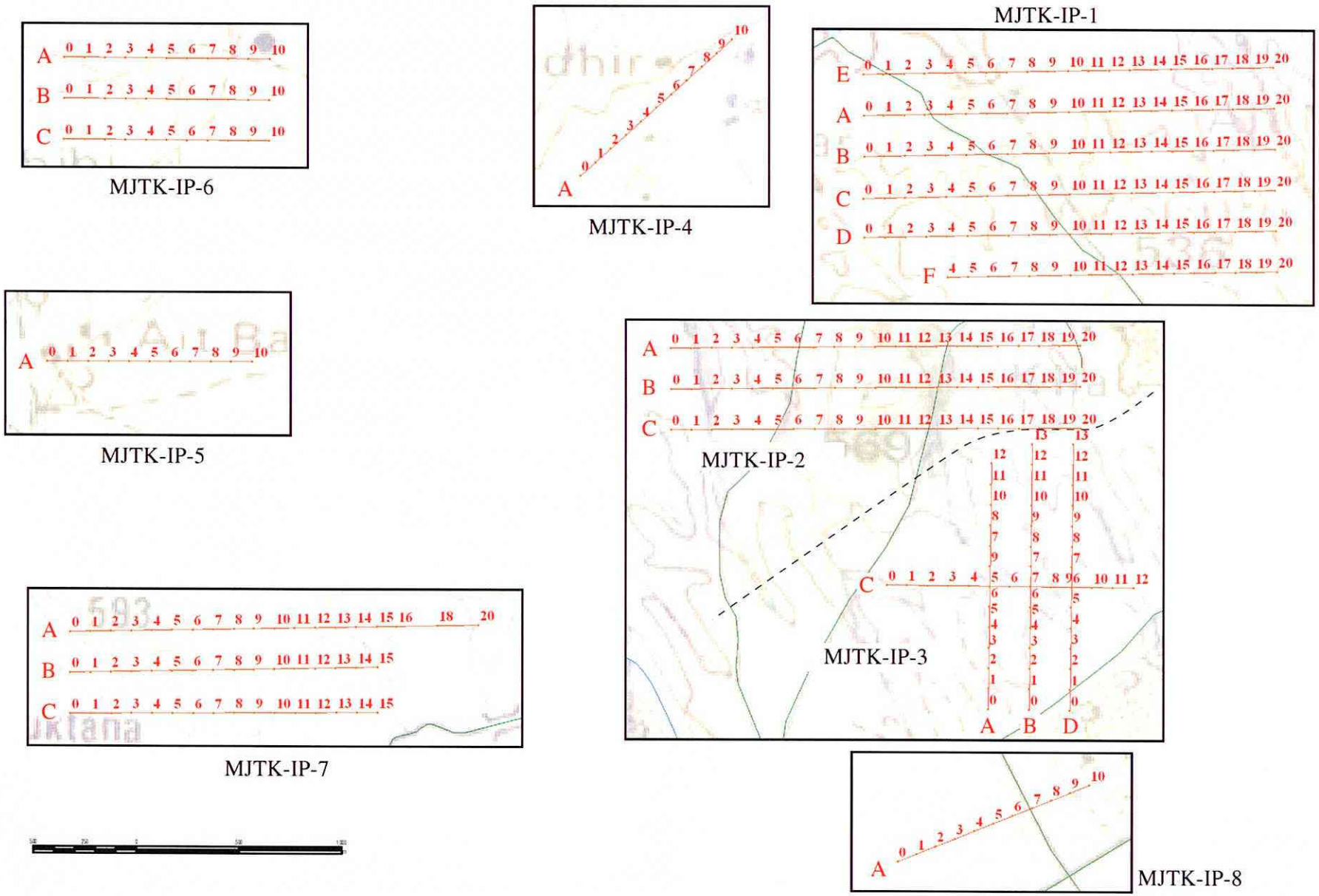

Fig.II-2-1-2 Outline map of Survey line

2-1-3 Survey Method

As we send an electric current into the earth, various electric chemical phenomena occur in the medium that composes the ground. IP method measures the following two phenomena.

"Over Voltage Effect"

The electric double layers occur on the surface of sulfide minerals or conductive metals due to electric current, and the charged electricity is discharged to the reverse direction when the current is cut. This phenomenon is of the combined effect of the ion conduct and electron conduct. The electron conductive minerals take place this phenomenon, and are good targets for the IP method.

"Polarization of Clay Mineral"

Common rocks are slightly polarized due to electric current, because of the membrane polarization of a small-amount of clay minerals in rock cavities. Montmorillonite shows the greatest membrane polarization, and kaolin shows low. The membrane polarization shows the greatest value when clay mineral content ratio is about 5 per cent, but decreases its value around such content.

The polarization value is much smaller compared with that of the Over Voltage Effect.

2) Measuring Method

The measuring method applied is the time-domain induced polarization method (TDIP method), and the electrode arrangement is the dipole-dipole, the electrode interval 100 meters, the electrode isolation factor n=1 to 5, and the survey line separation 200 meters.

The intermittent direct current, on/off 2.0 sec, has been employed between the current electrodes C1 and C2, and the primary potential Vp and damping secondary potential Vs have been measured right before and after the current interruption. The apparent resistivity is measured by the primary potential during current introduction, and the chargeability is measured by the damping secondary potential.

Figure II-2-1-3 shows the concept of operation, and Figure II-2-1-4 shows the concept of the measuring method. The sampling time is t4 to t14 after current interruption, as shown in Figure II-2-1-4.

The IP effect measurement value by the time domain method is called "chargeability, and represented by Vs/Vp[mV/V]. The chargeability is the integral data of 450 to 950 [msec].

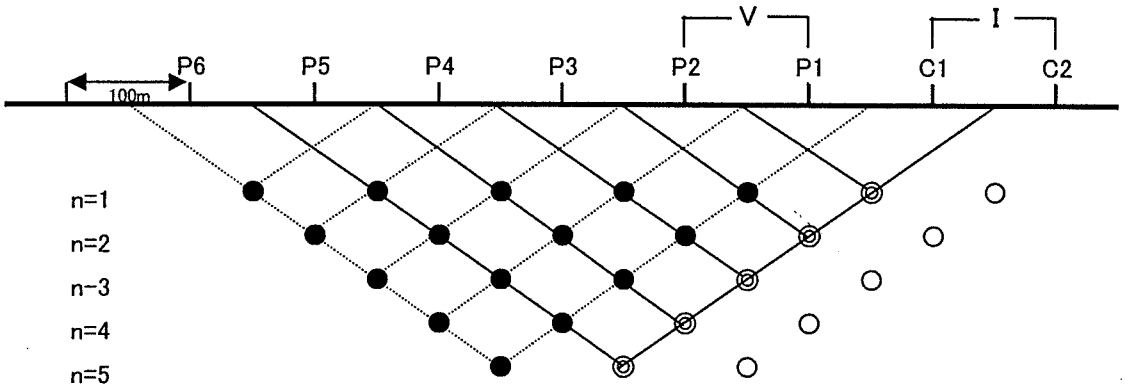

Fig. II -2-1-3 Concept of operation

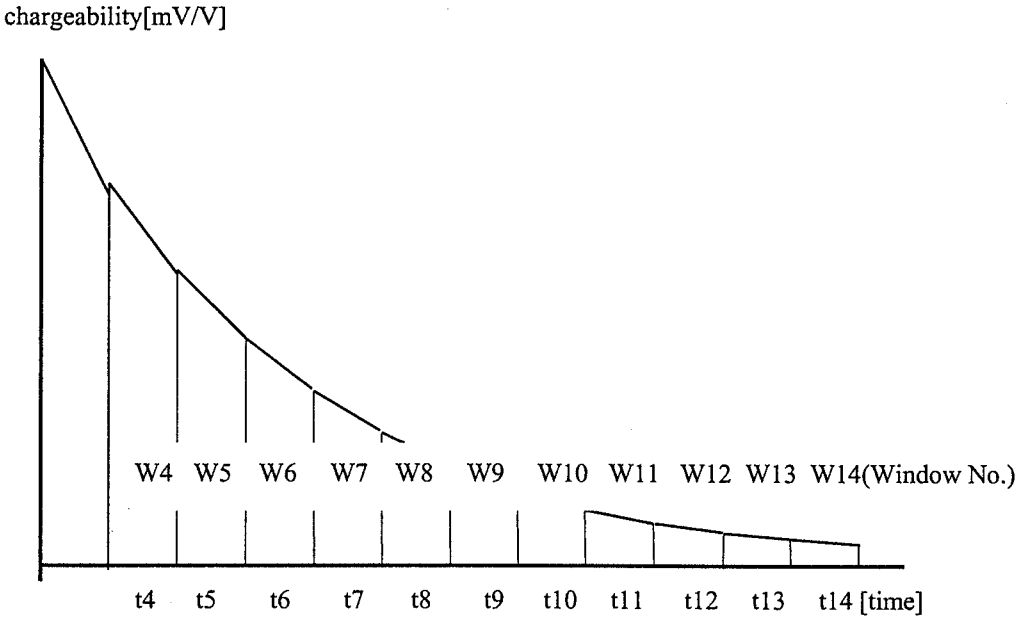

Fig. II -2-1-4 Concept of the method of measurement

Table II -2-1-3 List of sampling time

Window #	W4	W5	W6	W7	W8	W9	W10	W11	W12	W13	W14
Mid-point(msec)	60	90	130	190	270	380	520	705	935	1230	1590
Width(msec)	20	40	40	80	80	140	140	230	230	360	360

3) Equipment used

Table II-2-1-4 shows the specification of IP survey instrument used for the survey.

Table II-2-1-4 Specification of IP survey instrument

Equipment	Type	Maker	Specification	Amount
Transmitter	CH-97T,CH-97P	CHIBA Electronic	Max. output current 60A	2
	CH-98T,CH-98PA	Inc.	Max. output Volt. 880V	2
(Lab. Test)	IP-L	IRIS Instruments	1 μA～100 μA max 10V	1
Engine Generator	ET-4500	HONDA	Max. Power 4.5kW 3 φ, 220V	2
Receiver	IPR-12	SCINTREX	8ch., 14window Input Range:50 μV to 14V	2
Electrode	ASK System		PbCl	12
Measuring	Pocket compass	USHIKATA		2
	100m Esron tape			4
	GPS	GARMIN		3
Communication Device	TH-42	KENWOOD	Max. Power : 5W	12

2-1-4 Analysis Method

The two dimension inversion analysis combined the model calculated by the finite factor analysis and the auto-analysis by the nonlinear least squares method has been used for the study. In this method, the cross section showing the topography is divided into some blocks. These blocks are given their resistivity values and chargeability values, and the resistivity and chargeability structures are presented, then the model calculation by the finite factor method is performed.

Finally, the minimum resistivity structure and chargeability structure are gain by the auto-repeating analysis applied the last squares method. RES2DINV of GETOMO SOFTWARE has been used for the analysis.

2-1-5 Survey Result

2-1-5-1 Result of Measuring

1) MJTK-IP-1

Figures II-2-1-5 to II-2-1-7 show the sections of the apparent resistivity, chargeability, and metal factor, and Figures II-2-1-8 to II-2-1-10 show the planes.

The apparent resistivity ranges 12 to 132 Ω· m, and the average figure is 31 Ω· m. The apparent resistivity is generally low, below 50 Ω· m, except the survey lines of A and D showing highest figure of 130 Ω· m, and getting lower to the depth.

The resistivity distribution of n=1, reflecting near surface effect, is generally low, below 20 Ω· m.

The chargeability ranges 2.8 to 14.9 mV/V, and the average figure is 7.2 mV/V. The chargeability tends to show higher figure to depth, but generally low. Slightly higher chargeability zones are in the survey lines F, D, C, B, and eastern side of the deep part of A and E, extending to the east.

The metal factor is about 60 in maximum, extending northwest.

2) MJTK-IP-2

Figures IP-2-1-11 to II-2-1-13 show the cross sections of the apparent resistivity, chargeability, and metal factor, and Figures II-2-1-14 to II-2-1-16 show the planes.

The resistivity ranges 10 to 711 Ω· m, and the average figure is 89 Ω· m. The resistivity distribution shows a clear high resistivity zone on the summit near No.10 of the survey lines A, B, and C.

The chargeability ranges 0.9 to 20.5mV/V, and the average figure is 5.4 mV/V. The shallow anomaly is correlated with the high apparent resistivity zone. This zone possibly corresponds to the andesite outcropping there.

The metal factor shows generally low, below 20.

3) MJTK-IP-3

Figures II-2-1-17 to II-2-1-19 show the cross sections of the apparent resistivity, chargeability, and metal factor, and Figures II-2-1-20 to II-2-1-22 show the planes.

The apparent resistivity ranges 14 to 136 Ω· m, and the average figure is 44 Ω· m. The apparent resistivity distribution shows a very clear high resistivity zone on the survey lines A, B, and C, around No.6.

The chargeability ranges 0.9 to 5.9mV/V, and the average figure is 3.0mV/V. The chargeability is generally low.

The metal factor is generally low, below 20.

4) MJTK-IP-4

Figure II-2-1-23 shows the cross sections of the apparent resistivity, chargeability, and metal factor.

The apparent resistivity ranges 22 to 44 Ω· m, and the average figure is 31 Ω· m. No change appears in the apparent resistivity distribution.

The chargeability ranges 2.4 to 9.9mV/V, and the average figure is 5.5mV/V. The chargeability tends to higher in the shallow and deep parts in the central survey lines, but is generally low and flat.

The metal factor shows generally low figures, and the maximum figure is around 50.

5) MJTK-IP-5

Figures II-2-1-24 shows the cross section of the apparent resistivity, chargeability, and metal factor.

The apparent resistivity ranges 29 to 124 Ω· m, and the average figure is 57 Ω· m. The apparent resistivity distribution is high in shallow and low in deep.

The chargeability ranges 4.5 to 8.6mV/V, and the average figure is 6.6mV/V. The chargeability is slightly high, corresponding to the high resistivity zone in shallow part.

The metal factor is generally low, and the highest figure is 20.

5) MJTK-IP-6

Figures II-2-1-25 to 27 show the cross sections of the apparent resistivity, chargeability, and metal factor, and Figures II-2-1-28 to II-2-1-30 show the planes.

The apparent resistivity ranges 25 to 103 Ω· m, and the average figure is 35 Ω· m. The apparent resistivity distribution is even except survey line B, extending to the east.

The chargeability ranges 2.8 to 11.5mV/V, and the average figure is 5.1mV/V. The chargeability tends to show higher the deeper, but generally low.

The metal factor is 30 in the highest.

6) MJTK-IP-7

Figures II-2-1-31 to II-2-1-33 show the cross sections of the apparent resistivity, chargeability, and metal factor, and Figures II-2-1-34 to II-2-1-36 show the planes.

The apparent resistivity ranges 12 to 61 Ω· m, and the average figure is 24 Ω· m. The apparent resistivity distribution tends to show low in deeper. In the measuring of 200 meters interval on the survey line A, it shows the very low value of 15 Ω· m in the deep part.

The chargeability ranges 2.4 to 17.7mV/V, and the average figure is 5.9mV/V. The chargeability tends to be higher the deeper.

The metal factor is 10 in the highest in deep.

7) MJTK-IP-8

Figure II-2-1-37 shows the cross section of the apparent resistivity, chargeability, and metal factor.

The apparent resistivity ranges 28 to 47 Ω·m, and the average figure is 37 Ω·m. No change appears in the apparent resistivity distribution.

The chargeability ranges 2.3 to 5.4 mV/V, and the average figure is 3.2 mV/V. The chargeability tends to slightly high in deep.

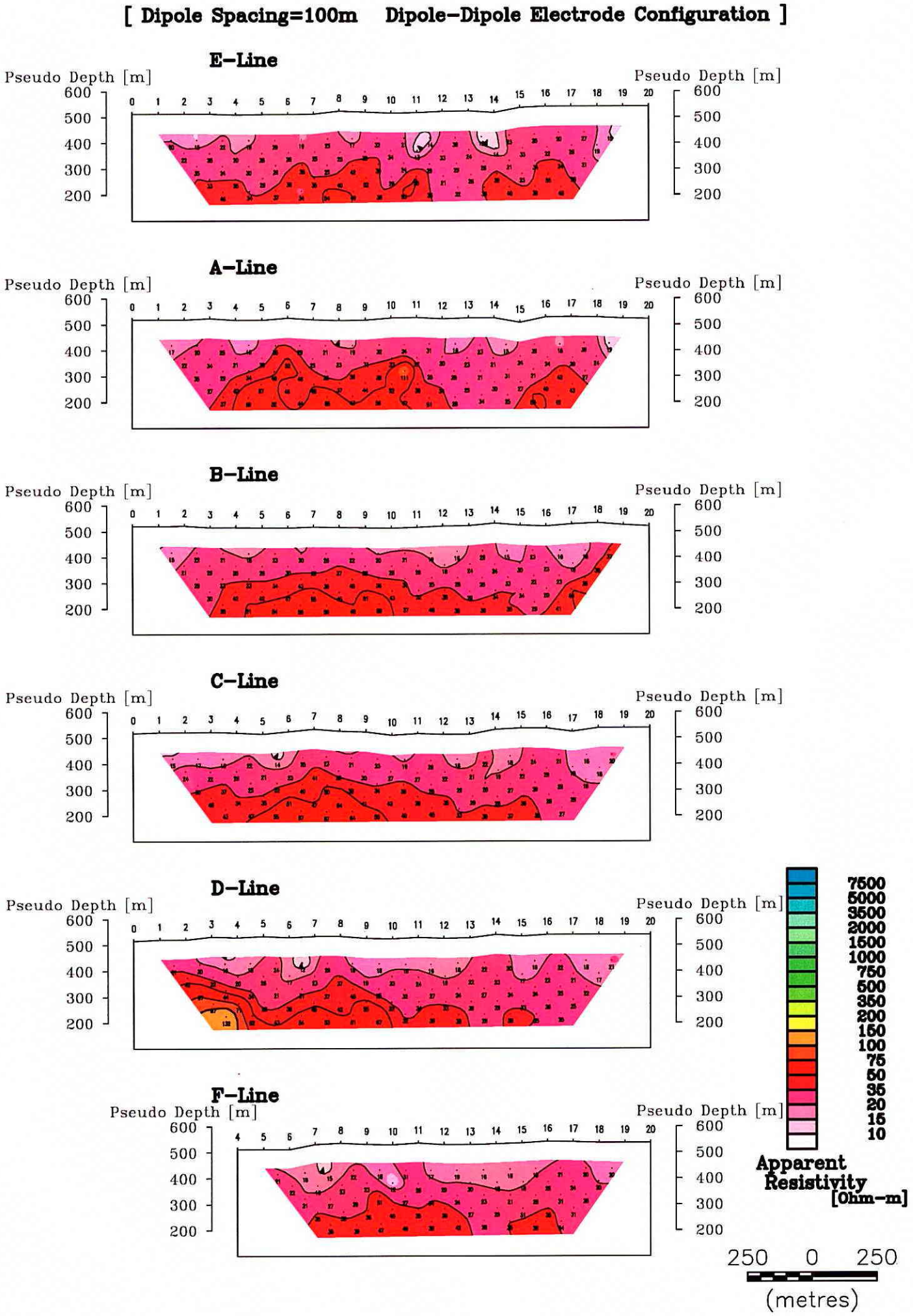

Fig.II-2-1-5 Section of apparent resistivity (MJTK-IP-1)

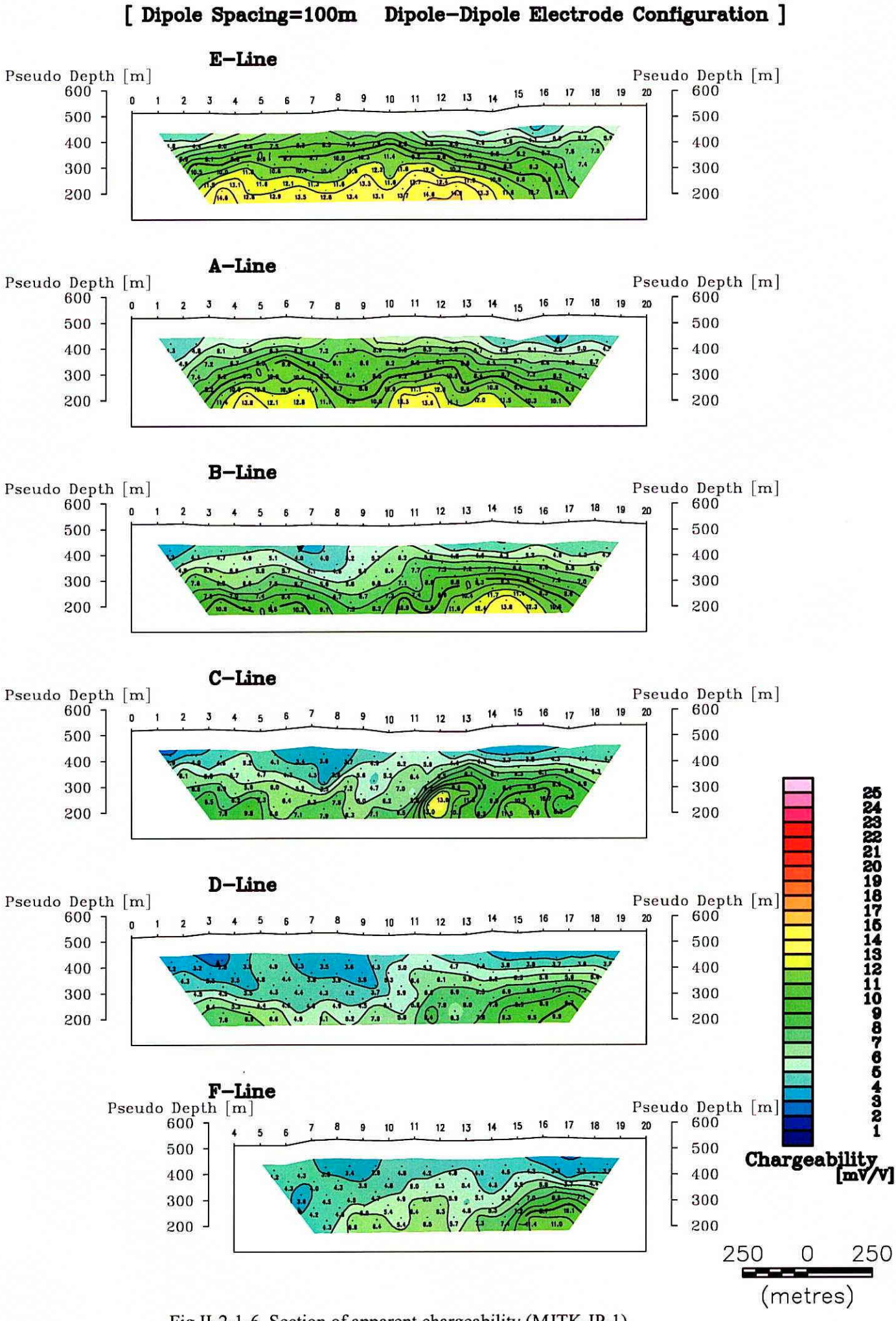

Fig.II-2-1-6 Section of apparent chargeability (MJTK-IP-1)

[Dipole Spacing=100m Dipole-Dipole Electrode Configuration]

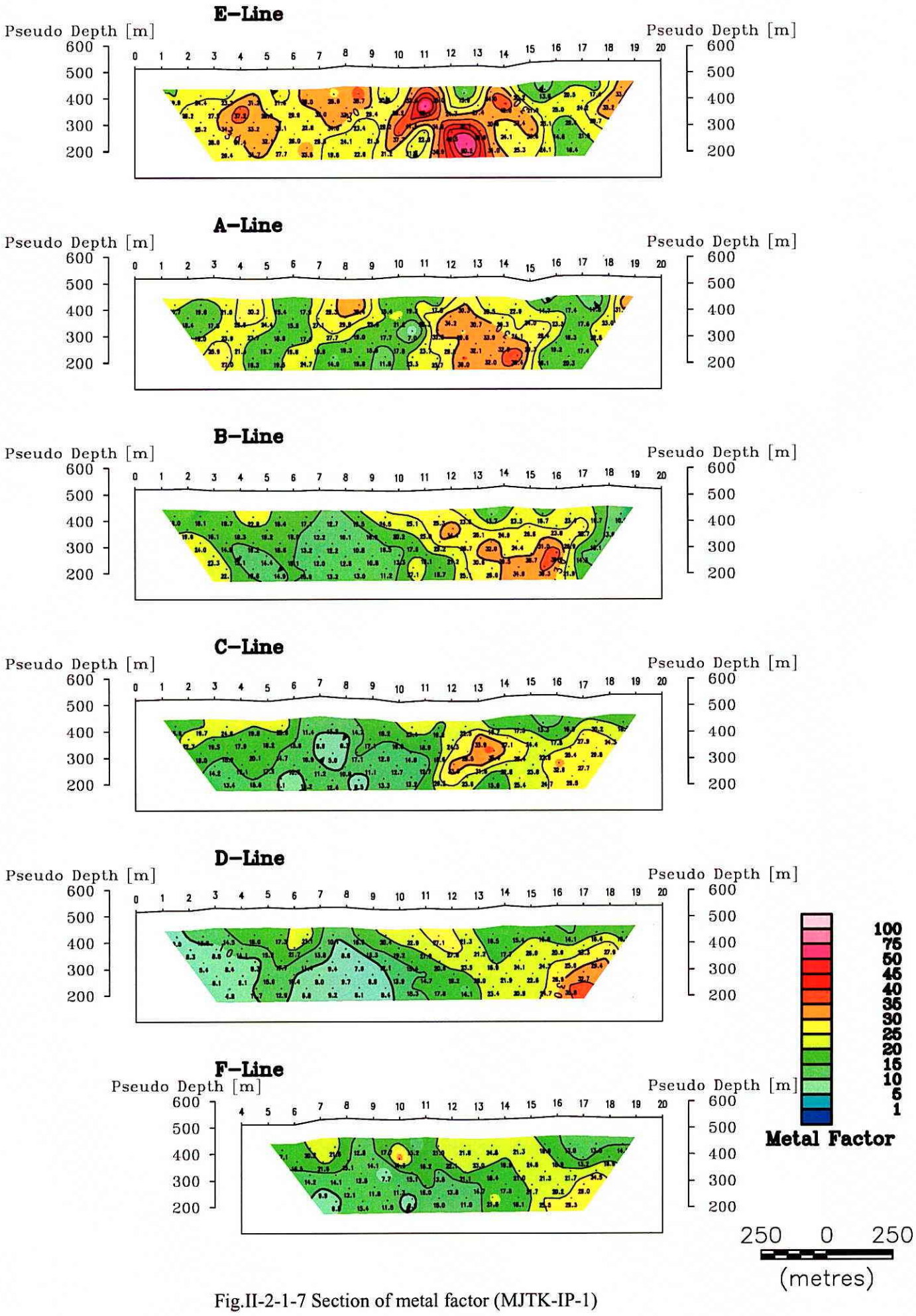

Fig.II-2-1-7 Section of metal factor (MJTK-IP-1)

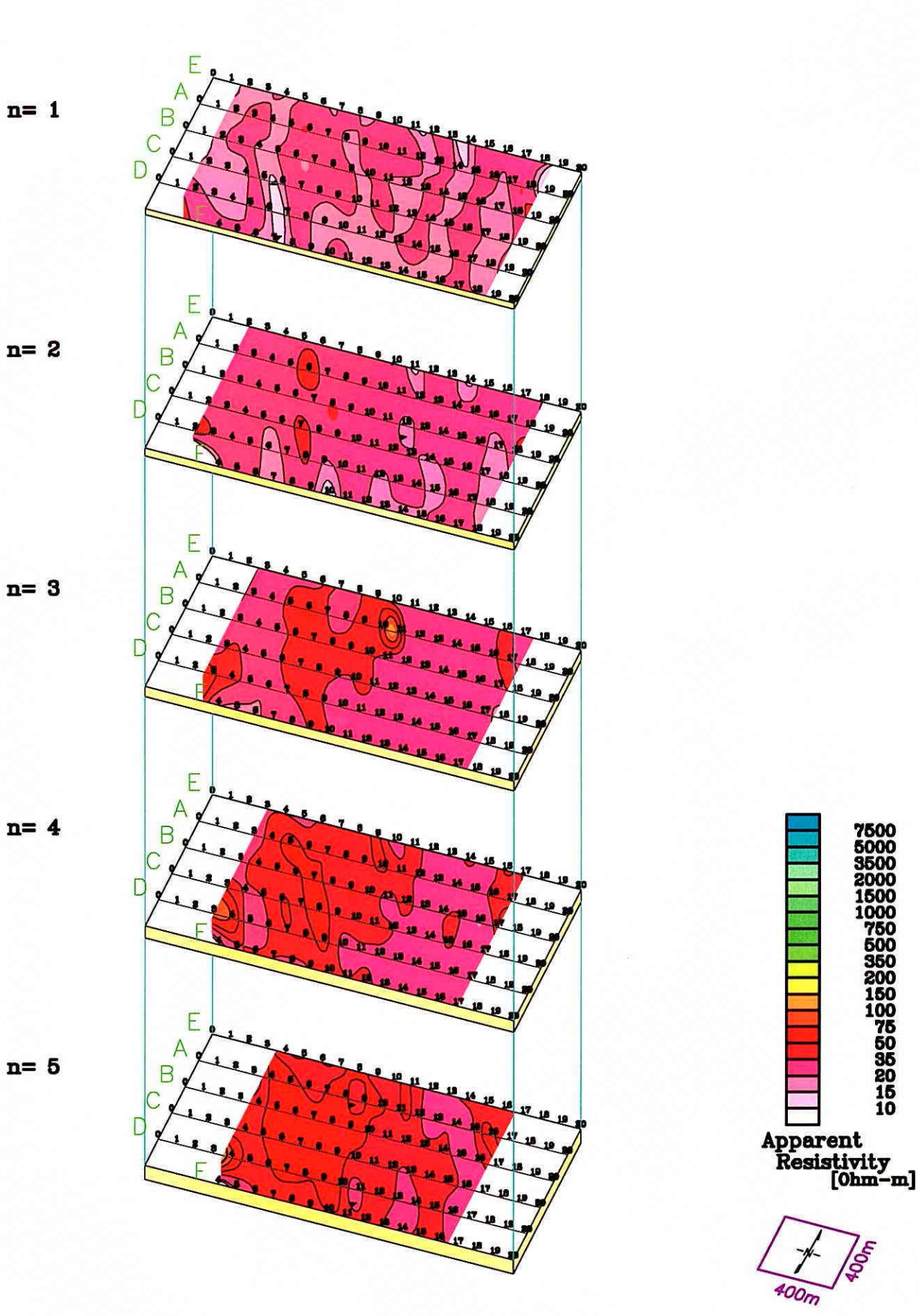

Fig.II-2-1-8 Plane map of apparent resistivity (MJTK-IP-1)

[Dipole Spacing=100m Dipole-Dipole Electrode Configuration]

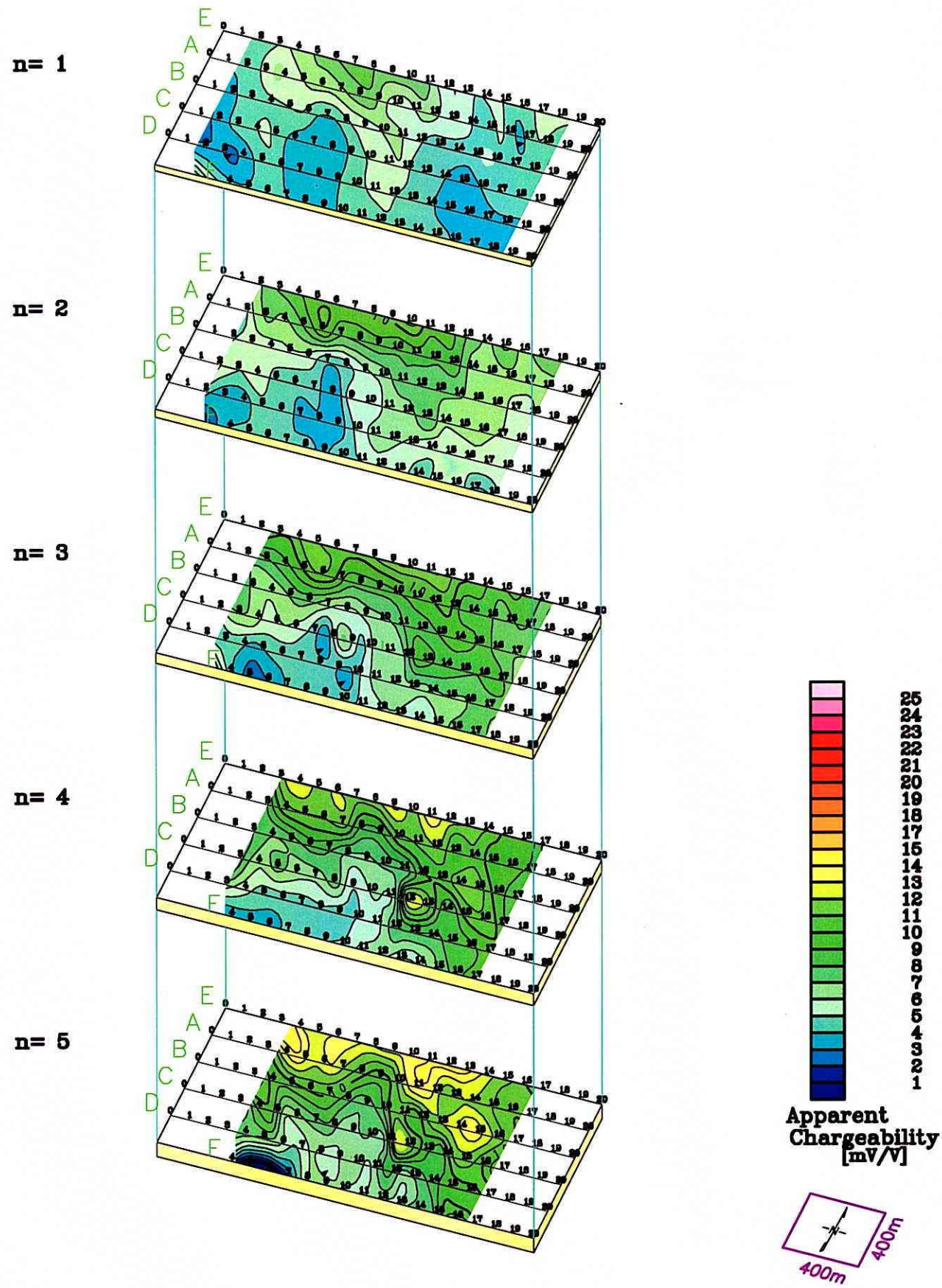

Fig.II-2-1-9 Plane map of apparent chargeability (MJTK-IP-1)

[Dipole Spacing=100m Dipole-Dipole Electrode Configuration]

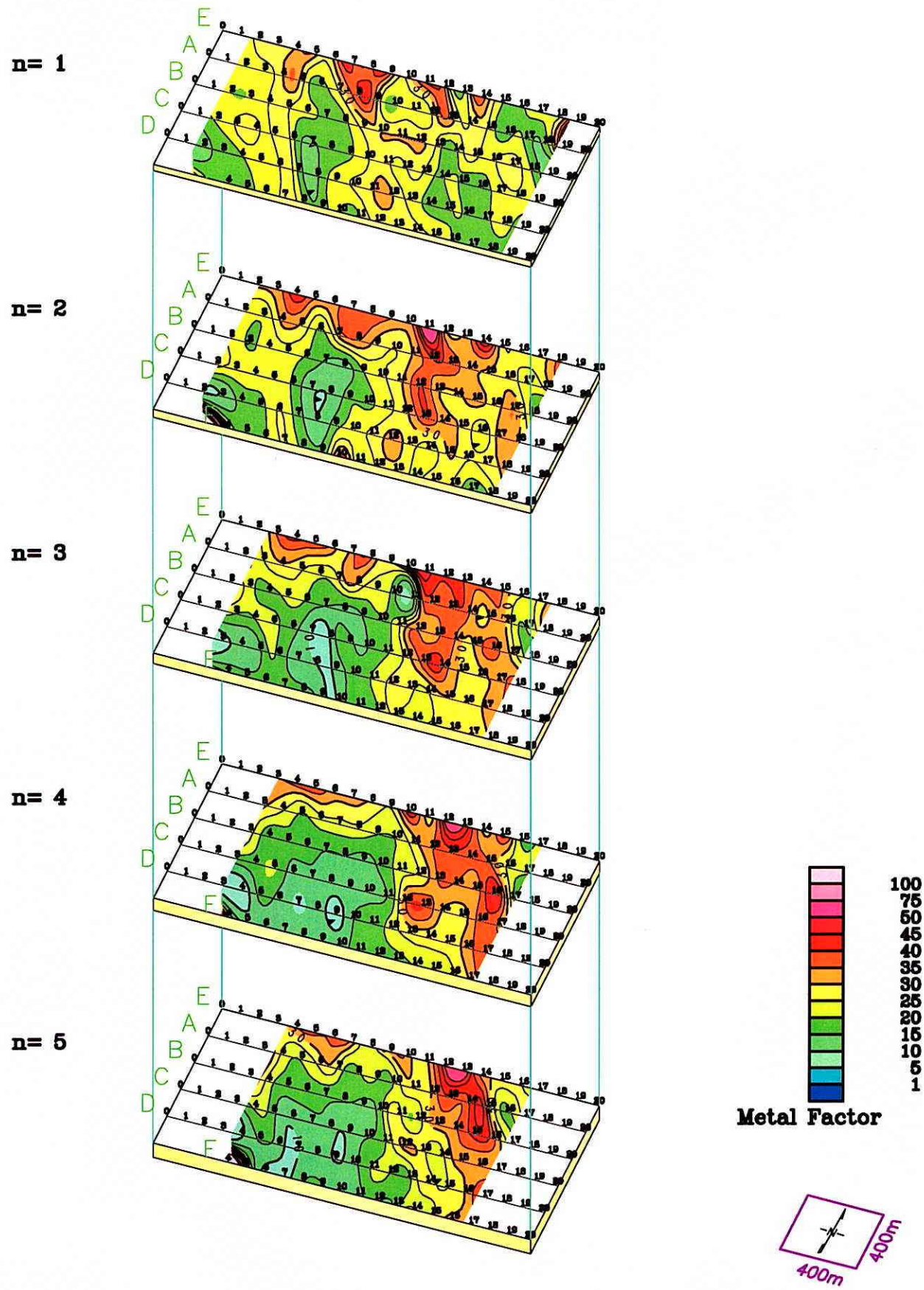

Fig.II-2-1-10 Plane map of metal factor (MJTK-IP-1)

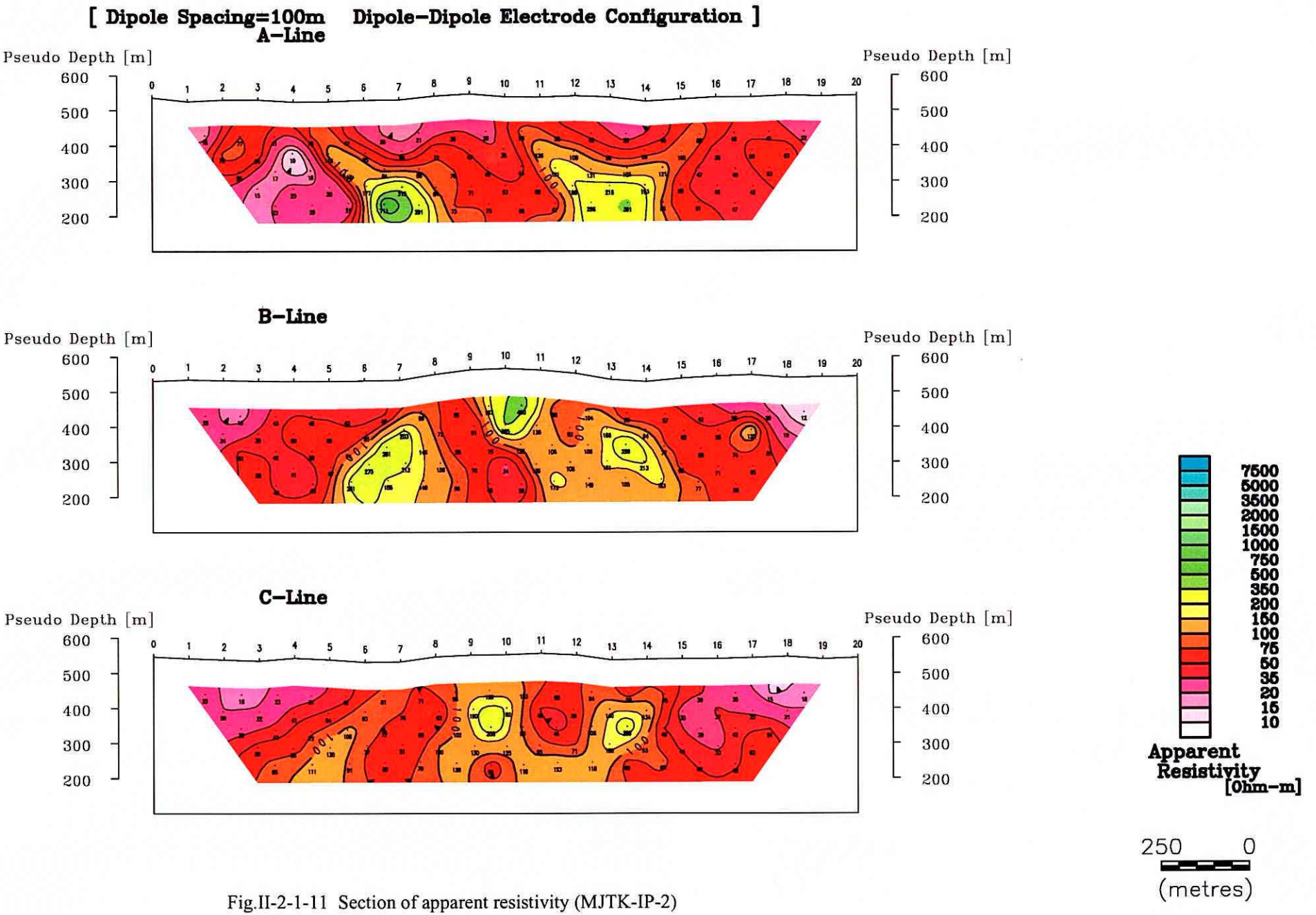

Fig.II-2-1-11 Section of apparent resistivity (MJTK-IP-2)

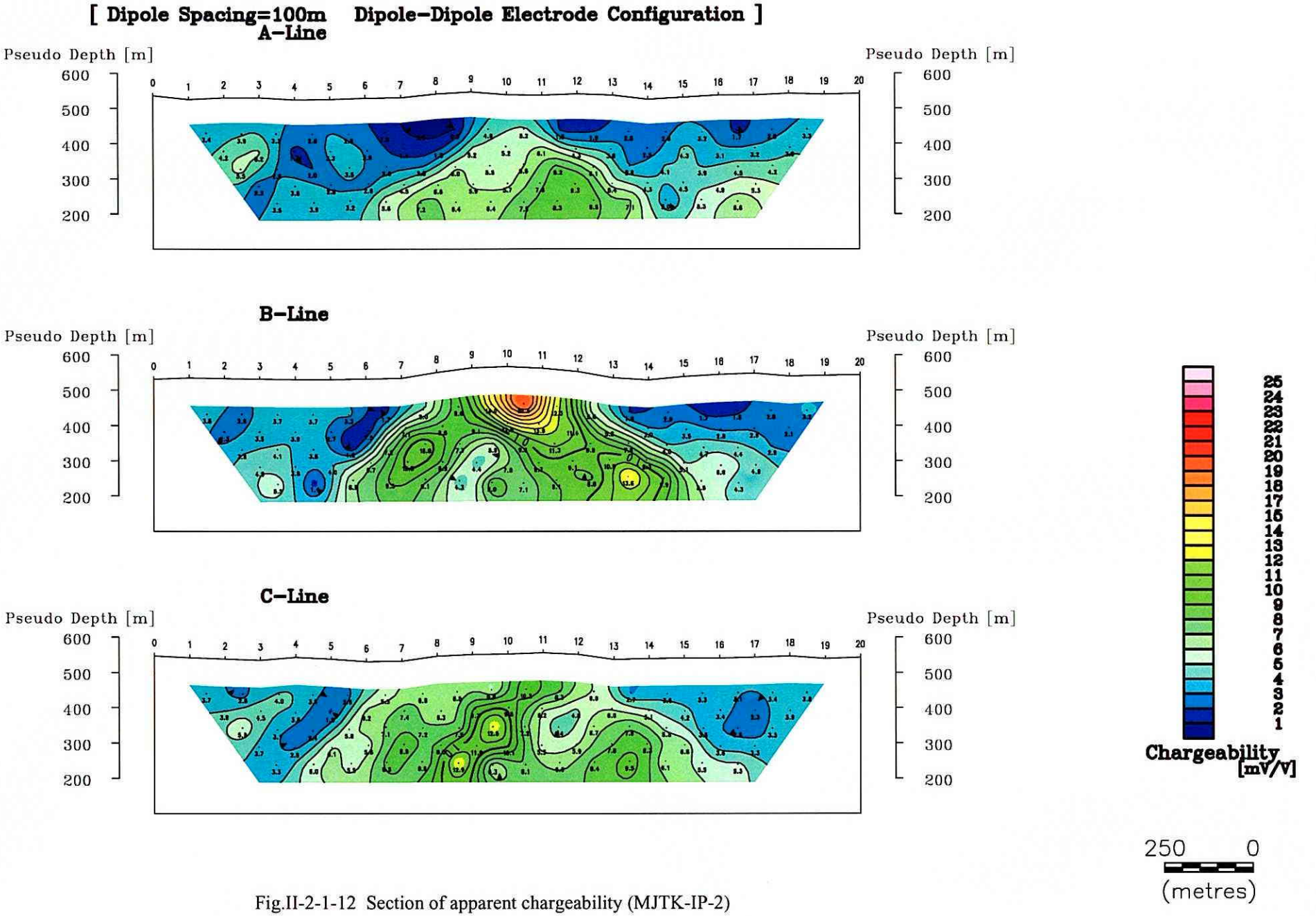

Fig.II-2-1-12 Section of apparent chargeability (MJTK-IP-2)

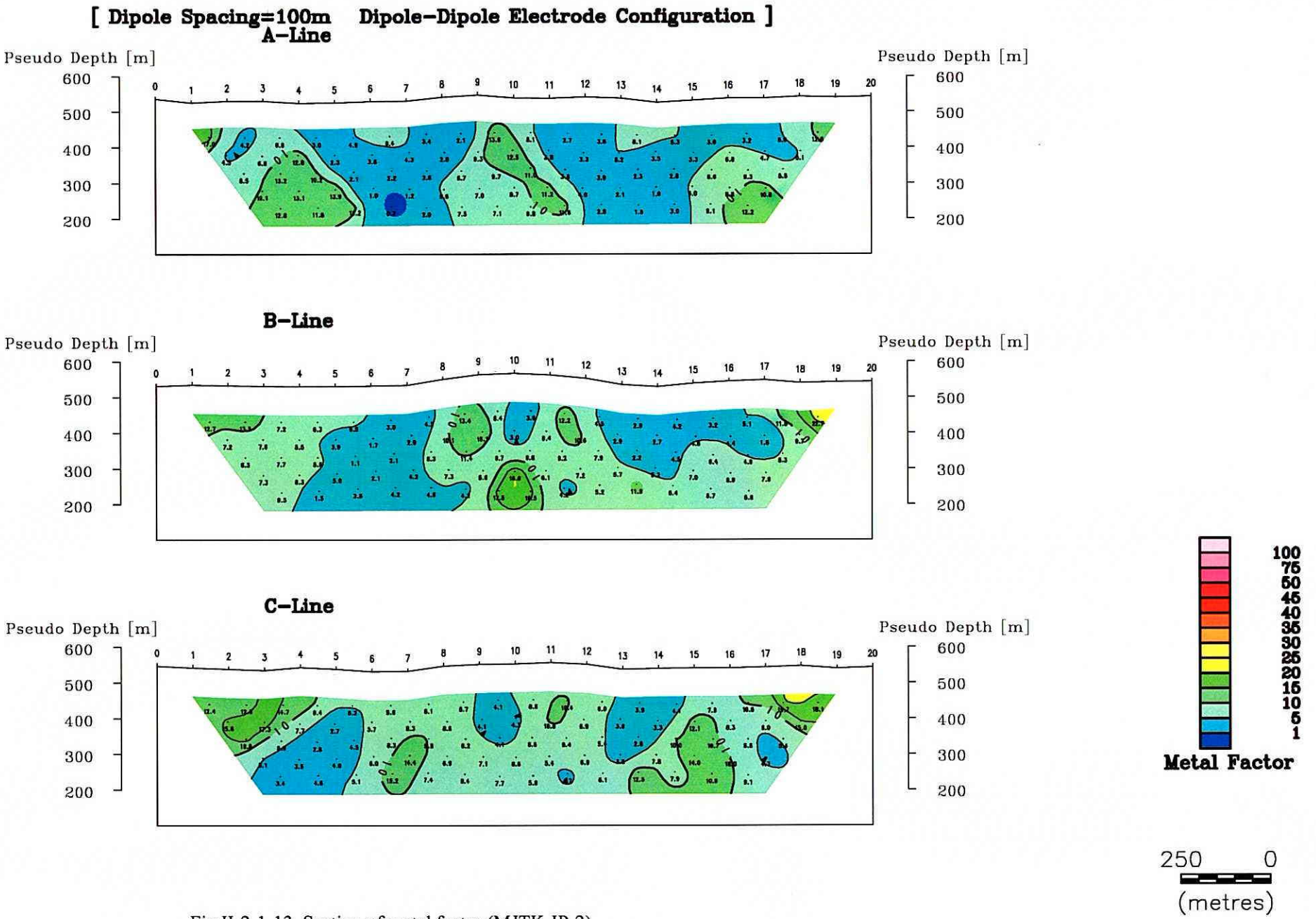

Fig.II-2-1-13 Section of metal factor (MJTK-IP-2)

[Dipole Spacing=100m Dipole-Dipole Electrode Configuration]

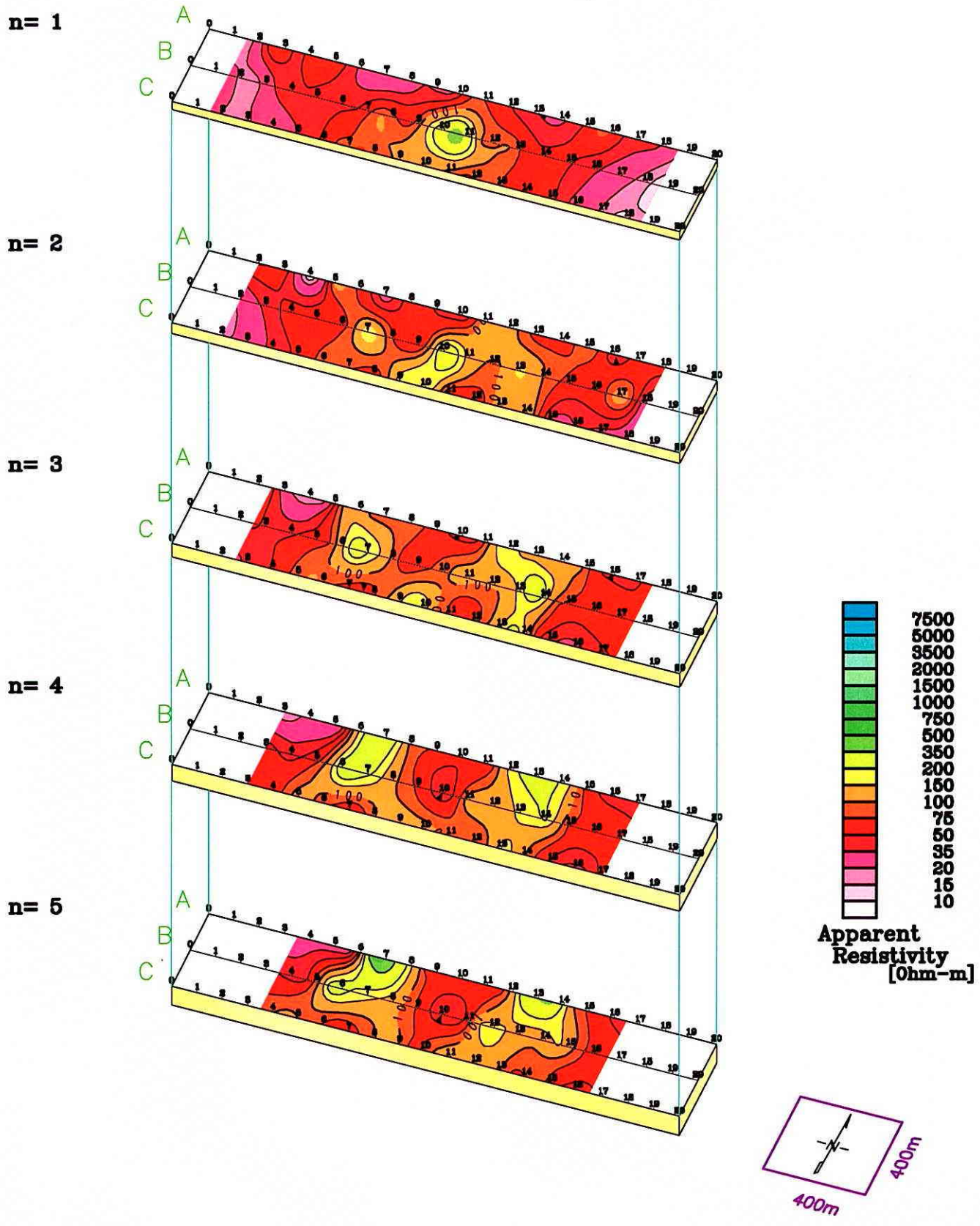

Fig.II-2-1-14 Plane map of apparent resistivity (MJTK-IP-2)

[Dipole Spacing=100m Dipole-Dipole Electrode Configuration]

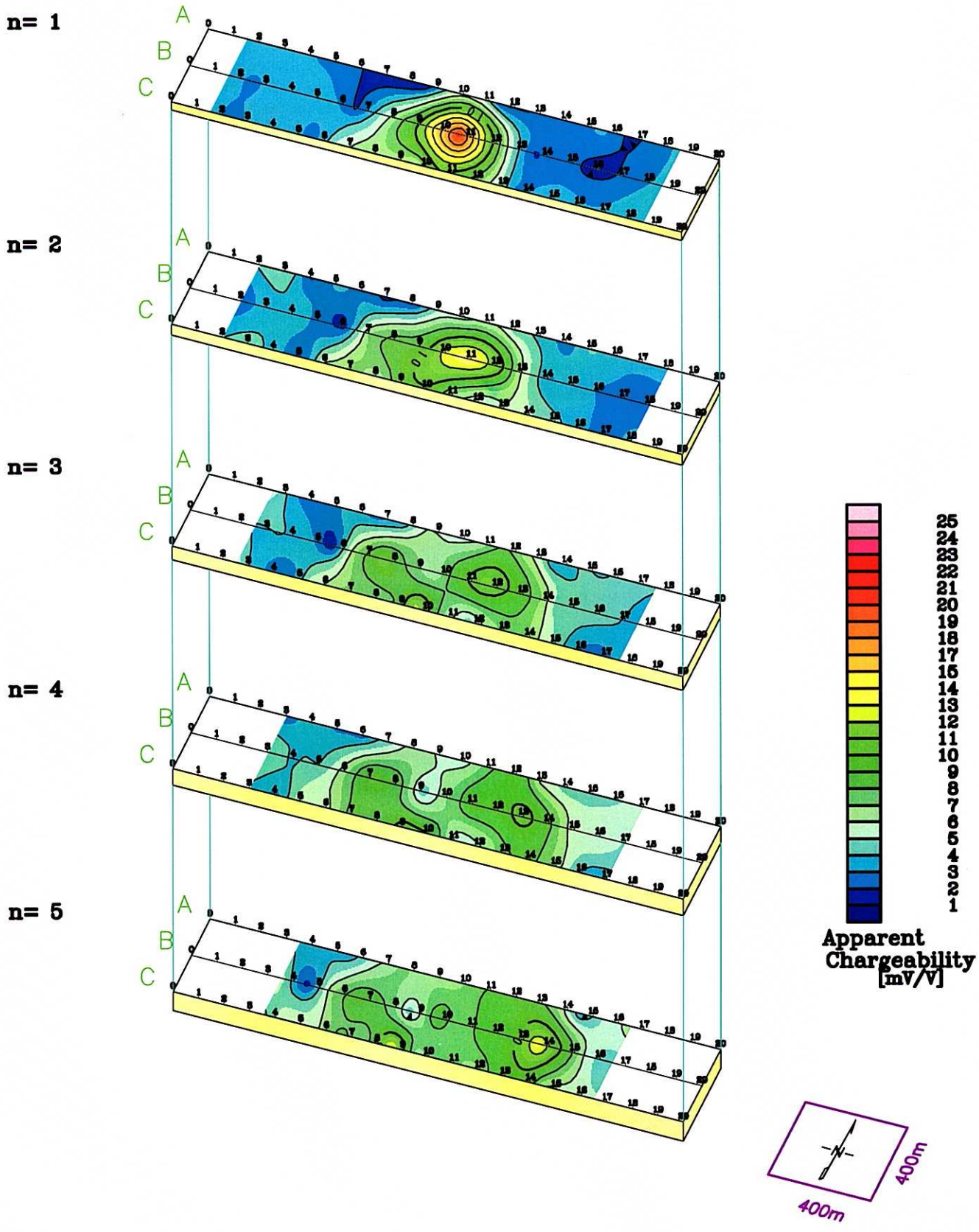

Fig.II-2-1-15 Plane map of apparent chargeability (MJTK-IP-2)

[Dipole Spacing=100m Dipole-Dipole Electrode Configuration]

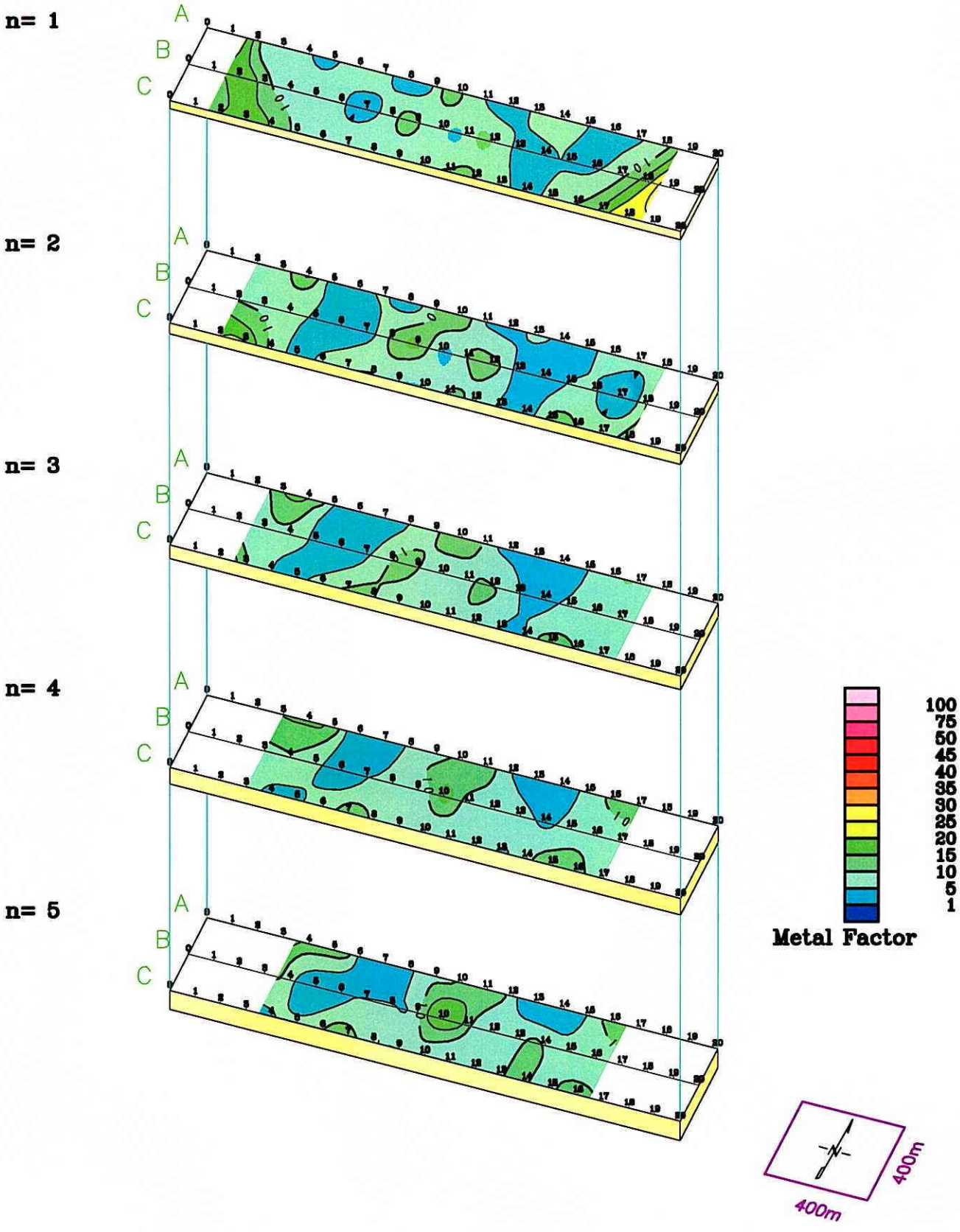

Fig.II-2-1-16 Plane map of metal factor (MJTK-IP-2)

[Dipole Spacing=100m Dipole-Dipole Electrode Configuration]

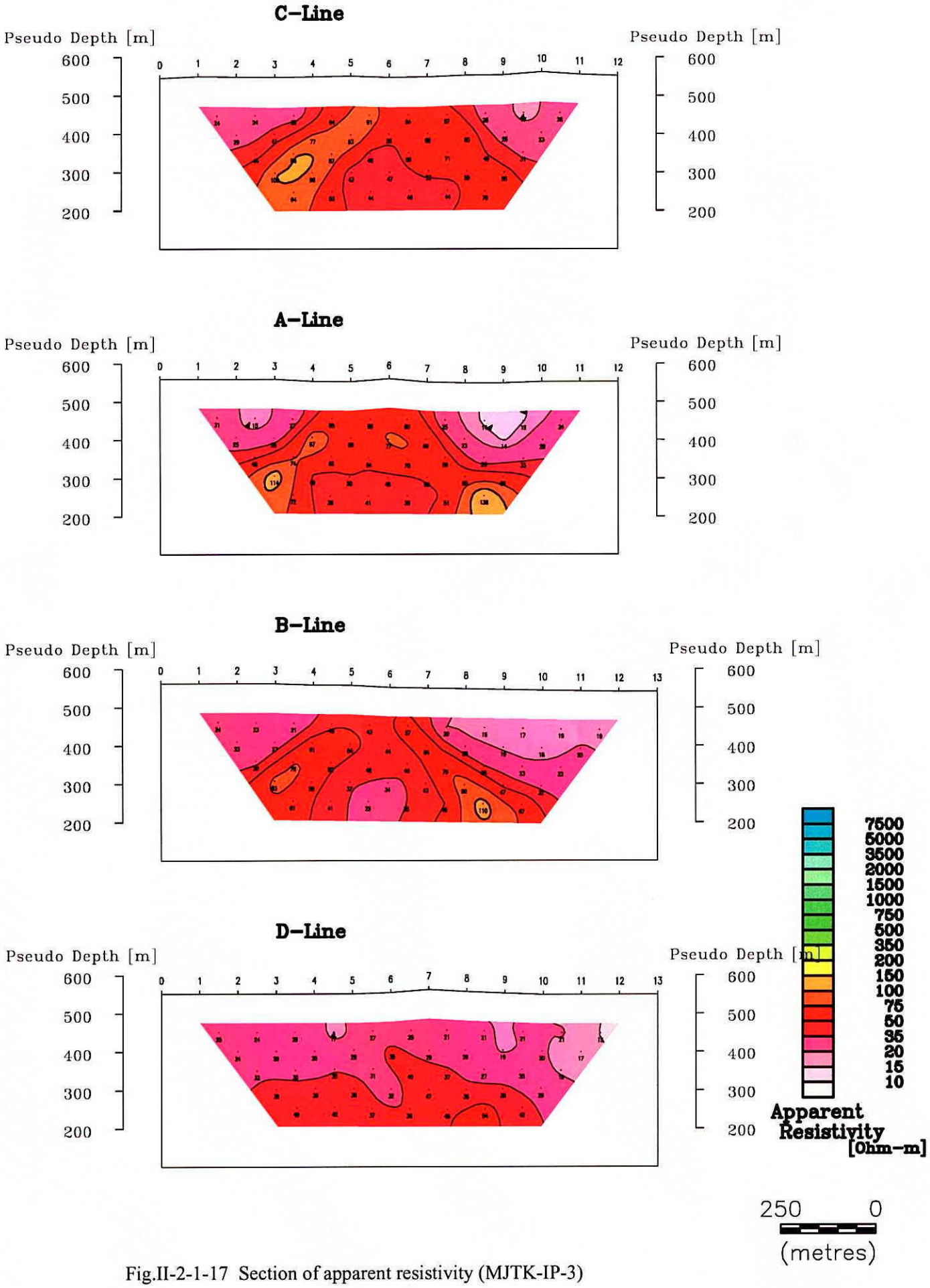

Fig.II-2-1-17 Section of apparent resistivity (MJTK-IP-3)

[Dipole Spacing=100m Dipole-Dipole Electrode Configuration]

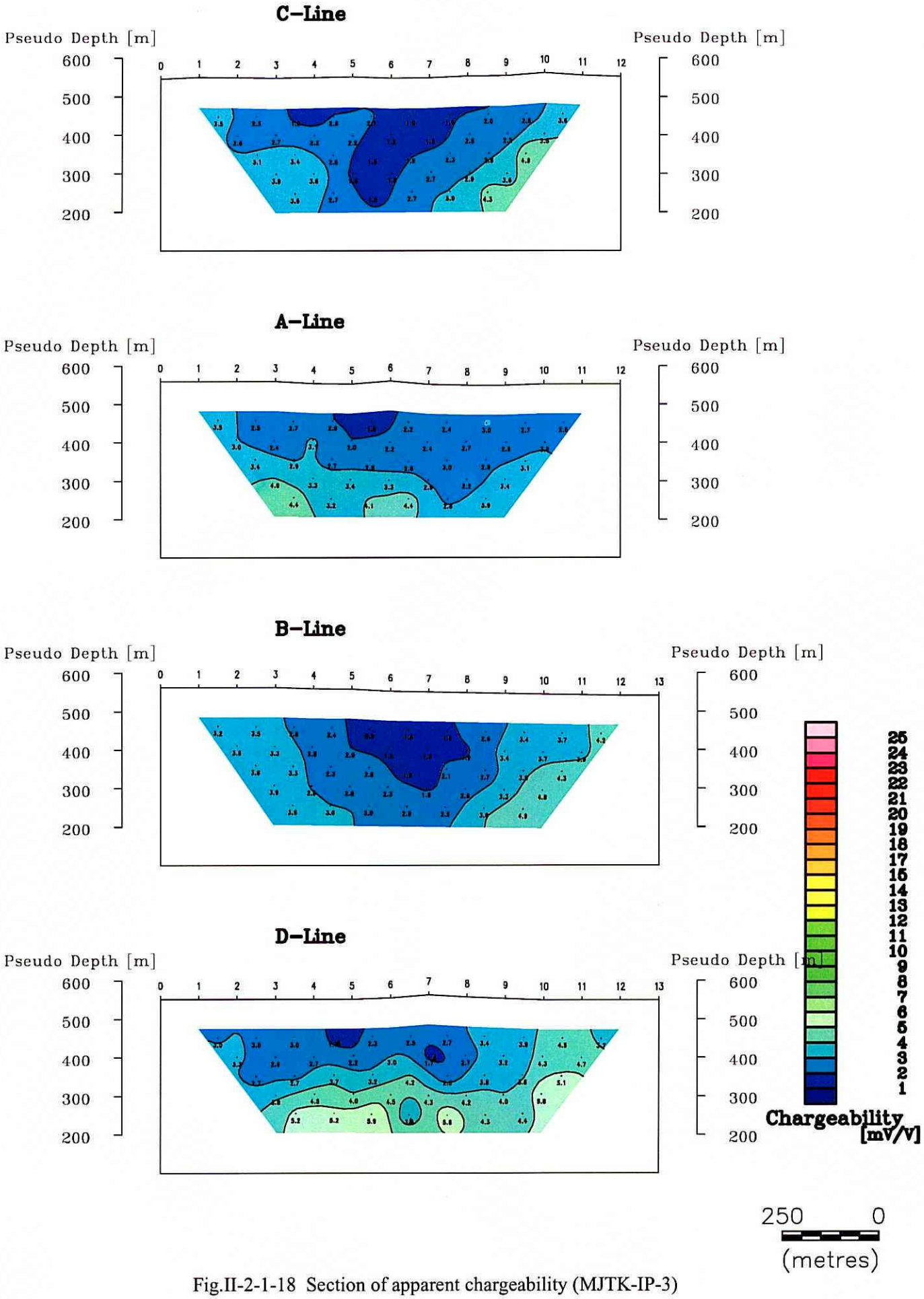

Fig.II-2-1-18 Section of apparent chargeability (MJTK-IP-3)

[Dipole Spacing=100m Dipole-Dipole Electrode Configuration]

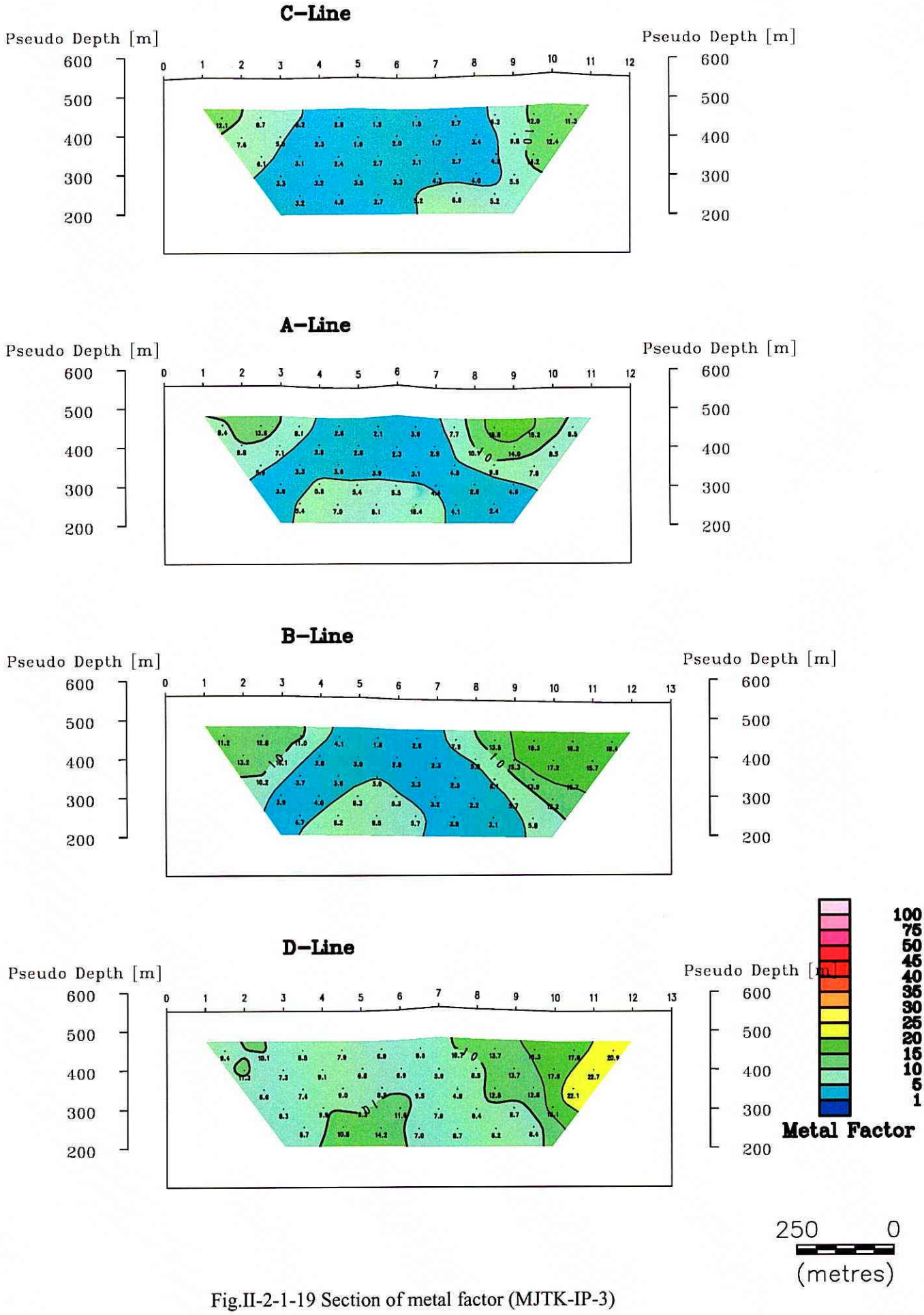

Fig.II-2-1-19 Section of metal factor (MJTK-IP-3)

[Dipole Spacing=100m Dipole-Dipole Electrode Configuration]

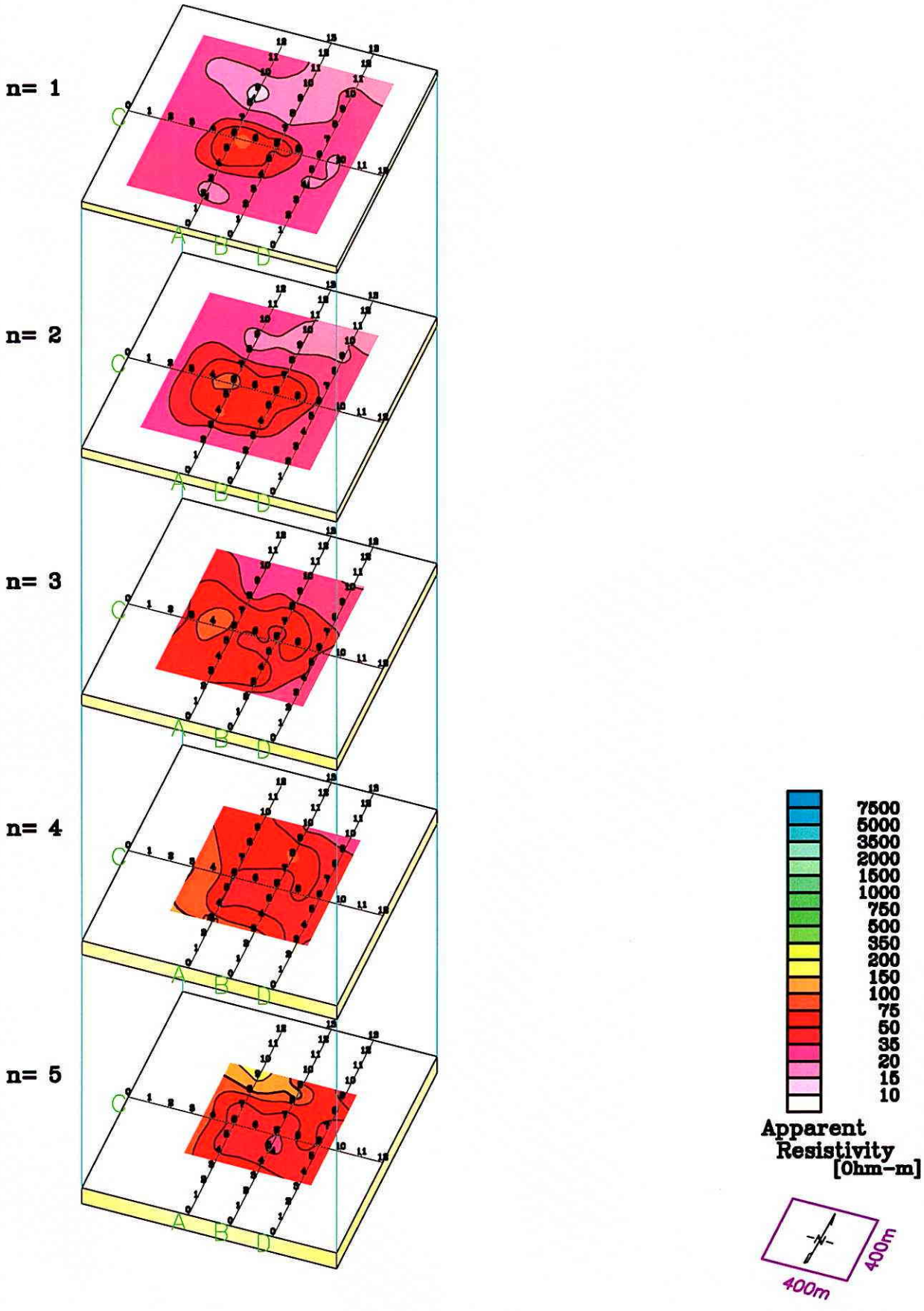

Fig.II-2-1-20 Plane map of apparent resistivity (MJTK-IP-3)

[Dipole Spacing=100m Dipole-Dipole Electrode Configuration]

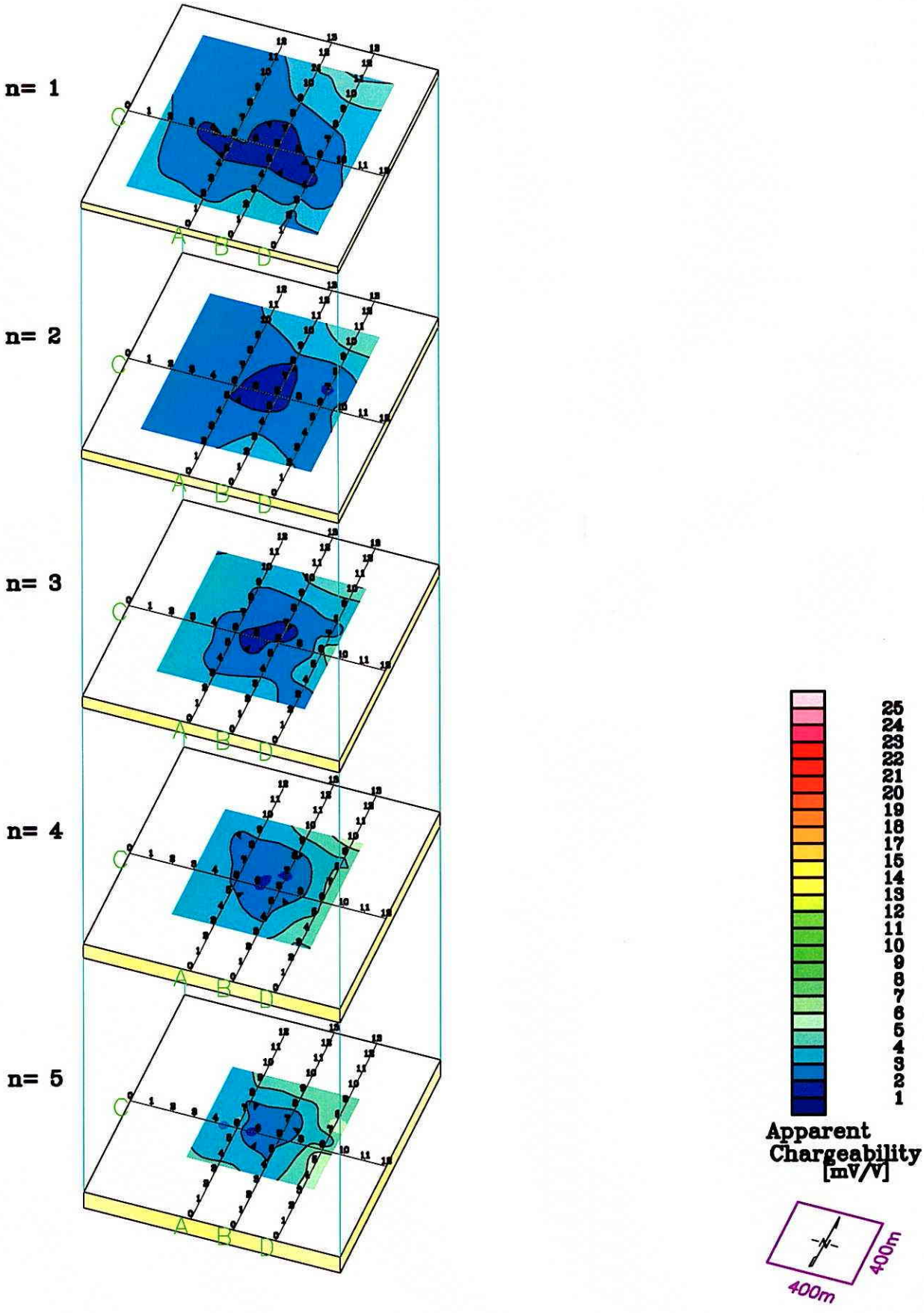

Fig.II-2-1-21 Plane map of apparent chargeability (MJTK-IP-3)

[Dipole Spacing=100m Dipole-Dipole Electrode Configuration]

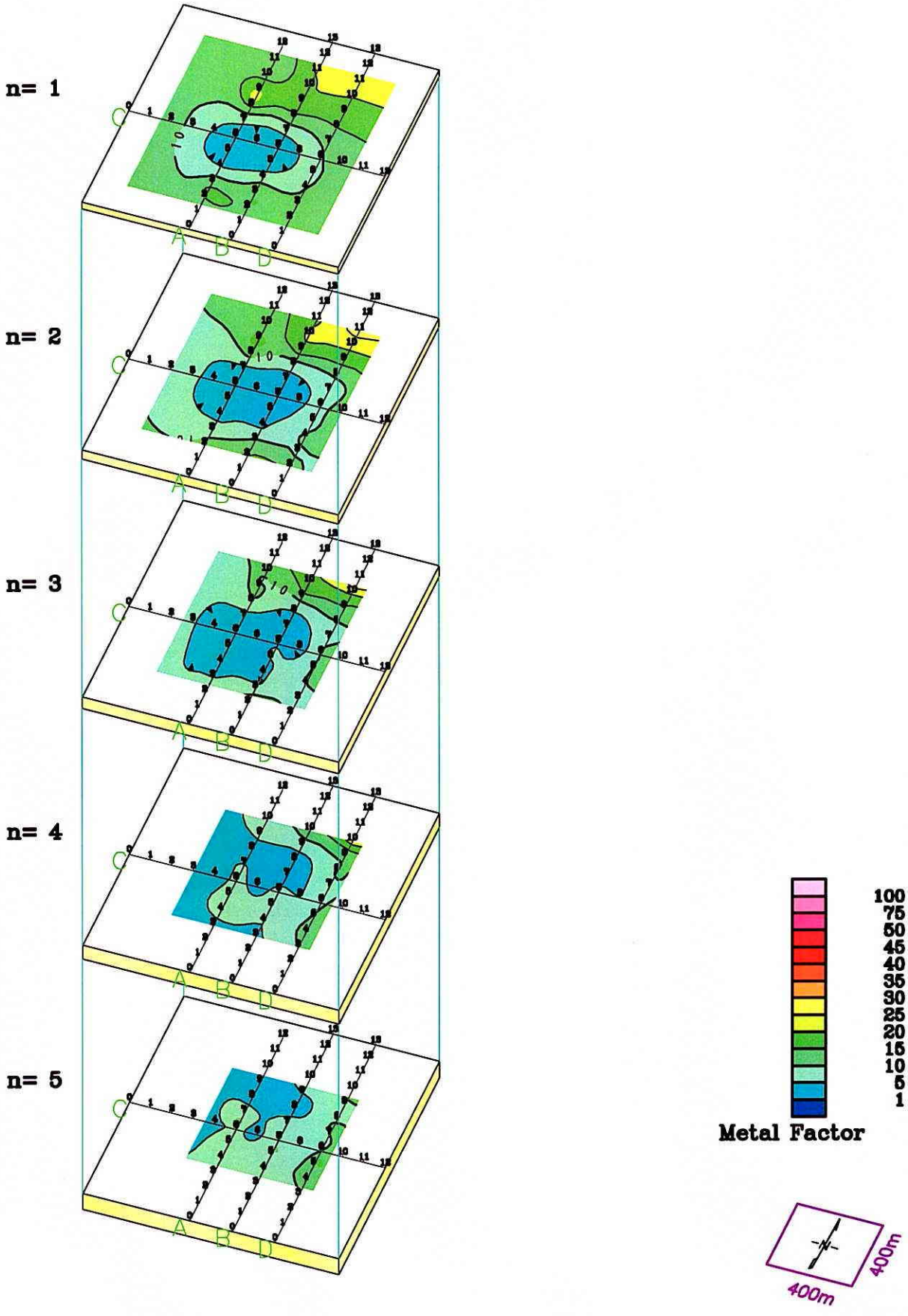

Fig.II-2-1-22 Plane map of metal factor (MJTK-IP-3)

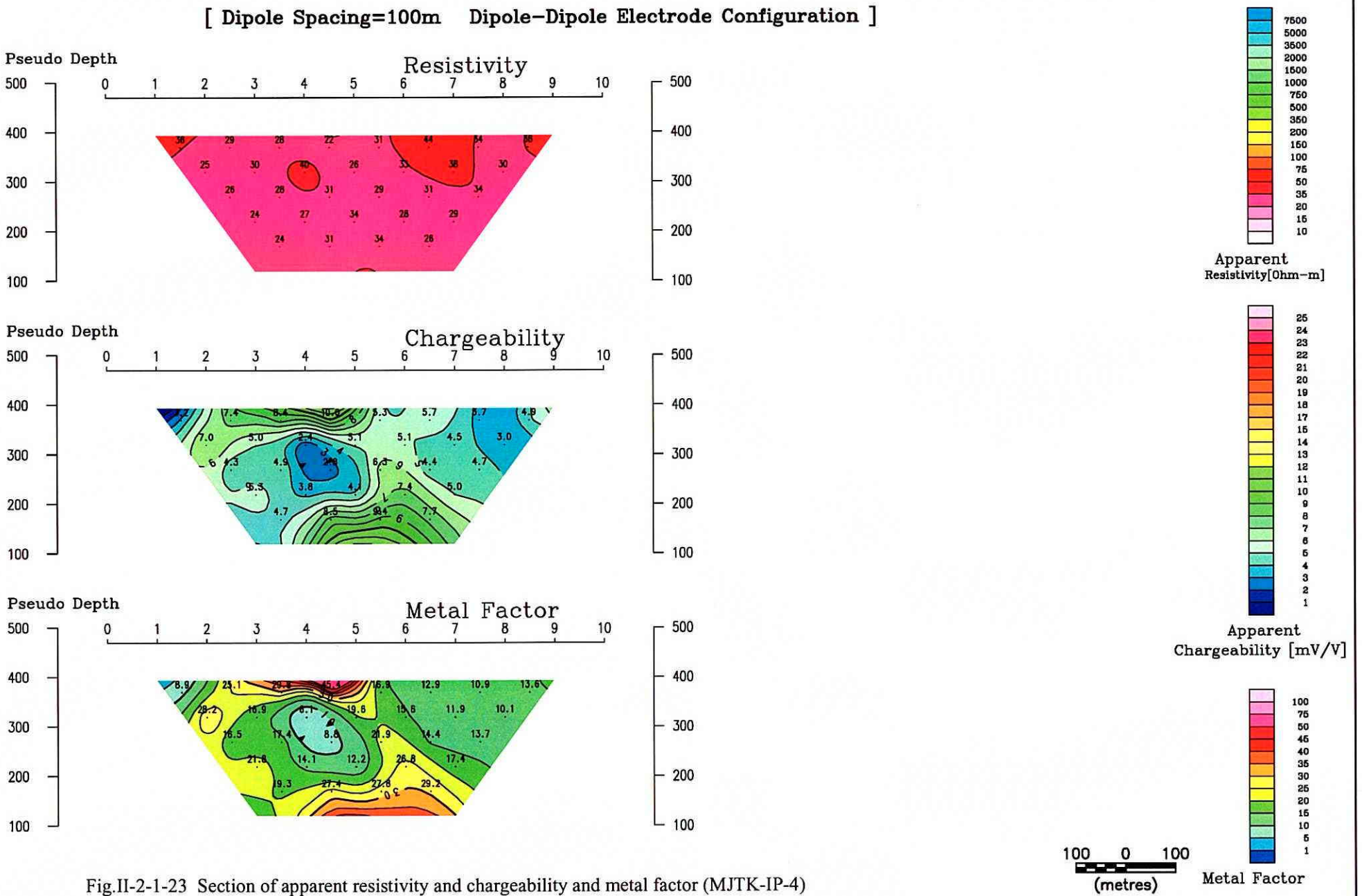

Fig.II-2-1-23 Section of apparent resistivity and chargeability and metal factor (MJTK-IP-4)

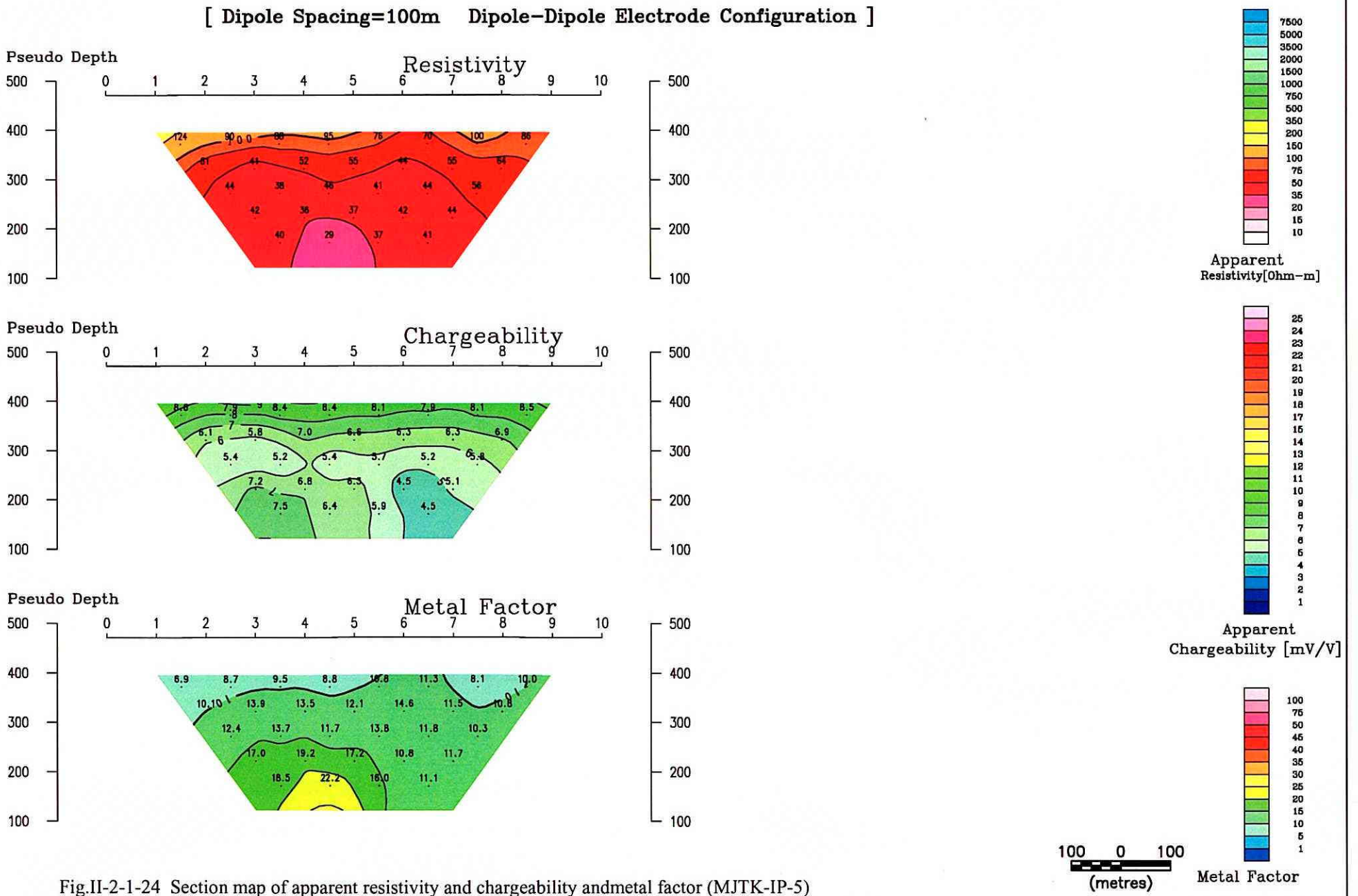

Fig.II-2-1-24 Section map of apparent resistivity and chargeability andmetal factor (MJTK-IP-5)

[Dipole Spacing=100m Dipole-Dipole Electrode Configuration]

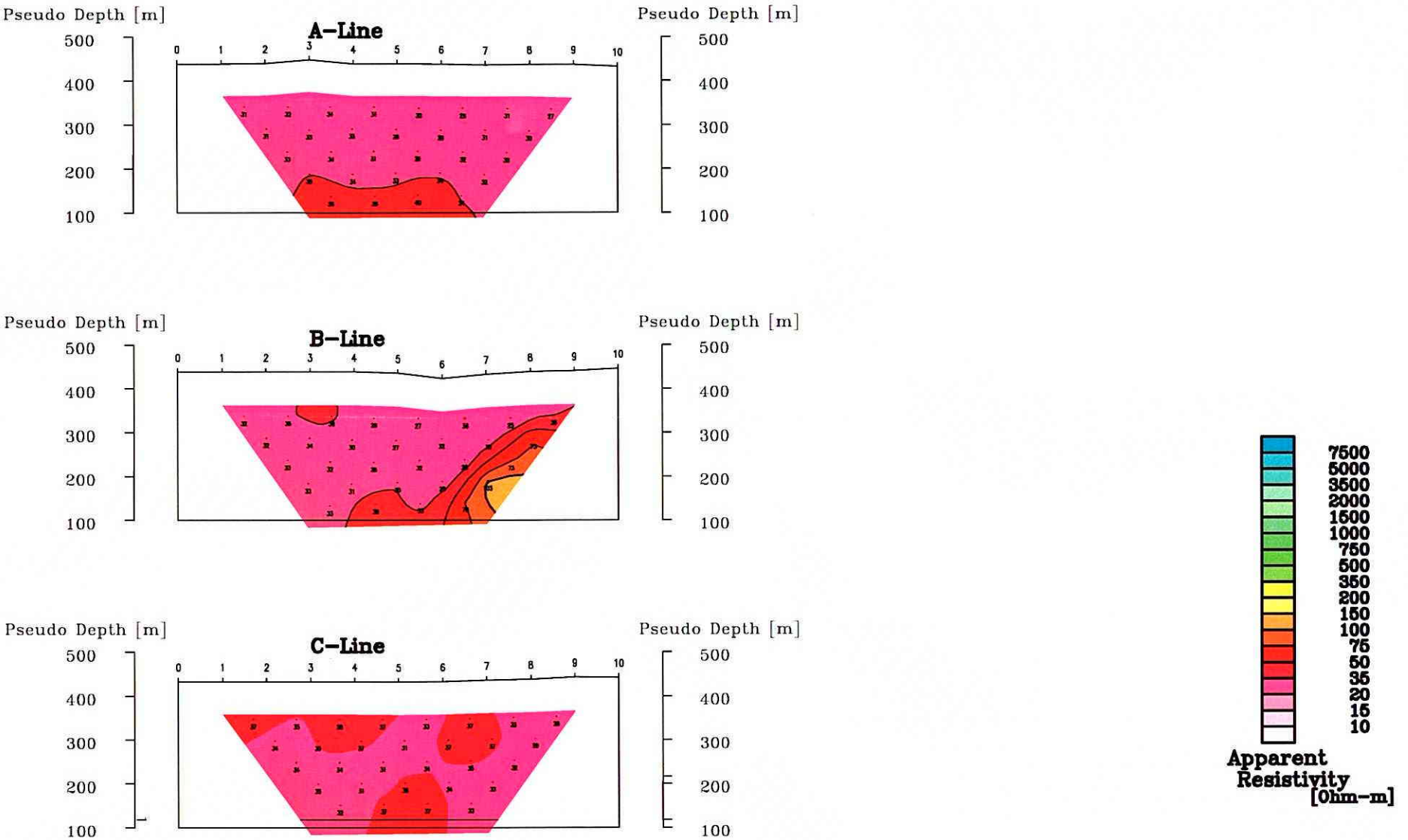

Fig.II-2-1-25 Section of apparent resistivity (MJTK-IP-6)

[Dipole Spacing=100m Dipole-Dipole Electrode Configuration]

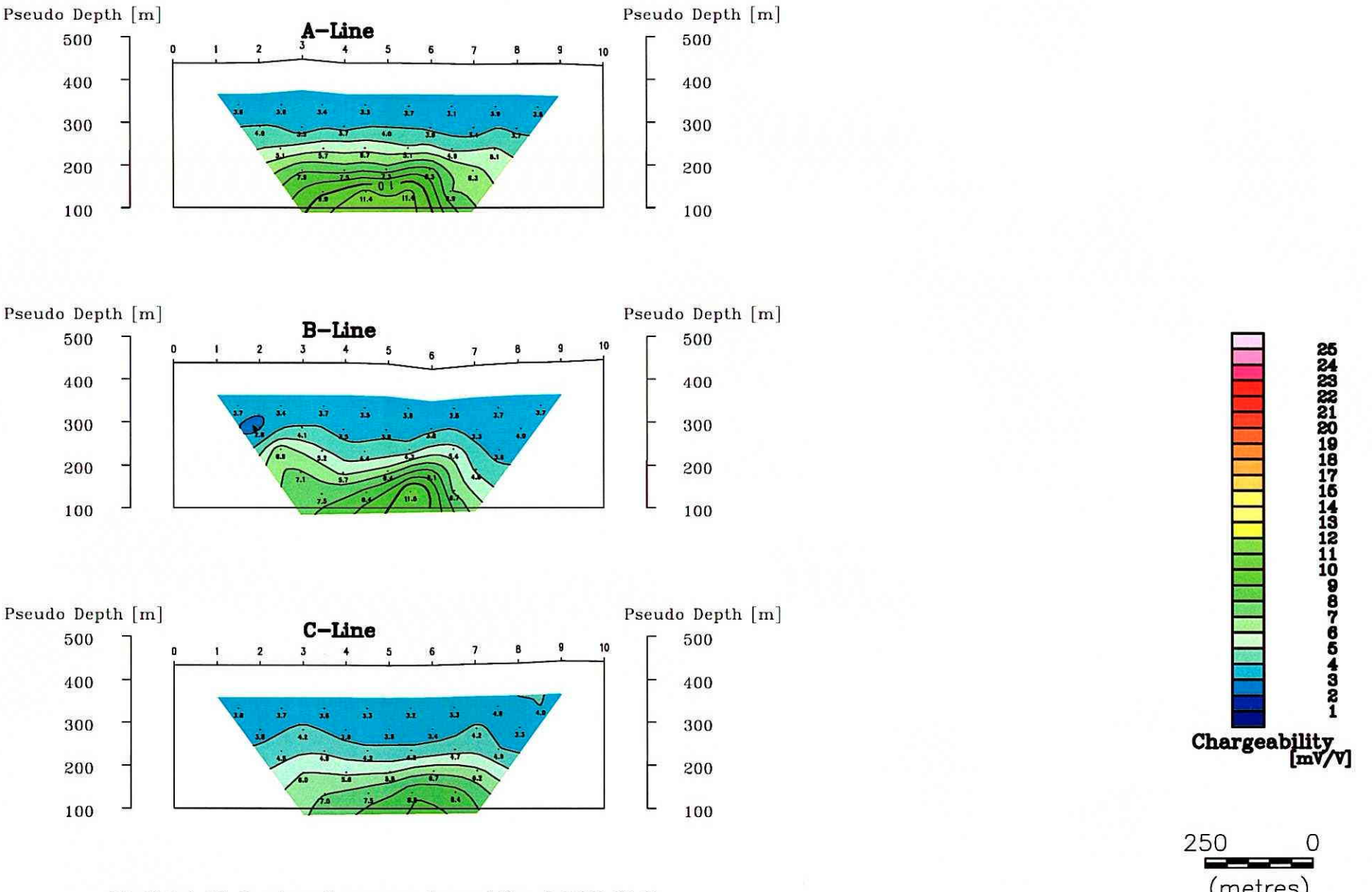

Fig.II-2-1-26 Section of apparent chargeability (MJTK-IP-6)

[Dipole Spacing=100m Dipole-Dipole Electrode Configuration]

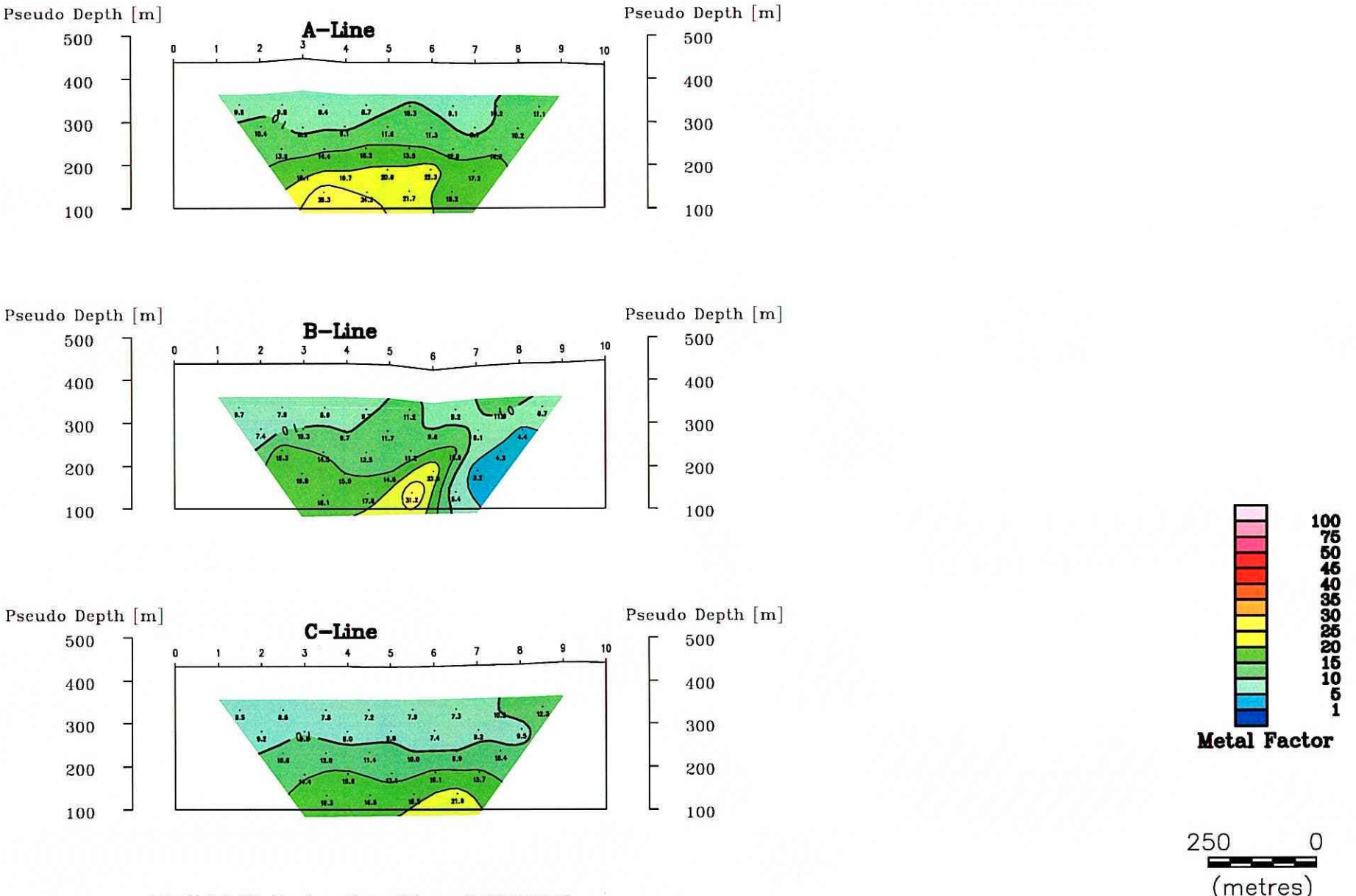

Fig.II-2-1-27 Section of metal factor (MJTK-IP-6)

[Dipole Spacing=100m Dipole-Dipole Electrode Configuration]

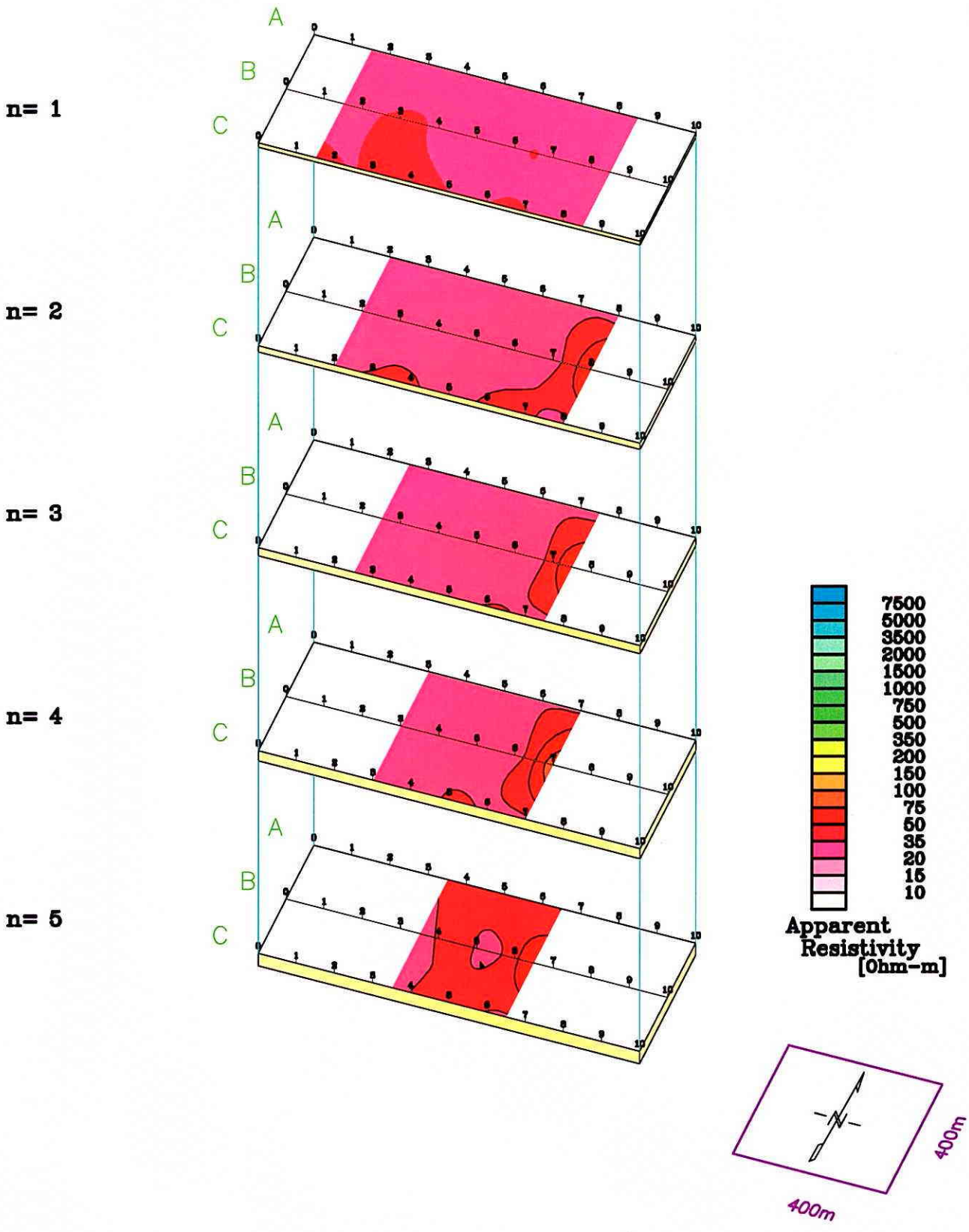

Fig.II-2-1-28 Plane map of apparent resistivity (MJTK-IP-6)

[Dipole Spacing=100m Dipole-Dipole Electrode Configuration]

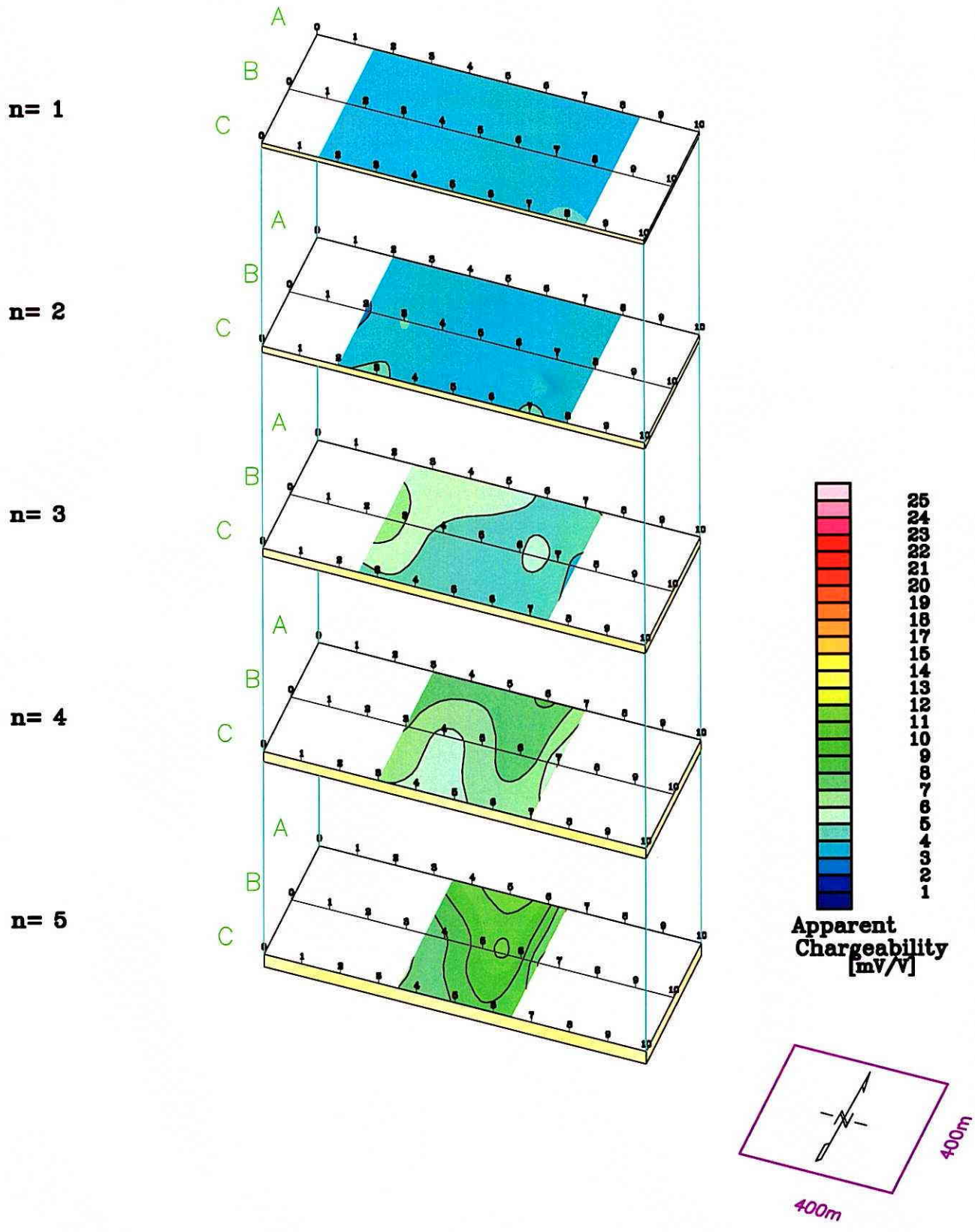

Fig.II-2-1-29 Plane map of apparent chargeability (MJTK-IP-6)

[Dipole Spacing=100m Dipole-Dipole Electrode Configuration]

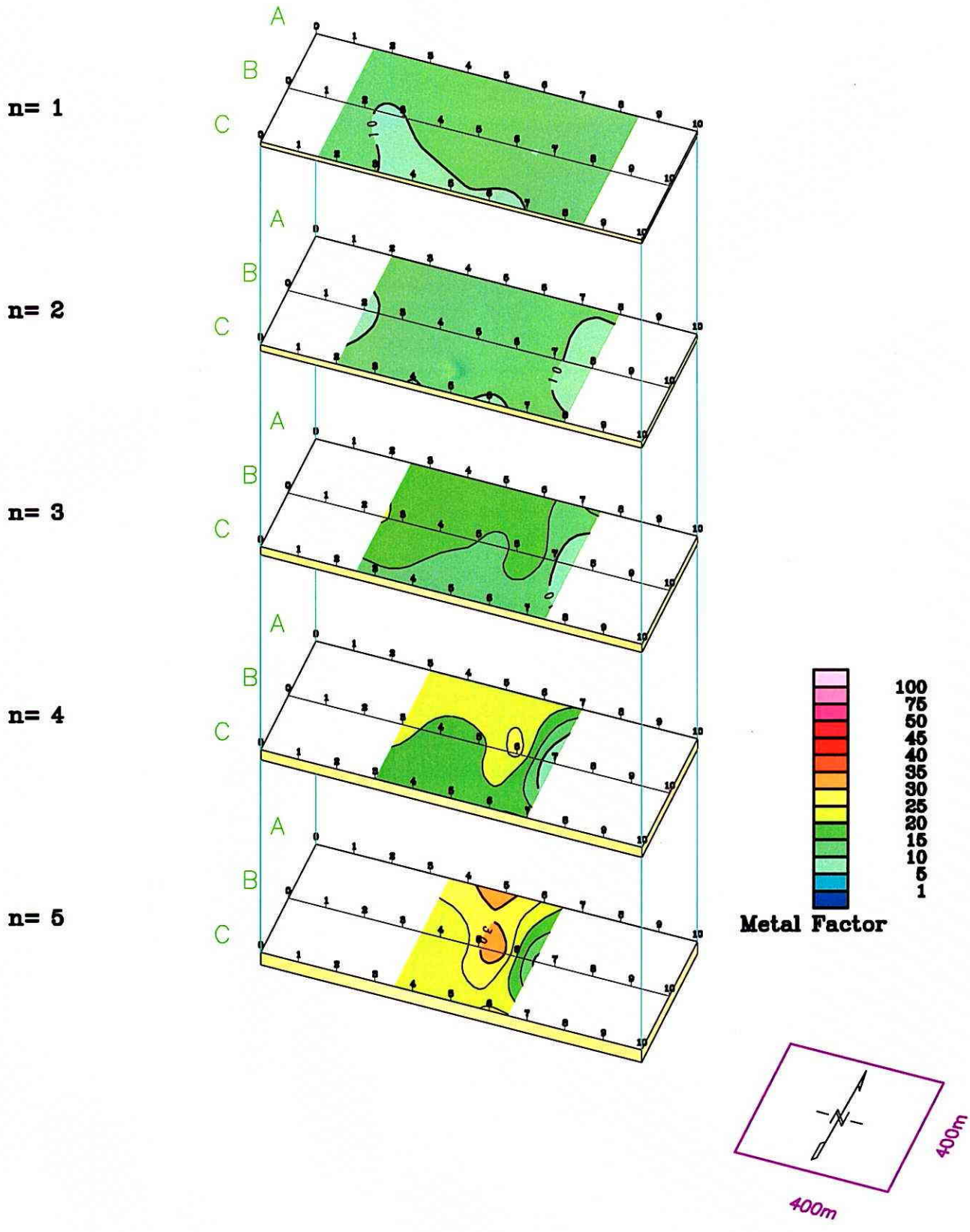

Fig.II-2-1-30 Plane map of metal factor (MJTK-IP-6)

[Dipole Spacing=100m Dipole-Dipole Electrode Configuration]

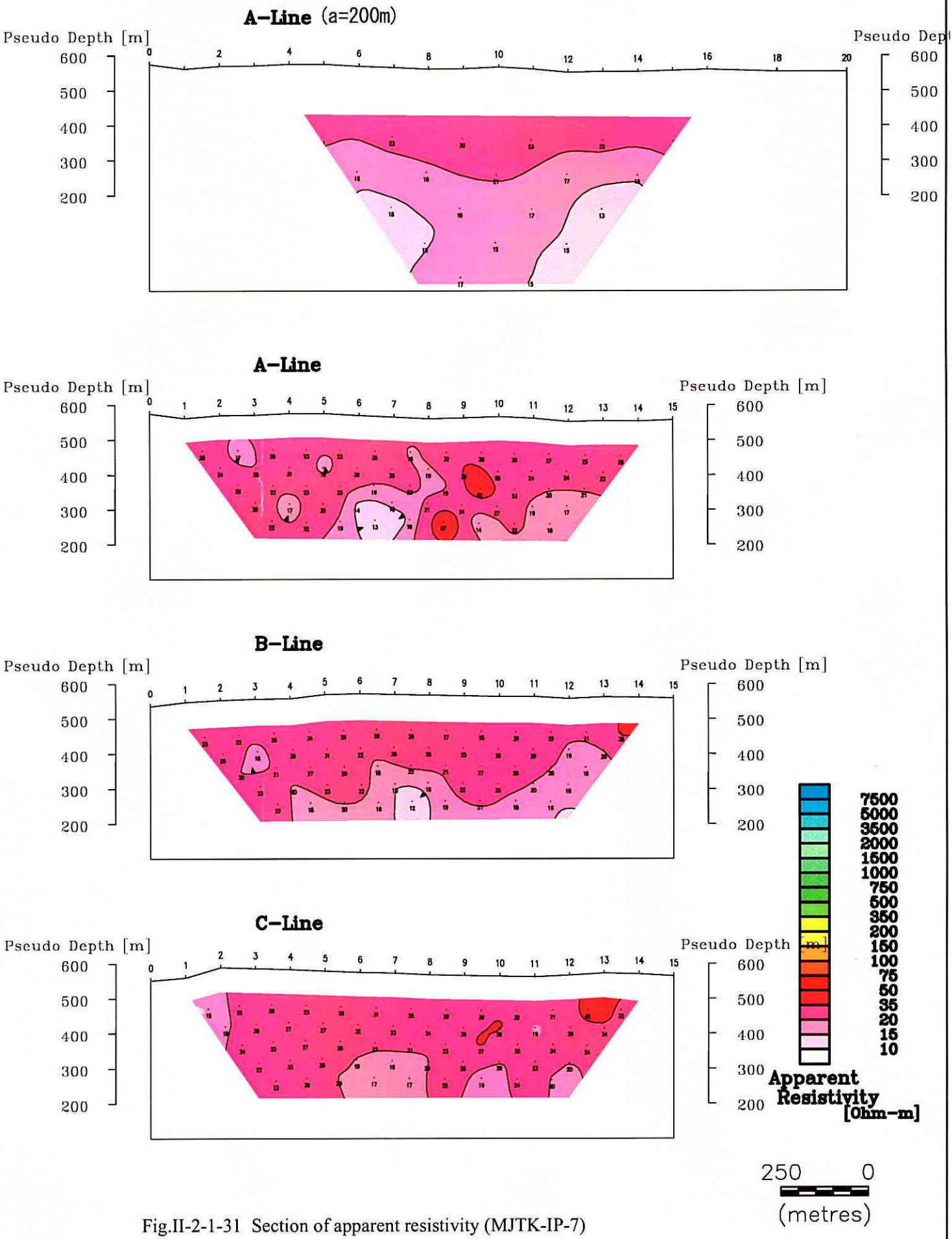

Fig.II-2-1-31 Section of apparent resistivity (MJTK-IP-7)

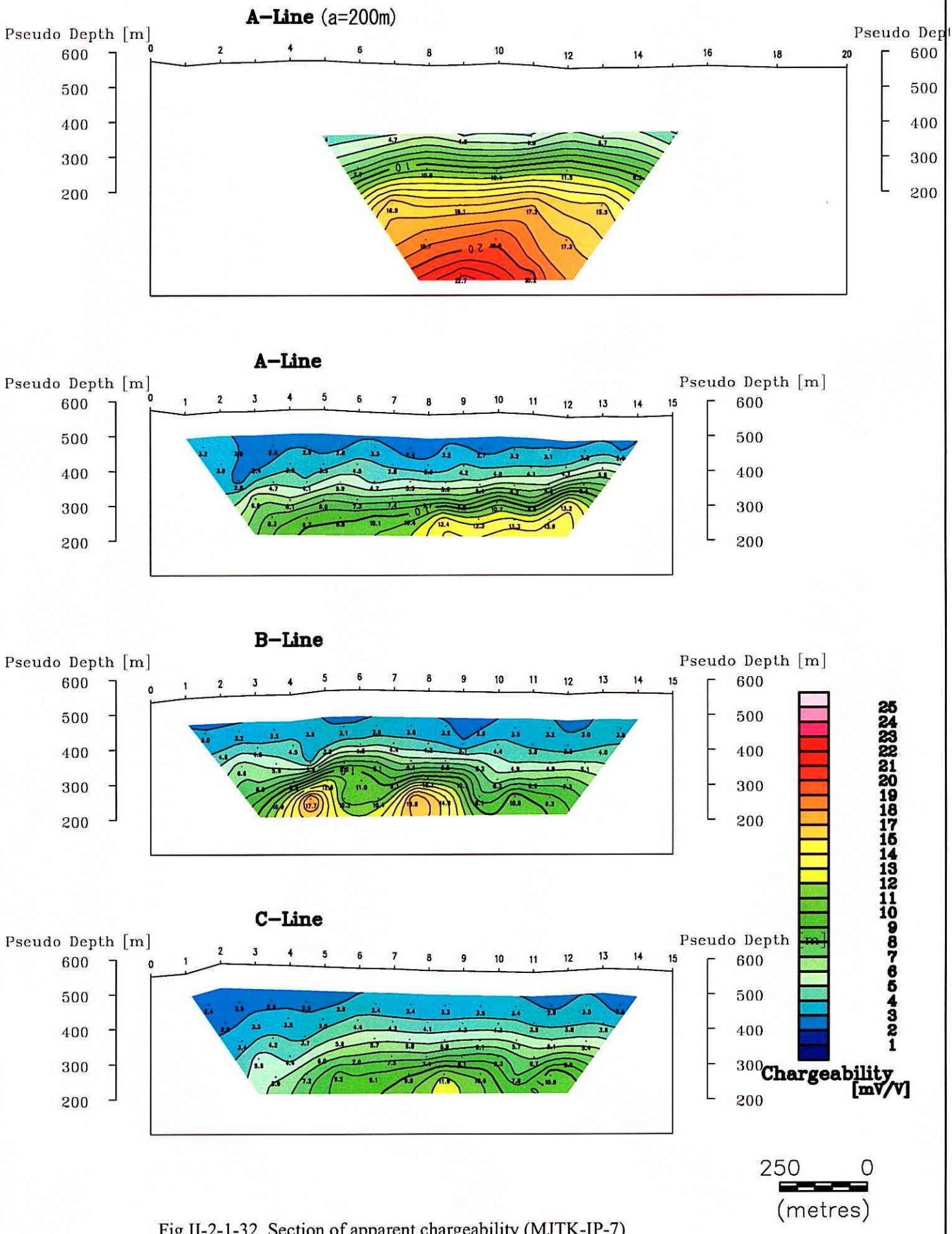

Fig.II-2-1-32 Section of apparent chargeability (MJTK-IP-7)

[Dipole Spacing=100m Dipole-Dipole Electrode Configuration]

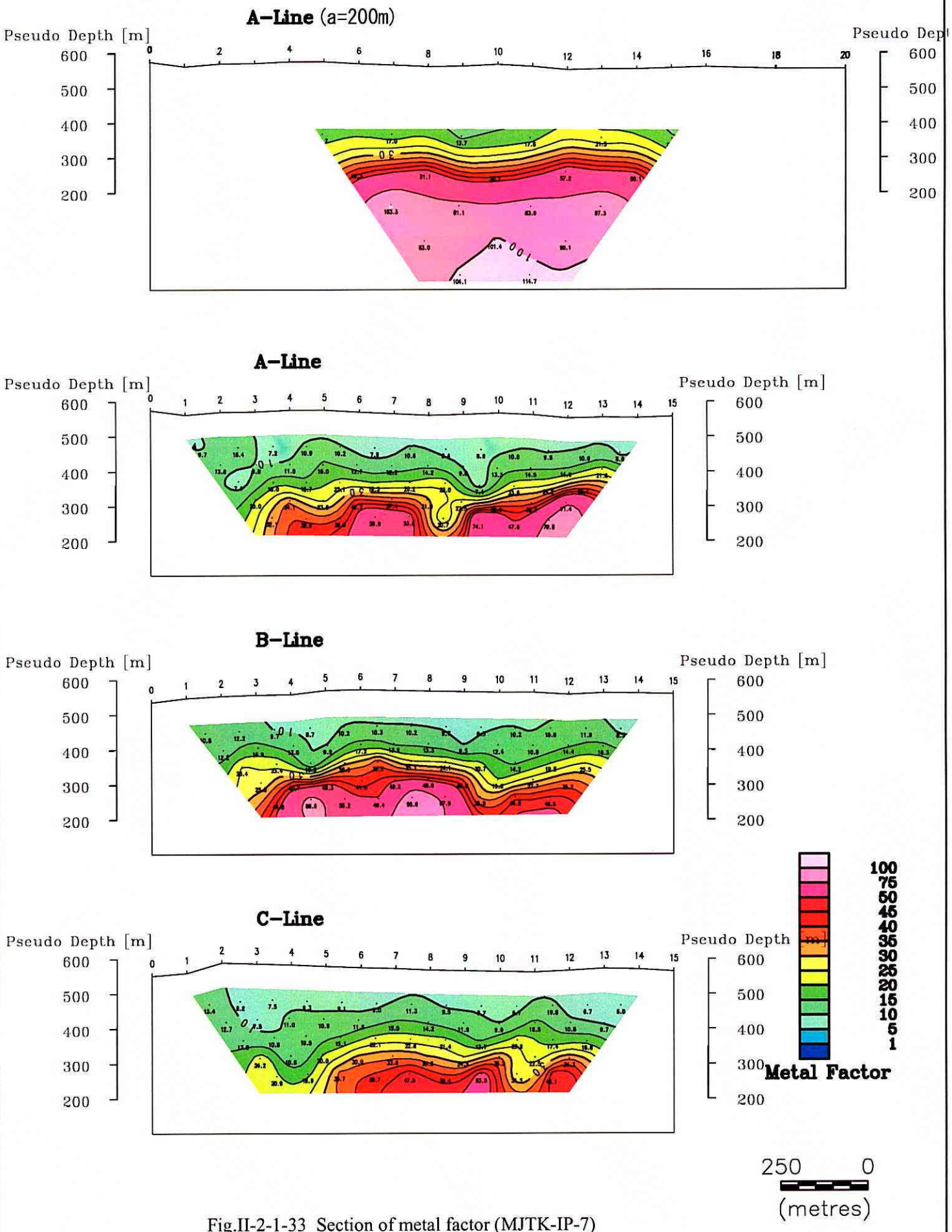

Fig.II-2-1-33 Section of metal factor (MJTK-IP-7)

[Dipole Spacing=100m Dipole-Dipole Electrode Configuration]

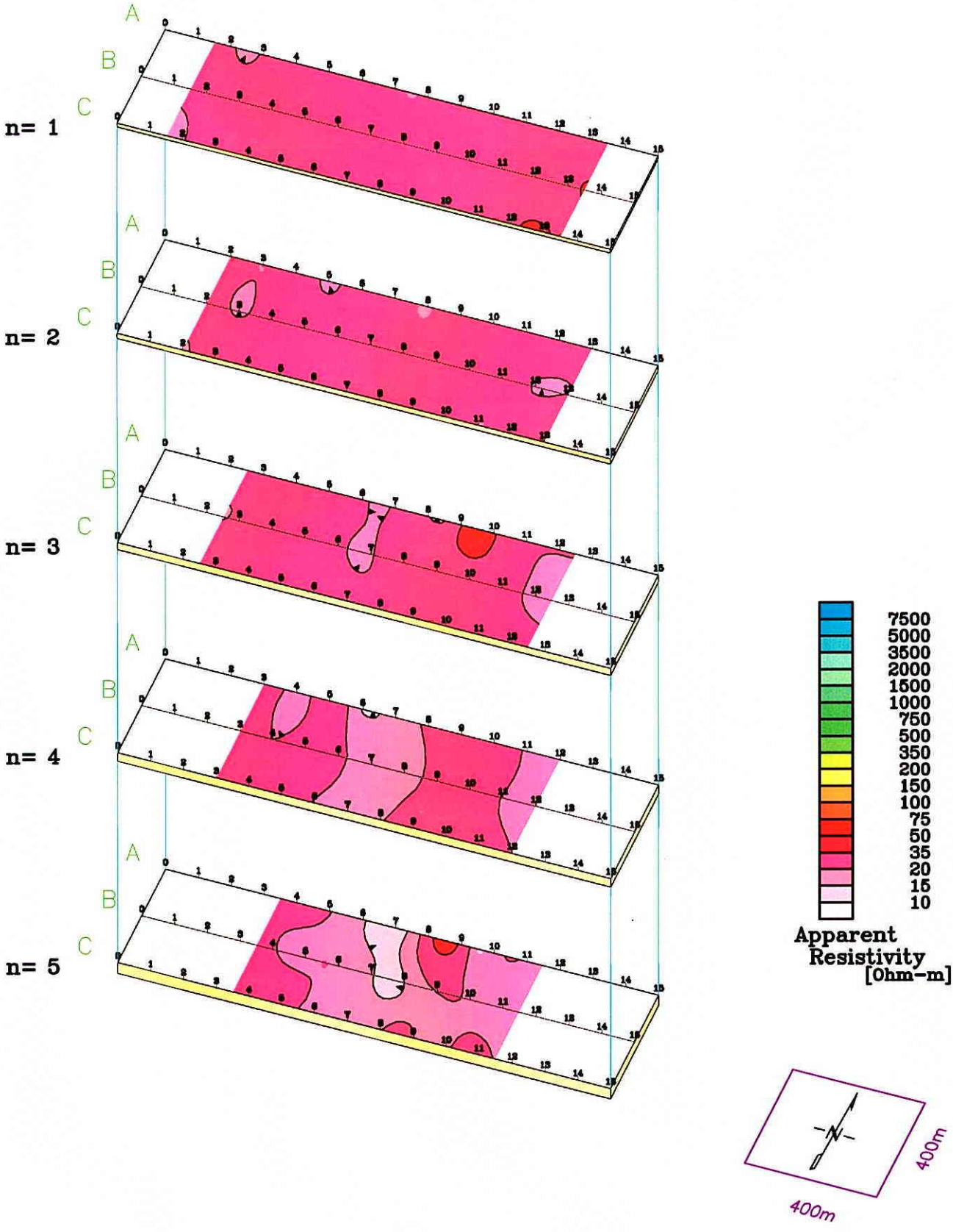

Fig.II-2-1-34 Plane map of apparent resistivity (MJTK-IP-7)

[Dipole Spacing=100m Dipole-Dipole Electrode Configuration]

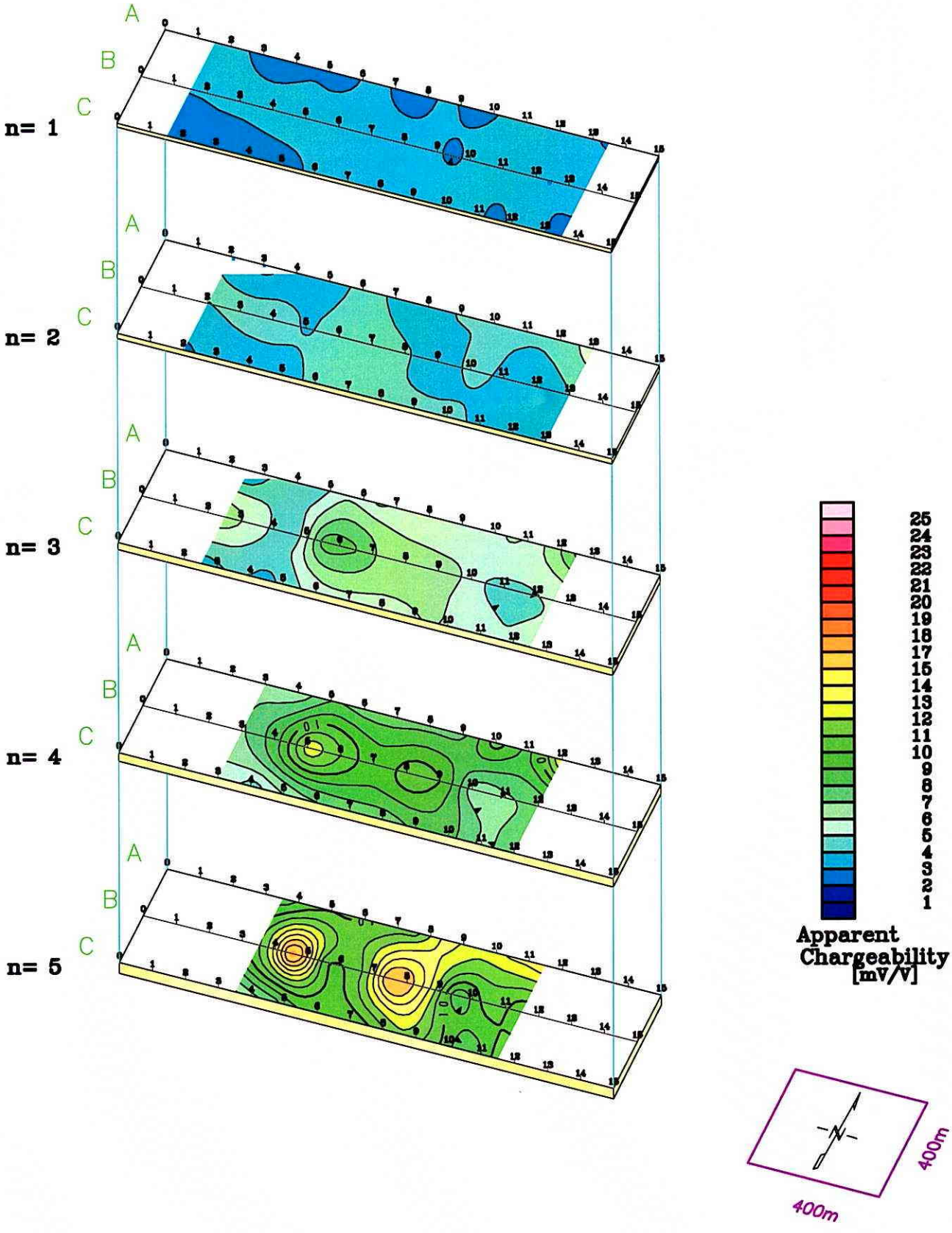

Fig.II-2-1-35 Plane map of apparent chargeability (MJTK-IP-7)

[Dipole Spacing=100m Dipole-Dipole Electrode Configuration]

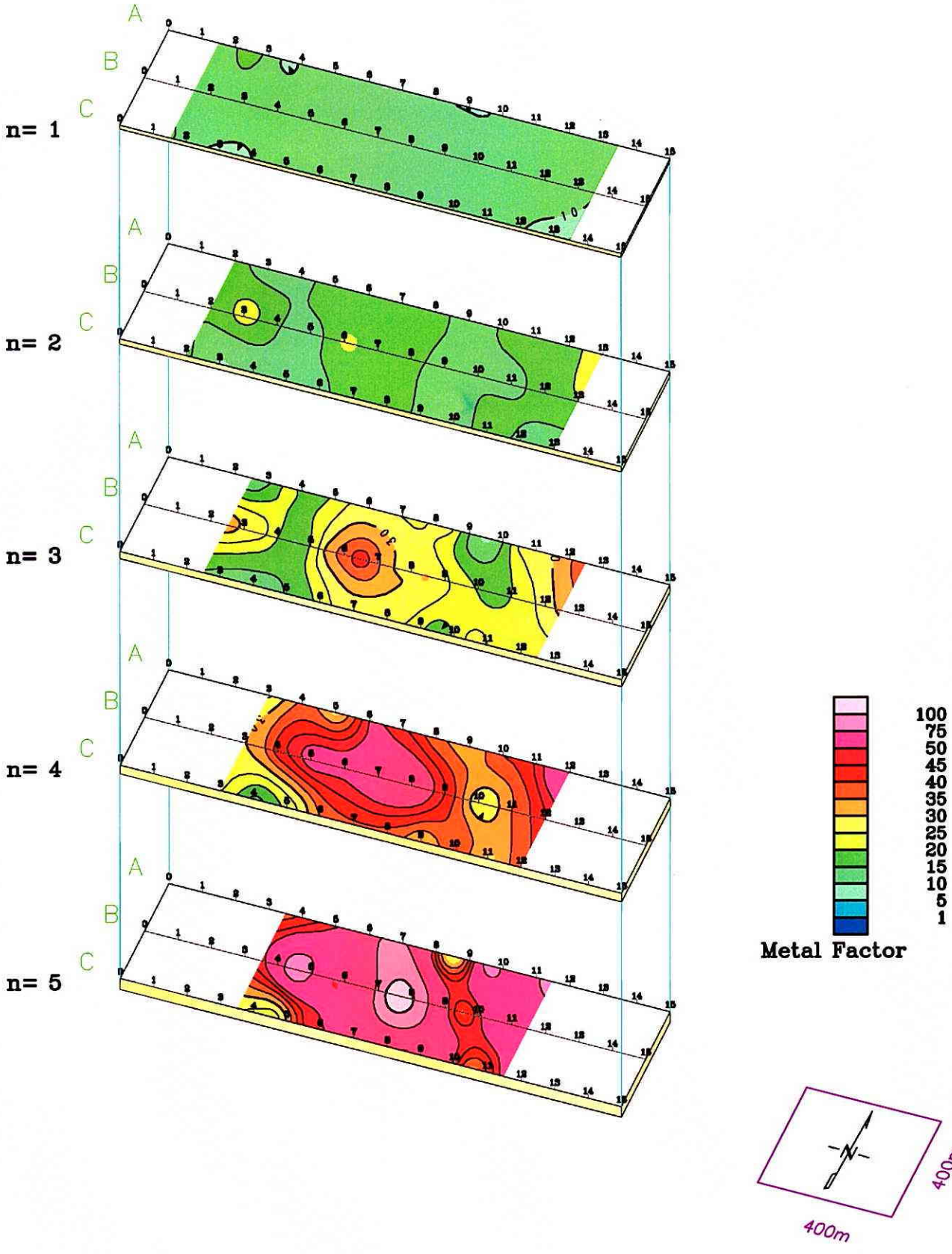

Fig.II-2-1-36 Plane map of metal factor (MJTK-IP-7)

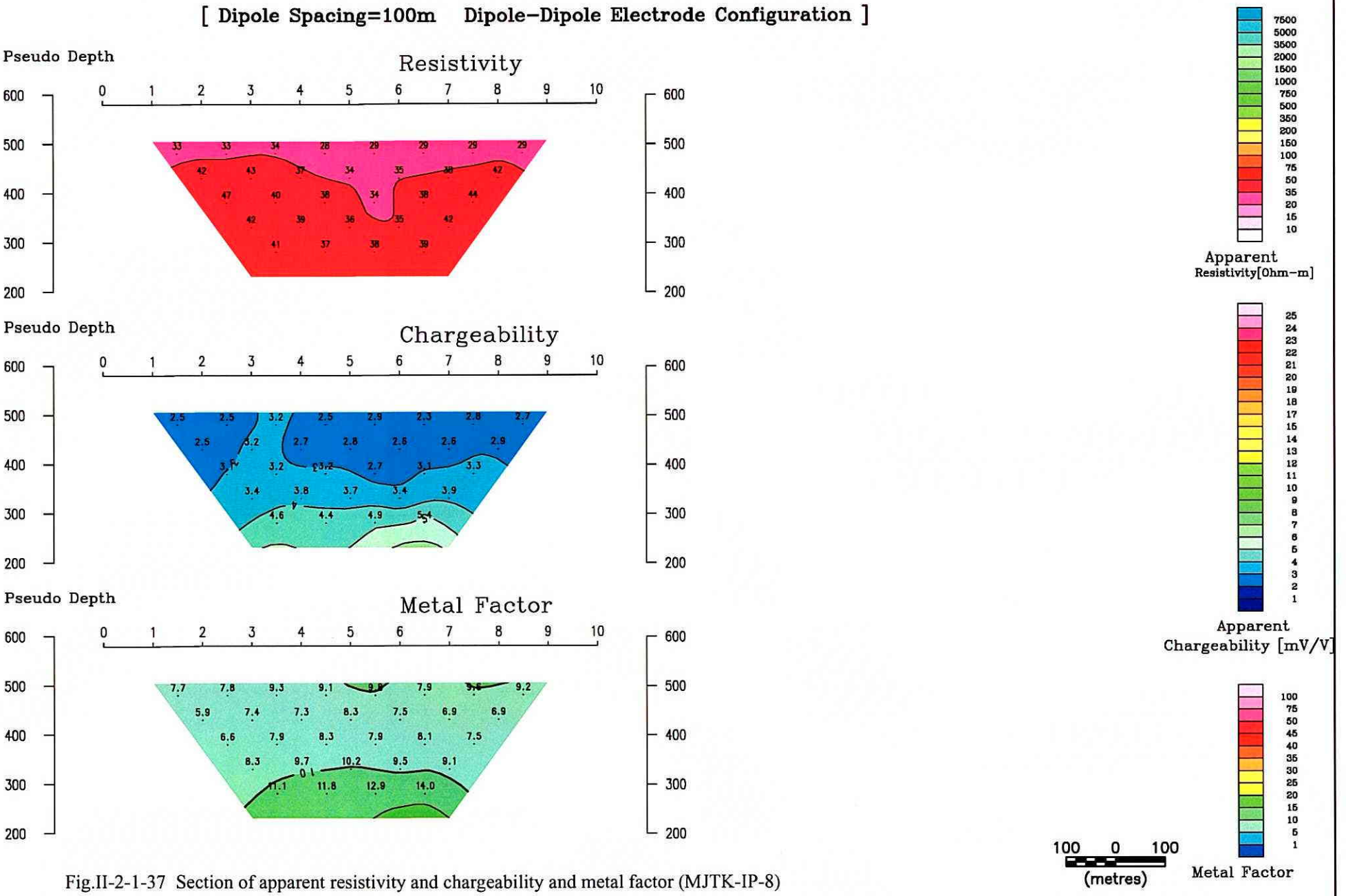

Fig.II-2-1-37 Section of apparent resistivity and chargeability and metal factor (MJTK-IP-8)

2-1-5-2 Result of Analysis

In the analysis, deep parts of both ends of the survey lines, in some places, have been analyzed as low or high resistivity and chargeability anomalies due to being presented in the same analyzing widths for both shallow and deep parts by using the expansion model. The reason of that is to have set some block structure for non-data parts, and those parts have been analyzed, in some cases, as extremely high values. In such case, it is better to neglect the data within around 300 meters from the ends of the survey lines at the highest analyzable depth.

1) MJTK-IP-1

Figures II-2-1-38 to II-2-1-40 show the cross sections of the analyzed resistivity, chargeability, and metal factor, and Figures II-2-1-41 to II-2-1-43 show the planes.

The analyzed resistivity in the district ranges 10 to 900 Ω· m. The resistivity shows low in shallow part, and wide swelled resistivity zones in deep parts around No.8 of the survey lines F, A, B, C, and D. In the last year's airborne magnetic survey, three airborne magnetic anomalies were detected at No.1 and No.8 of the survey line C, and No.14 of the survey line D. The above mentioned analyzed resistivity anomaly is corresponded with the airborne magnetic anomaly found at the No.8 of the Line C. The shallow part up to 120 meters is of low resistivity, below 50 Ω· m. It is thought that a low resistivity zone, about 15 Ω· m, spreads as a layer around the depth of 70 meters. This presumably is of silt or argillaceous layer containing a small-amount of pebble. It is presumed that these low resistivity zones are due to the young sediment, which extends to the east and north as a thick layer.

The chargeability is analyzed as37 mV/V in the highest. The chargeability is generally low, but slightly high and continuous in the deeper parts. It is analyzed extending north to south. Two zones, No.5 and No.14 of the lines E, A, B, have been analyzed as to high chargeability. The chargeability zone around No.14 on the east side corresponds to the low resistivity zone, below 75 Ω· m, and the slightly high chargeable zone on the west side, around No.5 of the lines A, B, and C, responds to the high resistivity zone of over 100 Ω· m.

In the metal factor, a relatively high value is detected horizontally in the deep, 70 to 90 meters. A vertical high value zone exists around No.11 to No.14 of the survey lines E, A, B, and C. This is corresponded with the low resistivity and slightly high chargeability zone, but it is not clear whether this indicates some ore minerals or not.

It is expected that the young sediments thickly and broadly deposit, judging from the airborne electromagnetic survey result. This is well coincident with the result of the resistivity structure analysis.

2) MJTK-IP-2

Figures II-2-1-44 to II-2-1-46 show the cross sections of the analyzed resistivity, chargeability, and metal factor, and Figures II-2-1-47 to II-2-1-49 show the planes.

The analyzed resistivity ranges 10 to 1,000 Ω· m. The resistivity distribution in the shallow part is characterized by a swelled high resistivity zone, highest over 100 Ω· m in at No.10 of the survey line B, surrounded by a low resistivity zone, below 100 Ω· m. The low resistivity zone is getting thicker from the summit. The deep part underneath the summit is of low resistivity, below 100 Ω· m.

The summit area is underlain by andesite, surrounded by calcareous siltstone, and the young sediments on the foot. It is thought that the resistivity of the young sediments is below 50 Ω· m. The low resistivity zone of the deep part underneath the summit possibly reflects cracked siltstone. The deep part of the summit and surrounding area, and the deep part on the northern side are in a high resistivity zone, over 500 Ω· m, suggesting deeper existence of andesite.

The high chargeability on the summit area is possibly correlated to the andesite, extending to the deeper north.

The metal factor is generally low, and no anomaly exists. The relatively high metal factor zone at No.10 to No.11 is in a low chargeability and low resistivity zone, therefore, this is not favorable zone for further exploration activity.

The airborne electromagnetic survey result tell us thicker anomaly at the ends of the survey lines as well as those of the resistivity structure sections.

In the airborne magnetic survey result, a weak anomaly exists at the summit area at No.10 of the survey line B. This is slightly higher in the shallow part, and correlated to the higher chargeability anomaly zone in the deep part and northern deep part, suggesting existing of some igneous body containing magnetic minerals.

3) MJTK-IP-3

The district is situated about one kilometer southeast of above-mentioned summit in MJTK-IP-2.

Figures II-2-1-50 to 52 show the cross sections of the analyzed resistivity, chargeability ., and metal factor, and Figures II-2-1-53 to 55 show the planes.

The airborne magnetic anomaly is seen at the cross point of the survey lines B and C.

The resistivity distribution is characterized by a dome-shape high-resistivity zone, 100 to 350 Ω· m, surrounded by a low resistivity zone, below 50 Ω· m. This pattern is situated in the central district at 70 meters depth.

The chargeability is corresponded with the dome-shape resistivity zone, showing lower than that of the surrounding area.

The metal factor is slightly higher corresponding with the low resistivity zone representing the young sediments, but anomalous.

The airborne magnetic anomaly is well corresponded with the analyzed dome-shape low resistivity zone, therefore it well reflect the rock facies of high magnetic and low IP effect.

4) MJTK-IP-4

Figure II-2-1-56 shows the cross section of the analyzed resistivity, chargeability, and metal factor.

The airborne magnetic survey result shows a widespread anomalous zone here. Also the airborne electromagnetic survey indicates a highly conductive anomaly here.

The resistivity is generally below 50 Ω· m, reflecting the young sediments.

The chargeability is about 10mV/V, and no anomaly is recognized.

It is thought that the airborne magnetic anomaly reflects some deep buried igneous bodies due to no existence of resistivity and chargeability anomaly.

The analyzed resistivity and chargeability show higher on the west side deep part, but this is caused by the analytical end effect.

5) MJTK-IP-5

Figure II-2-1-57 shows the cross section of the analyzed resistivity, chargeability, and metal factor.

The airborne magnetic survey result shows about 3 kilometers long and extending north to south anomaly.

The resistivity shows about 200 Ω· m down to the depth of 40 meters, and 20 to 50 Ω· m below it. It is judged that this low resistivity zone is generally due to the young sediments, and some high resistivity zones in the shallow part are due to some gravel layers.

The chargeability tends to shoe slightly higher near the surface, but generally low.

6) MJTK-IP-6

Figures II-2-1-58 to II-2-1-60 show the analyzed resistivity, chargeability, and metal factor, and Figures II-2-1-61 to II-2-1-63 show the planes.

The airborne magnetic survey result shows a weak anomaly near the central part of the survey line C.

The resistivity shows a slightly high anomaly in the central deep part of the survey line B, but the other area is generally low resistivity zone, below 50 Ω· m.

The chargeability tends to show a slightly high below the depth of 150 meters, and no anomalous zone has detected.

The metal factor shows a locally high zone in the deep part of No.8 and No.9 of the survey line B, but this is due to a low resistivity zone, below 10 Ω· m. The deep part of the western side of the line shows higher, but this is due to the analytical end effect.

It is thought that the weak airborne magnetic anomaly reflects Paleozoic rocks, corresponding with a high resistivity, over 100 Ω· m, and in deeper high chargeability zone at the central part of the survey line B.

7) MJTK-IP-7

Figures II-2-1-58 to II-2-1-60 show the cross sections of the analyzed resistivity, chargeability, and metal factor, and Figures II-2-1-61 to II-2-1-63 show the planes.

The airborne electromagnetic survey result shows generally high conductivity zone.

The resistivity becomes generally low to the deeper, about 10 Ω· m.

The chargeability tends to be higher to the deeper, corresponding with low resistivity, indicating Paleozoic rocks.

This district does not show any change in the resistivity structure, therefore, the depth of the Paleozoic is unclear.

The metal factor shows little higher in the deeper, but this is due to low resistivity, about 10 mV/V.

8) MJTK-IP-8

The airborne electromagnetic survey result shows a high conductive anomaly in this district.

The resistivity and chargeability reflect some stratigraphic structure. The resistivity shows 70 Ω· m at the highest, and the chargeability shows 6mV/V at the highest. No anomaly exists in both.

It is thought that the high conductive anomaly reflects some underground buried material.

Table II-2-1-5 shows the summary of the IP survey

Table II-2-1-5 Result of the IP survey

Survey District	Characteristic of Survey Result
MJTK-IP-1	Resistivity: 10 to 900 Ω· m Chargeability: Highest 360mV/V Below 50 Ω· m low resistivity down to 120m Widespread low resistivity, about 15 Ω· m, around depth of 70m. Presumably pebble-poor silt or argillaceous layer.

MJTK-IP-1	Deep part: swelled resistivity structure, over 100 Ω· m, in No.8 of lines F, A, B, C, D Chargeability: Highest 37mV/V. Two slightly high chargeability zones in deep part, elongating N-S. Through No.5 and No.13 of lines E, A, B, C. Around No.14 corresponds to low resistivity zone. Three Airborne Magnetic Anomaly: High resistivity and low chargeability zone in analyzed depth 147m and 0m.
MJTK-IP-2	Resistivity: 10 to 1,000 Ω· m Chargeability: Highest 37mV/V Hill-shape high resistivity distribution zone, over 100 Ω· m, centering No.10 of Line B, surrounded by low resistivity zone, below 100 Ω· m . Low resistivity zone of young sediments get thicker from summit as same as airborne EM result. Deep part underneath summit: Low resistivity zone below 100 Ω· m. Summit: Andesite, Surrounding: Calcareous silt ? Summit, surrounding, northern deep part: High resistivity zone, over 500 Ω· m. Andesite ?
MJTK-IP-3	Resistivity: 10 to 360 Ω· m Chargeability: Highest 11mV/V Airborne magnetic anomaly: Cross point of Line B and C Resistivity distribution: Dome-shape high resistivity zone, 100 to 350 Ω· m, in low resistivity zone, below 50 Ω· m. Central part below 70m depth Airborne magnetic anomaly: Reflect high resistivity and low IP effect rocks ?
MJTK-IP-4	Resistivity: 13 to 65 Ω· m Chargeability: Highest 16mV/V. No anomaly Generally reflect young sediments.
MJTK-IP-5	Resistivity: 24 to 310 Ω· m Chargeability: Highest 11mV/M High resistivity zone relating to gravel layer: 200 Ω· m down to 40m depth. Low resistivity zone, 20 to 50 Ω· m in deep. Generally reflect younger sediments. chargeability: Slightly higher in high resistivity zone near surface. No anomaly

MJTK-IP-6	Resistivity: 20 to 300 Ω· m. Chargeability: Highest 20mV/V. Resistivity: Generally low resistivity zone, below 50 Ω· m. Chargeability: Slightly higher below depth 150m. No anomaly. Airborne magnetic anomaly: Weak. Reflect deep sitting Paleozoic rocks ?
MJTK-IP-7	Resistivity: 4 to 80 Ω· m. Chargeability: Highest 20mV/V. Resistivity: about 10 Ω· m at deep. Chargeability: Slightly higher at deep. Reflect Paleozoic rocks ? Thickness of younger sediments: Not clear. Chargeability: No anomaly.
MJTK-IP-8	Resistivity: 16 to 70 Ω· m. Chargeability: Highest 6mV/V. Resistivity and Chargeability: Reflect stratigraphic structure of young sediments. No anomaly.

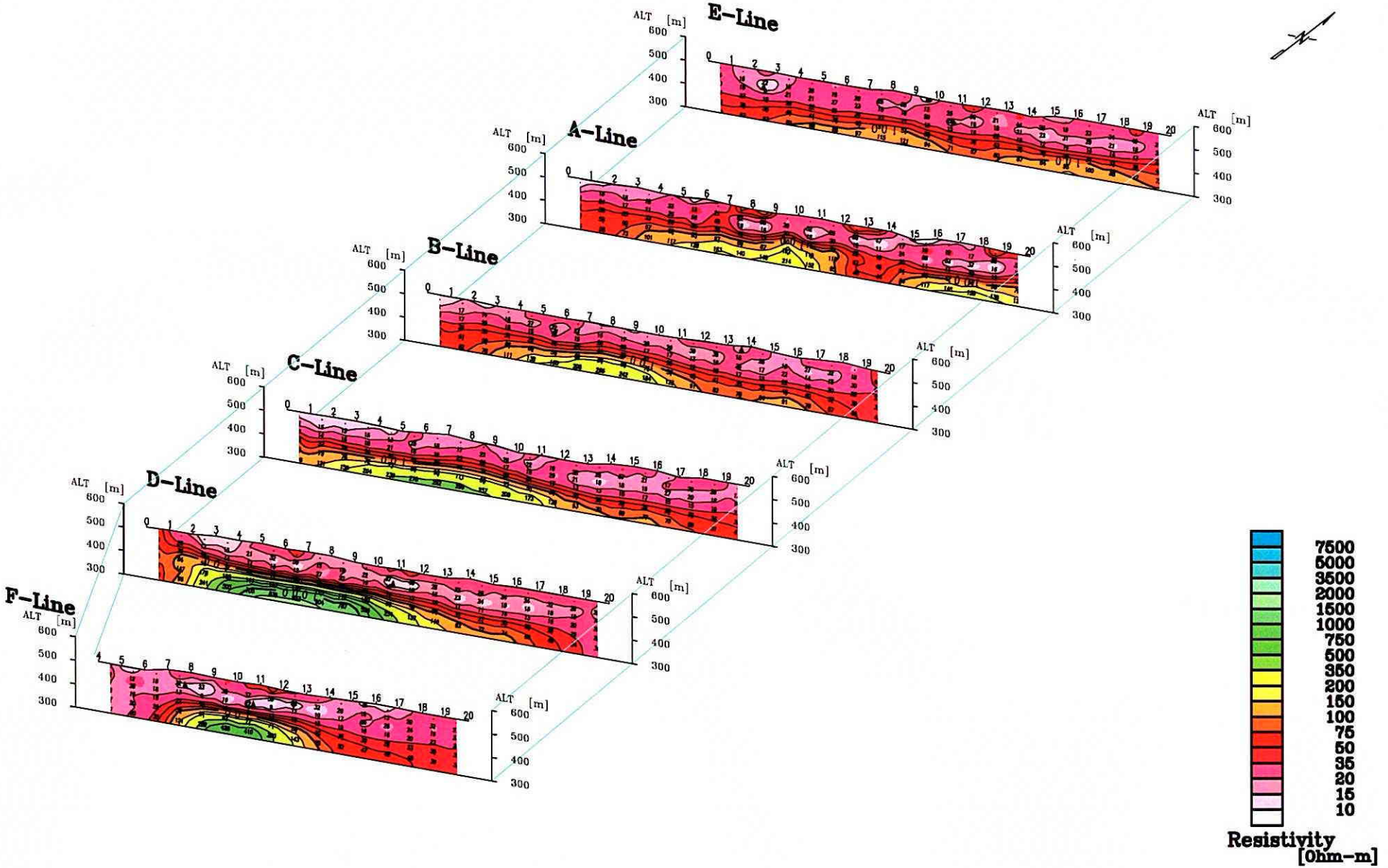

Fig.II-2-1-38 2D Analysis section of resistivity (MJTK-IP-1)

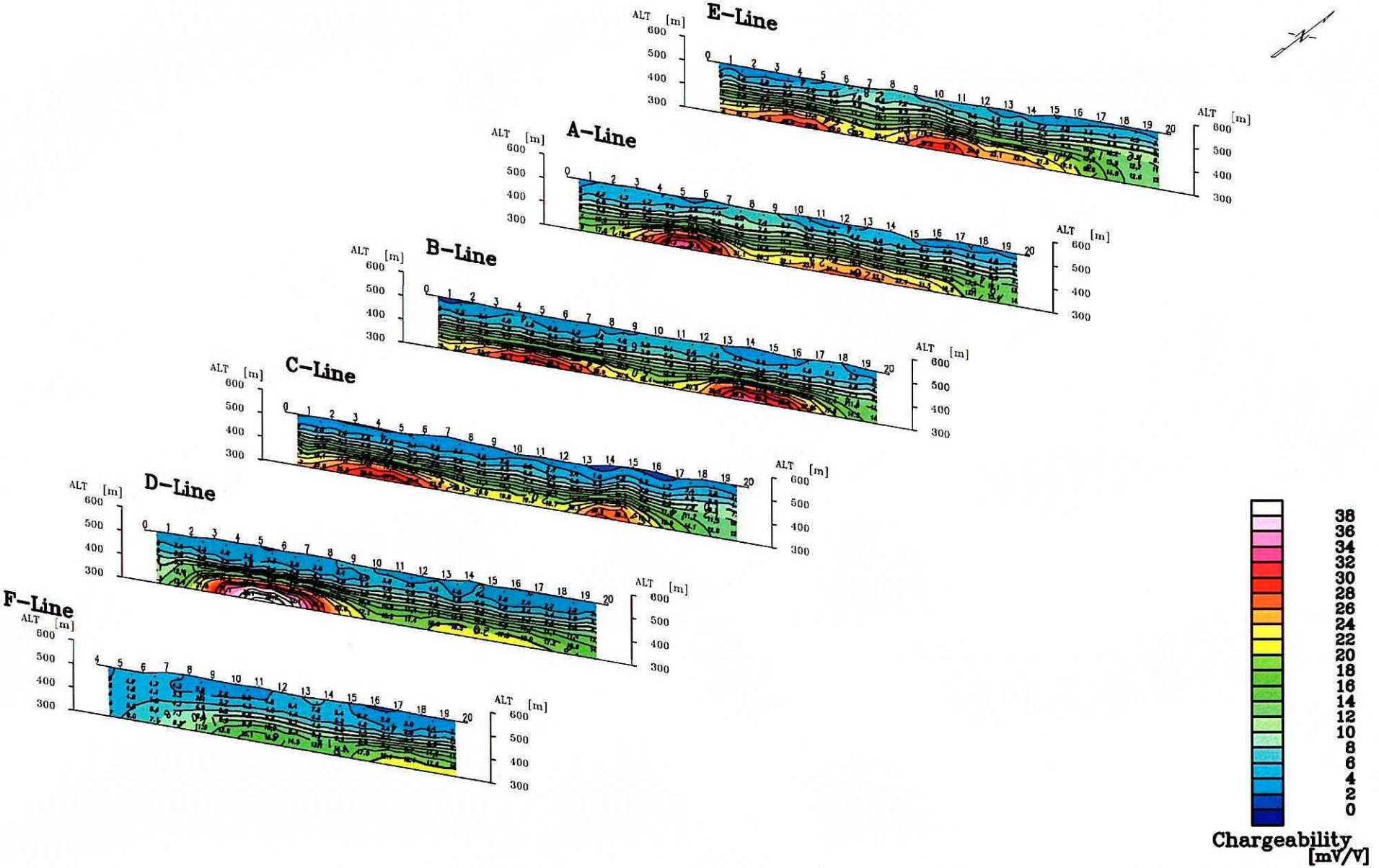

Fig.II-2-1-39 2D Analysis section of chargeability (MJTK-IP-1)

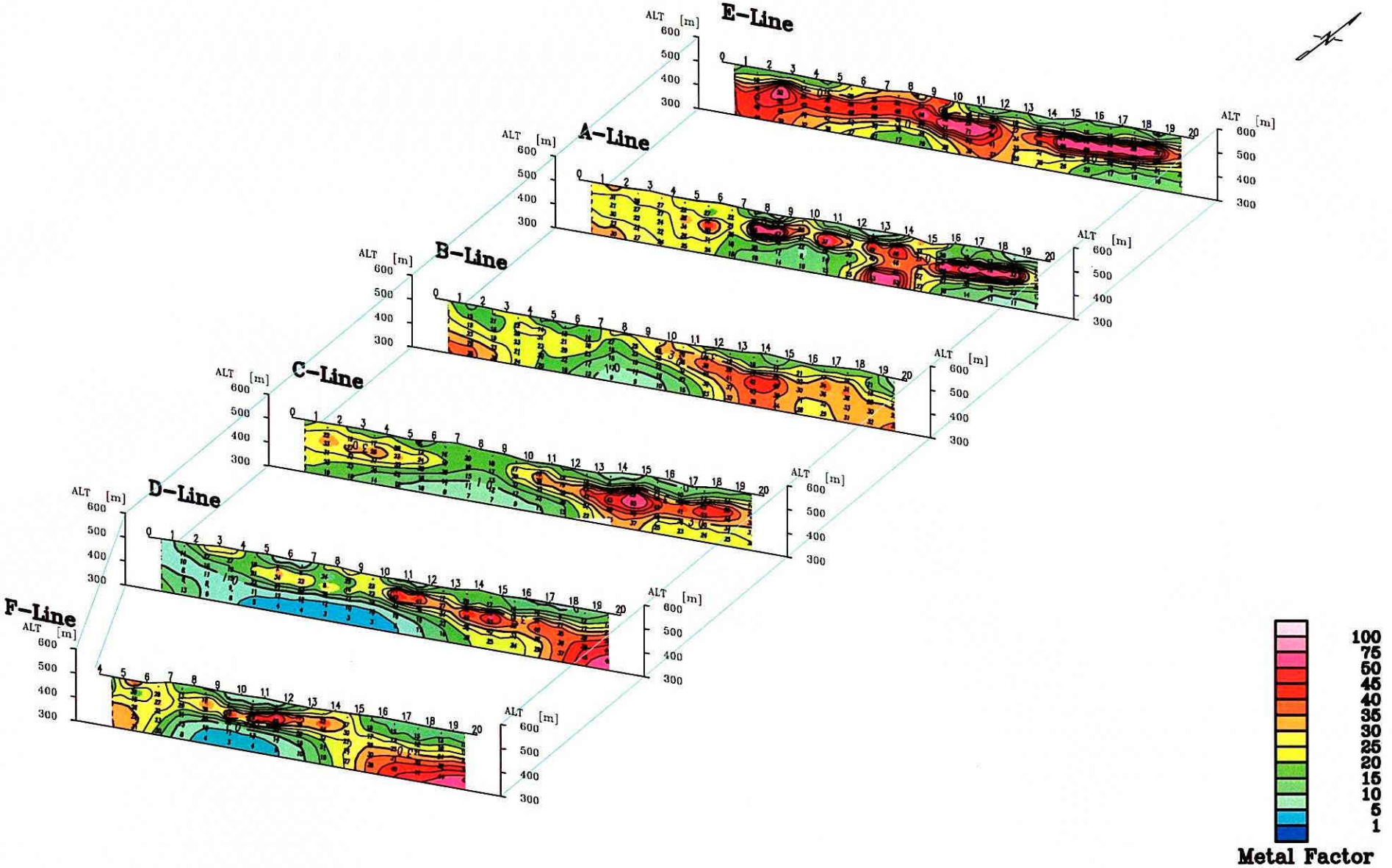

Fig.II-2-1-40 2D Analysis section of metal factor (MJTK-IP-1)

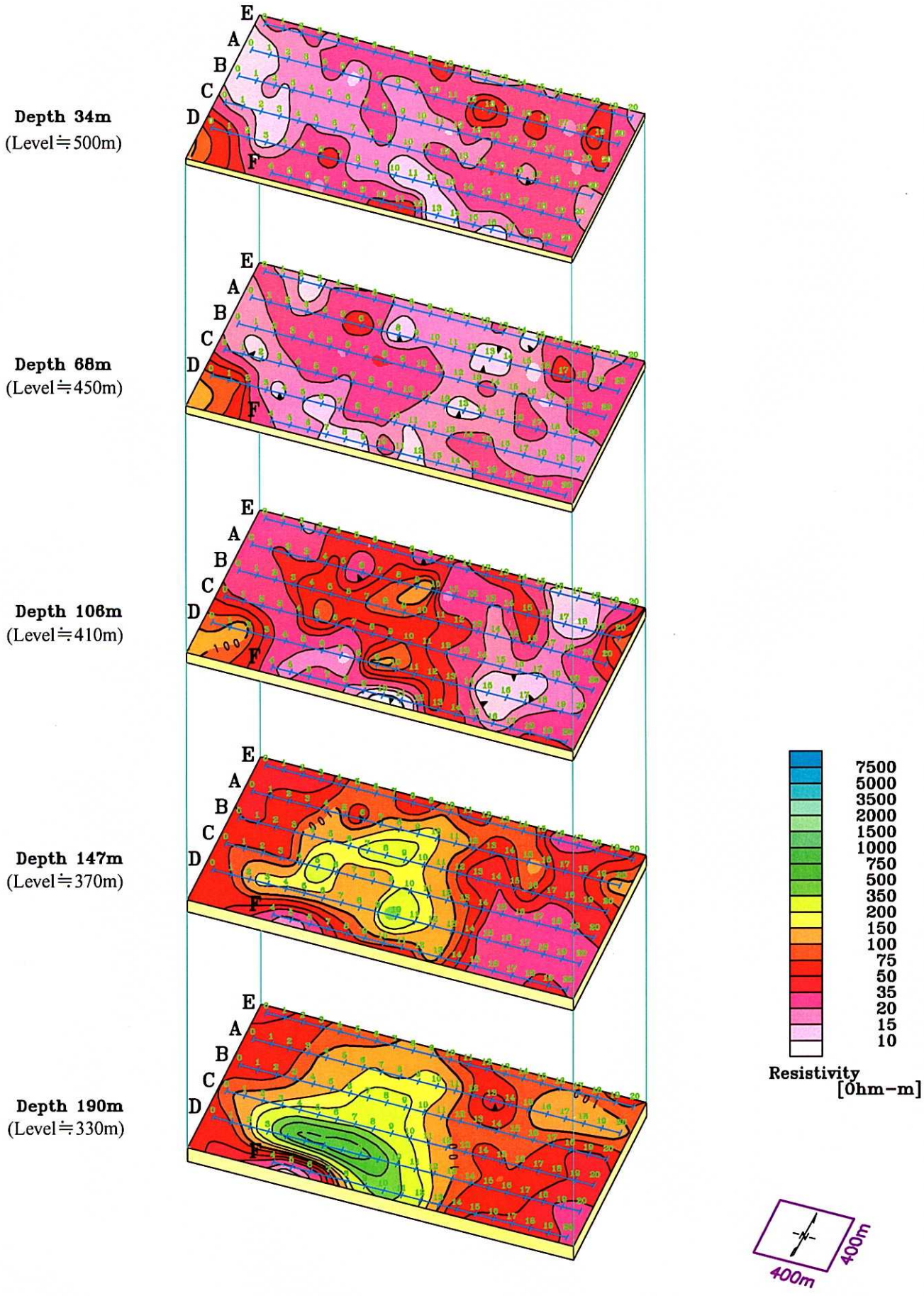

Fig.II-2-1-41 2D Analysis plane map of resistivity (MJTK-IP-1)

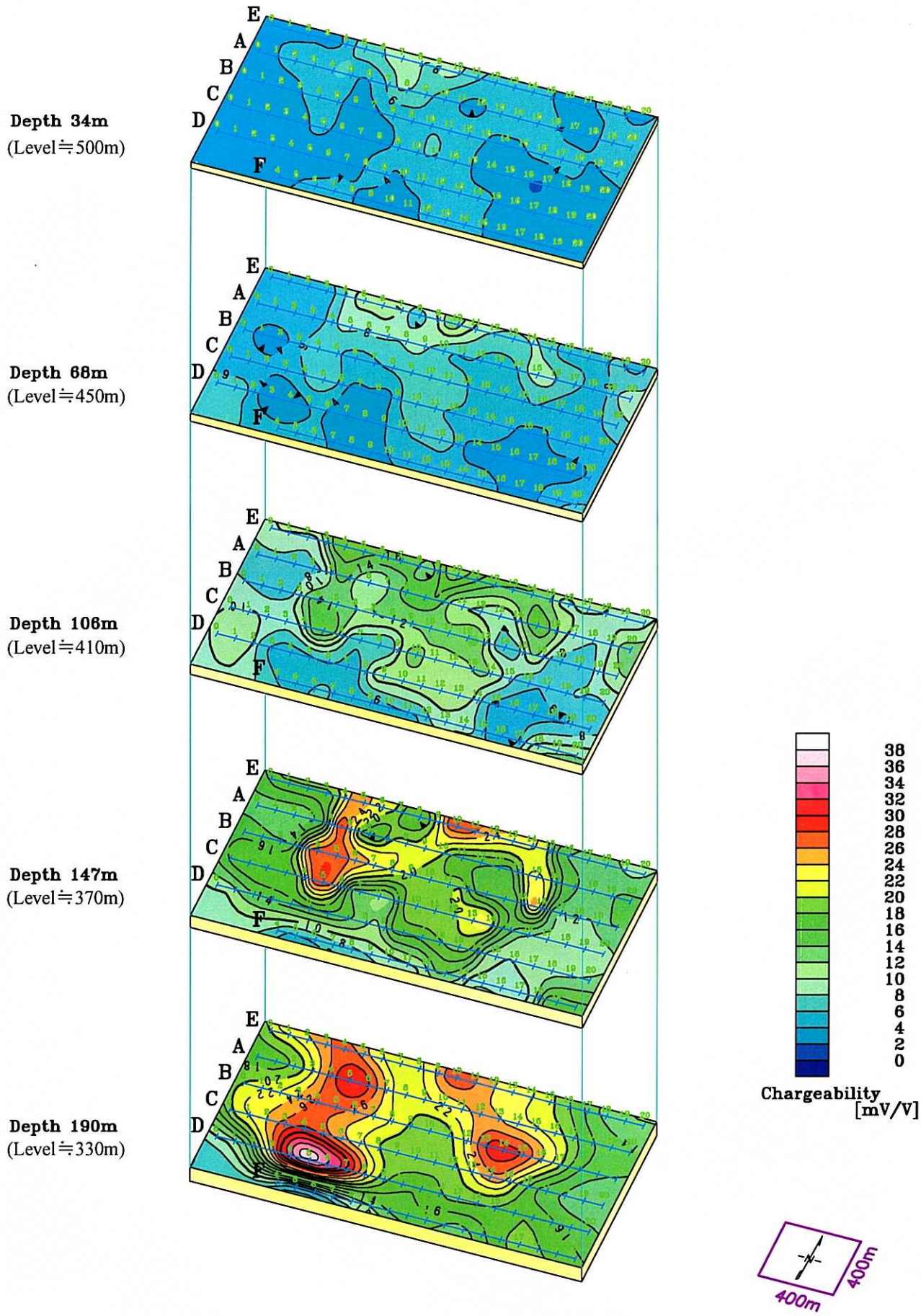

Fig.II-2-1-42 2D Analysis plane map of chargeability (MJTK-IP-1)

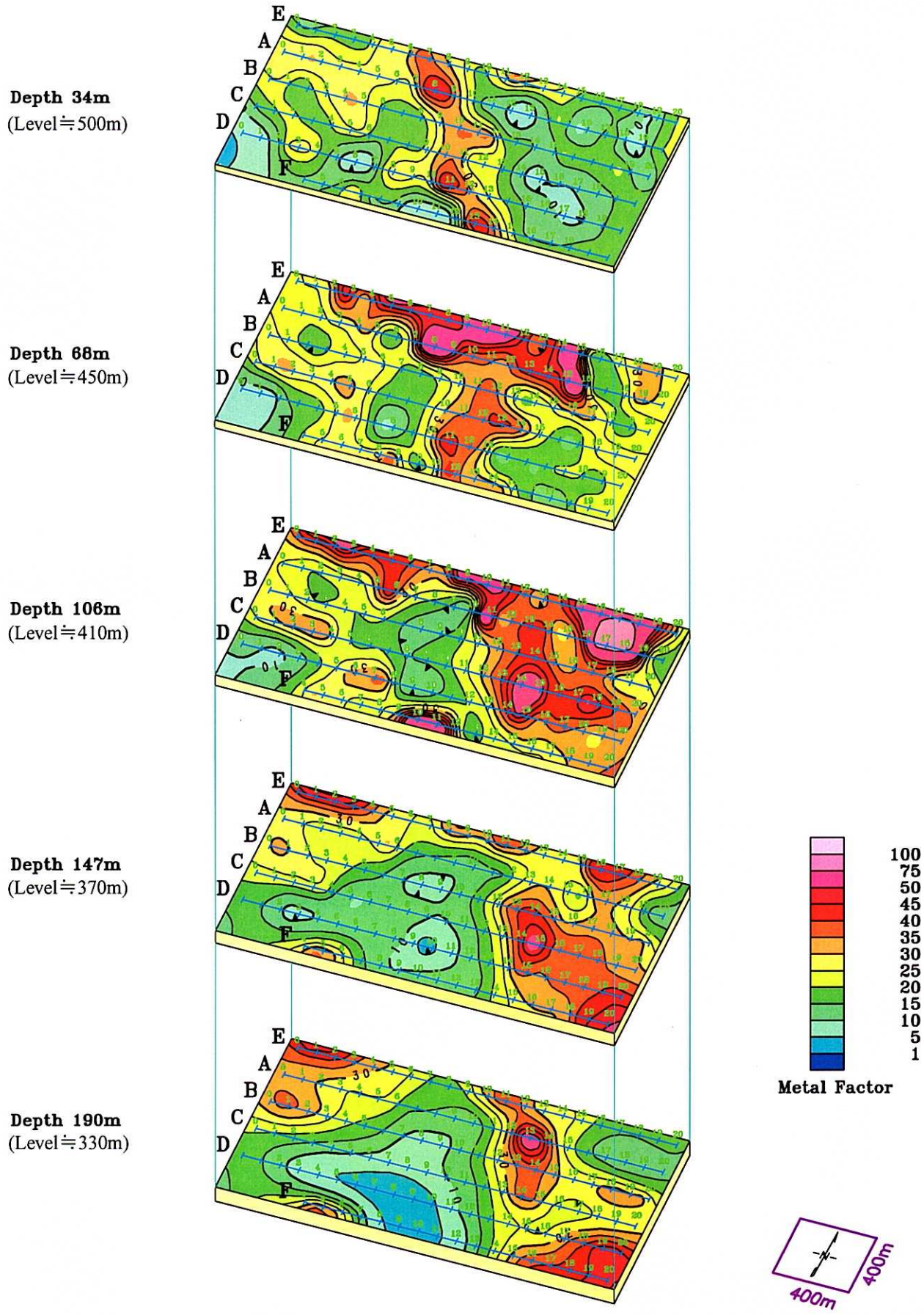

Fig.II-2-1-43 2D Analysis plane map of metal factor (MJTK-IP-1)

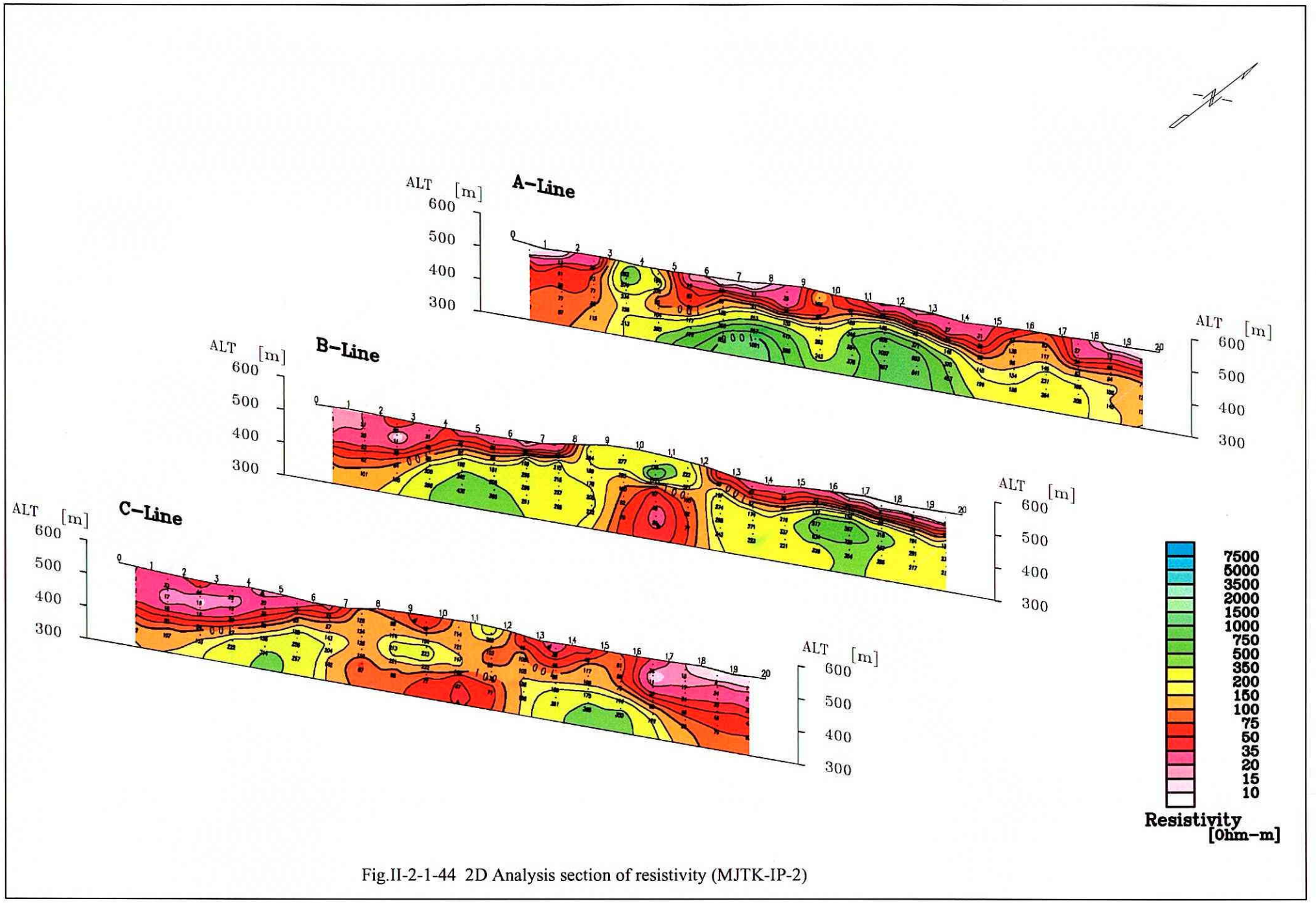

Fig.II-2-1-44 2D Analysis section of resistivity (MJTK-IP-2)

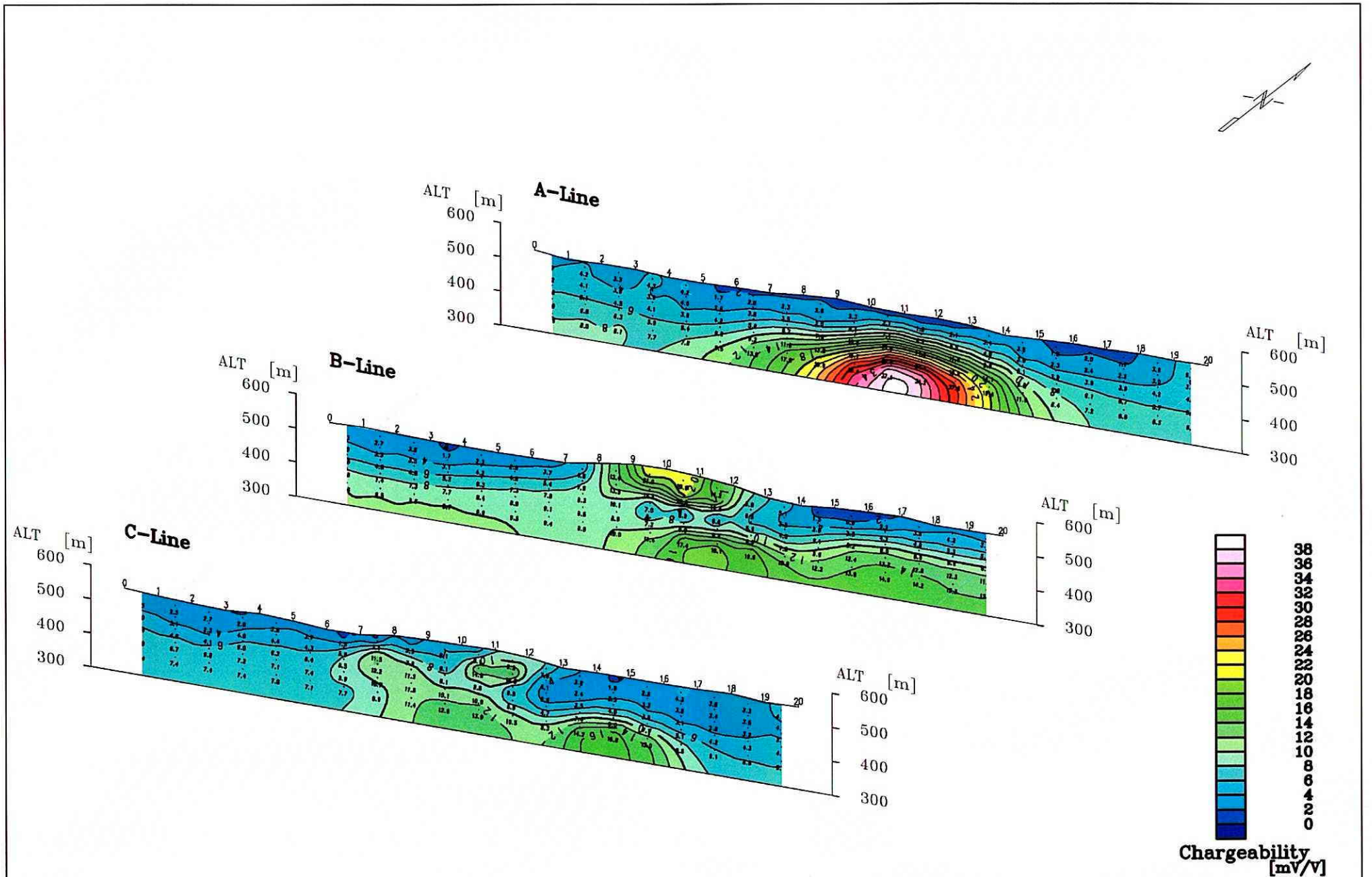

Fig.II-2-1-45 2D Analysis section of chargeability (MJTK-IP-2)

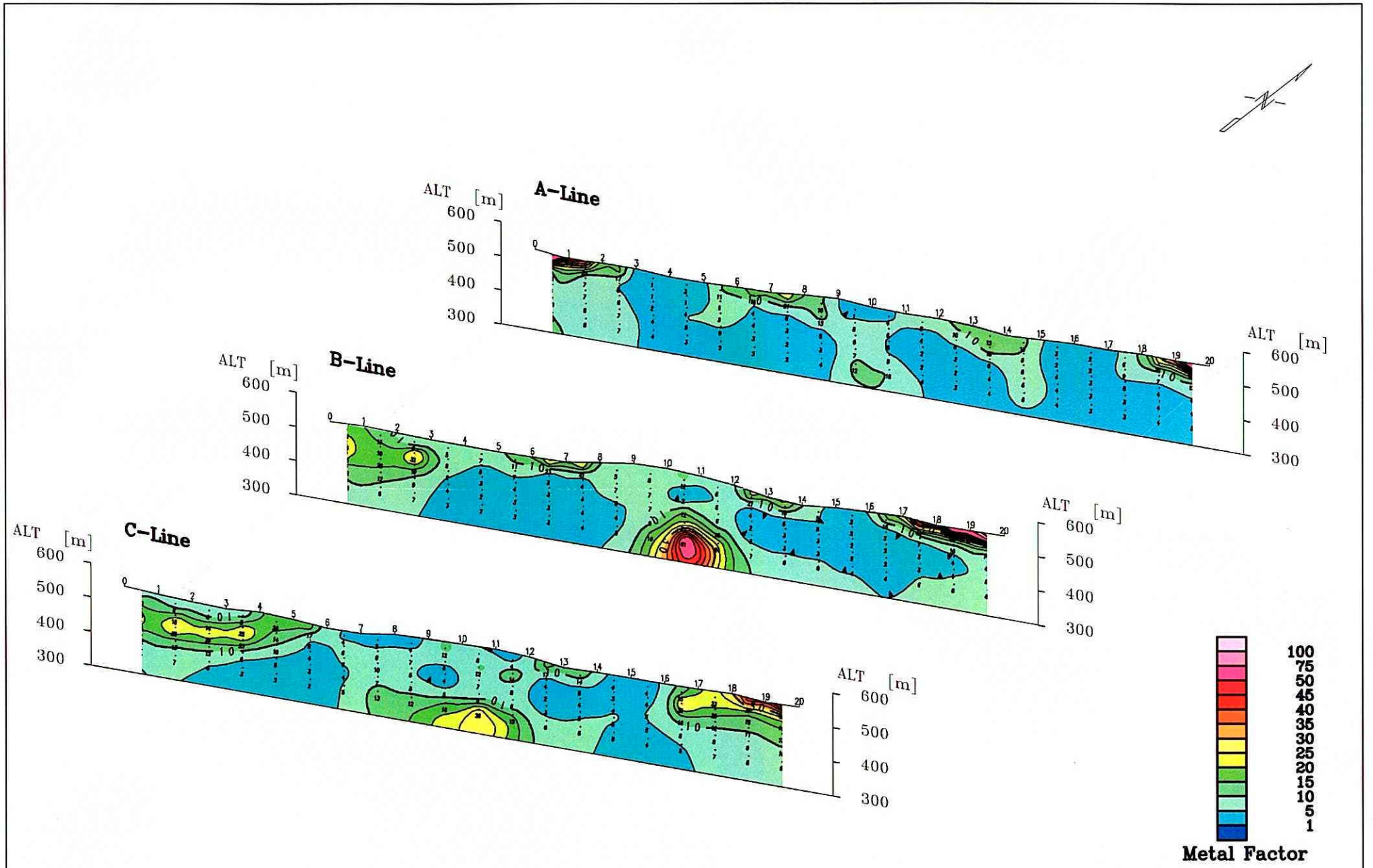

Fig.II-2-1-46 2D Analysis section of metal factor (MJTK-IP-2)

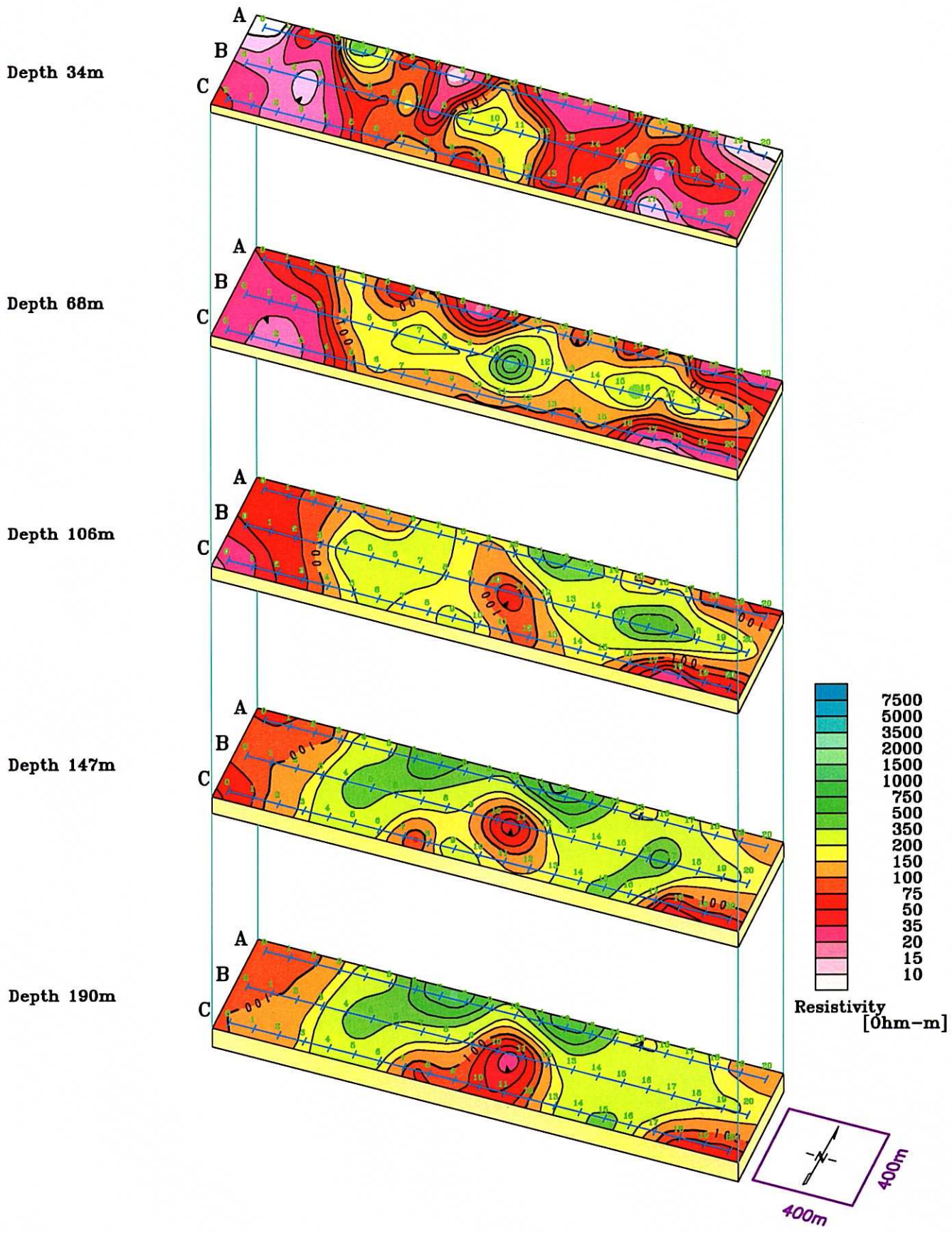

Fig.II-2-1-47 2D Analysis plane map of resistivity (MJTK-IP-2)

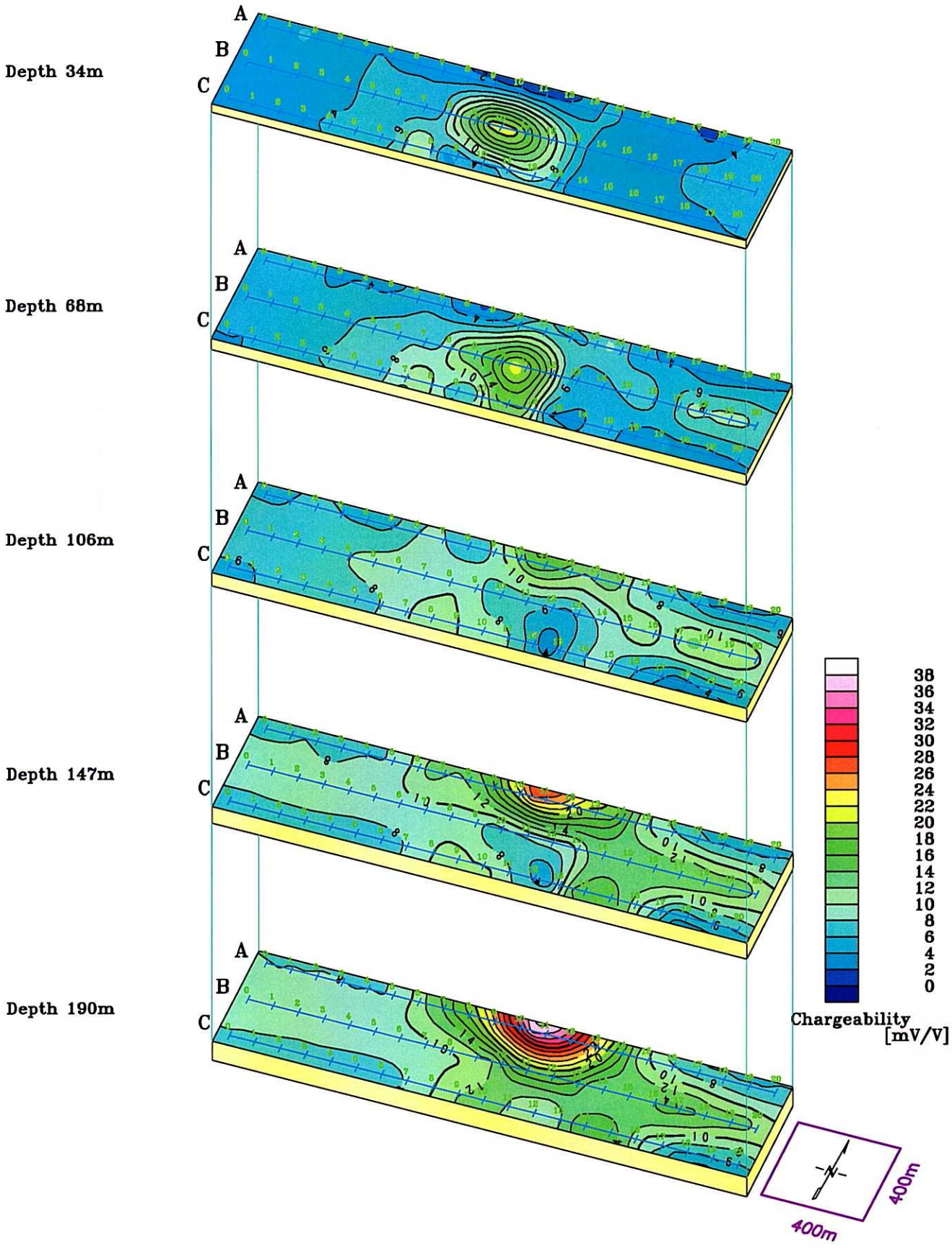

Fig.II-2-1-48 2D Analysis plane map of chargeability (MJTK-IP-2)

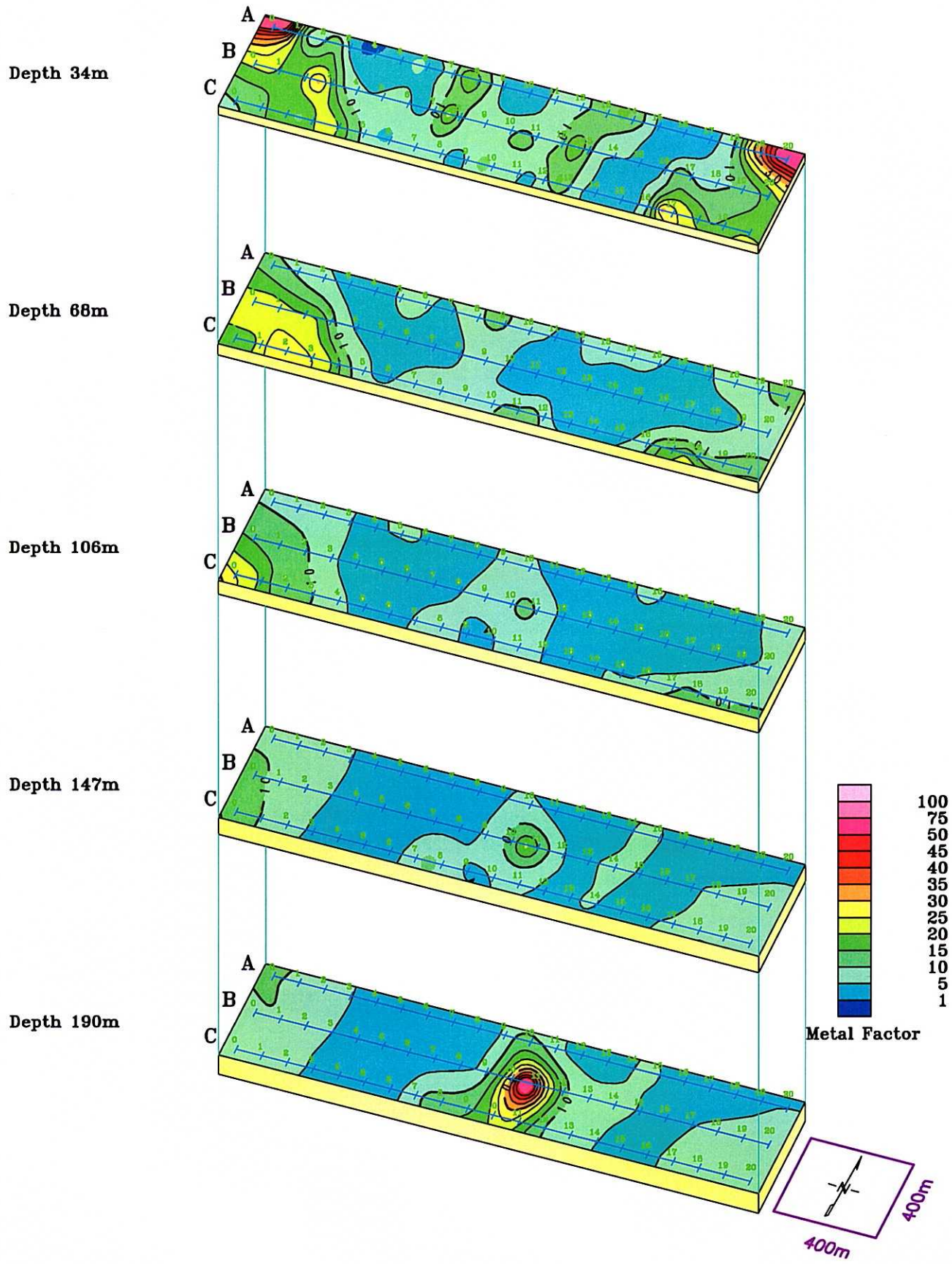

Fig.II-2-1-49 2D Analysis plane map of metal factor (MJTK-IP-2)

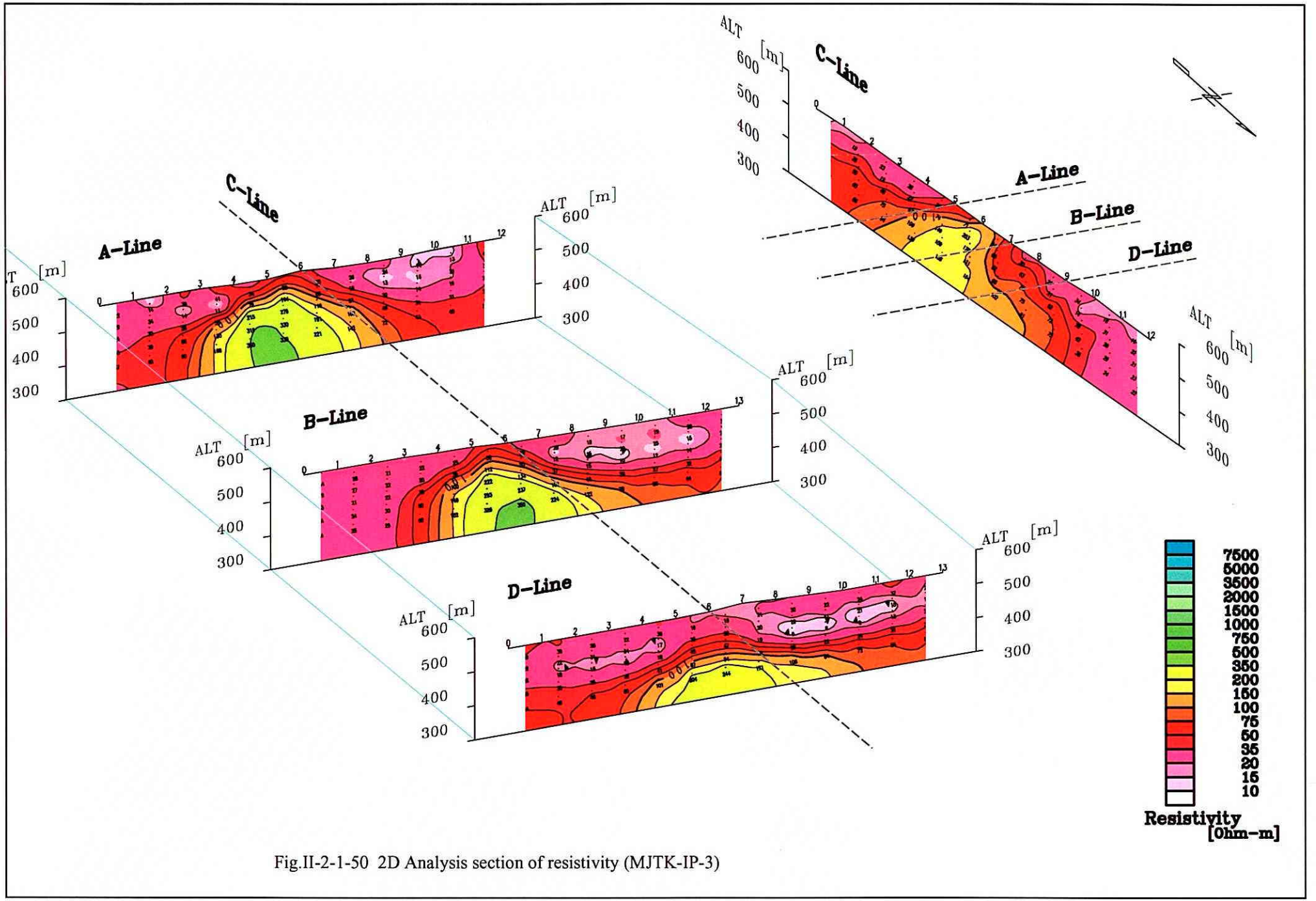

Fig.II-2-1-50 2D Analysis section of resistivity (MJTK-IP-3)

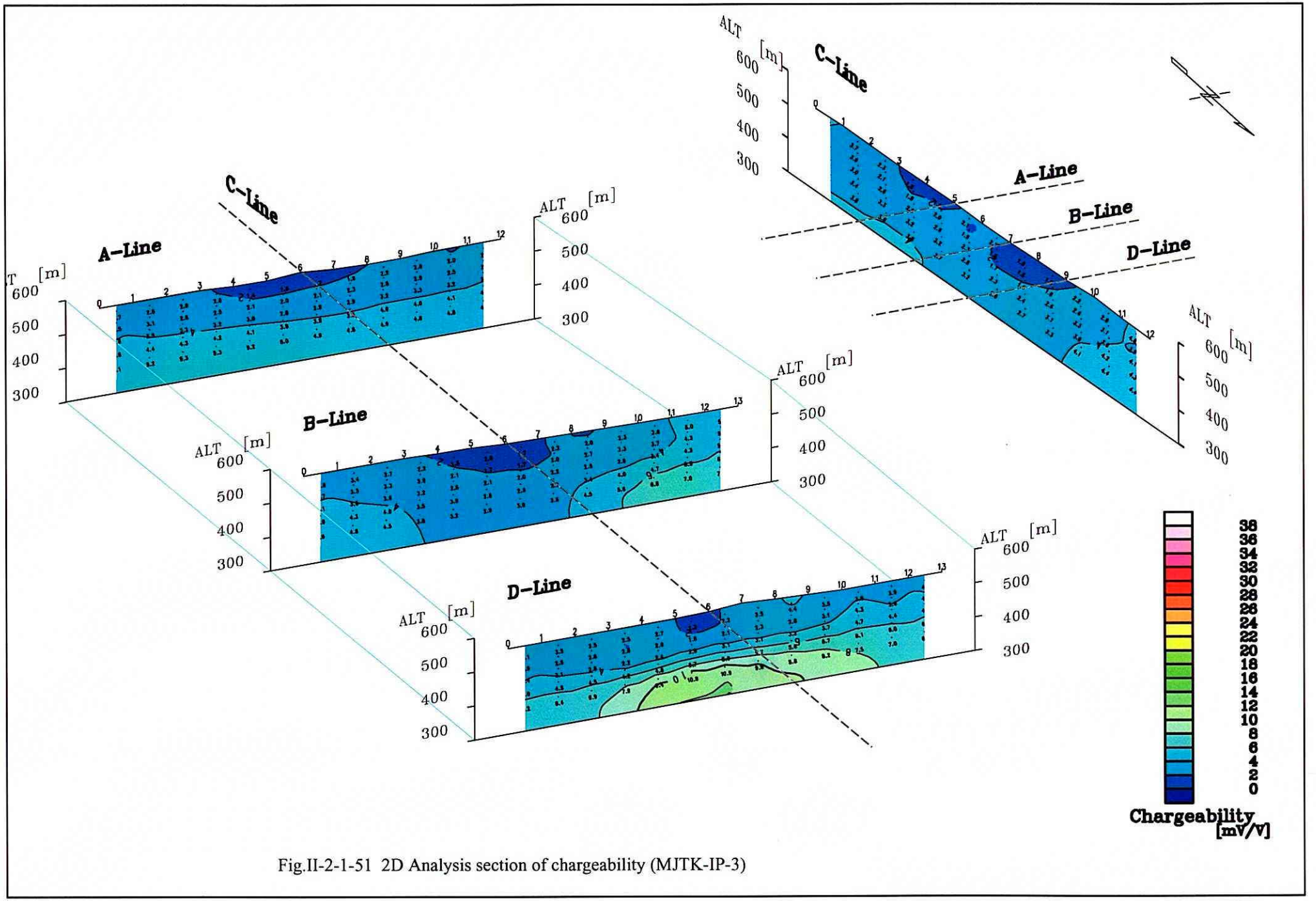

Fig.II-2-1-51 2D Analysis section of chargeability (MJTK-IP-3)

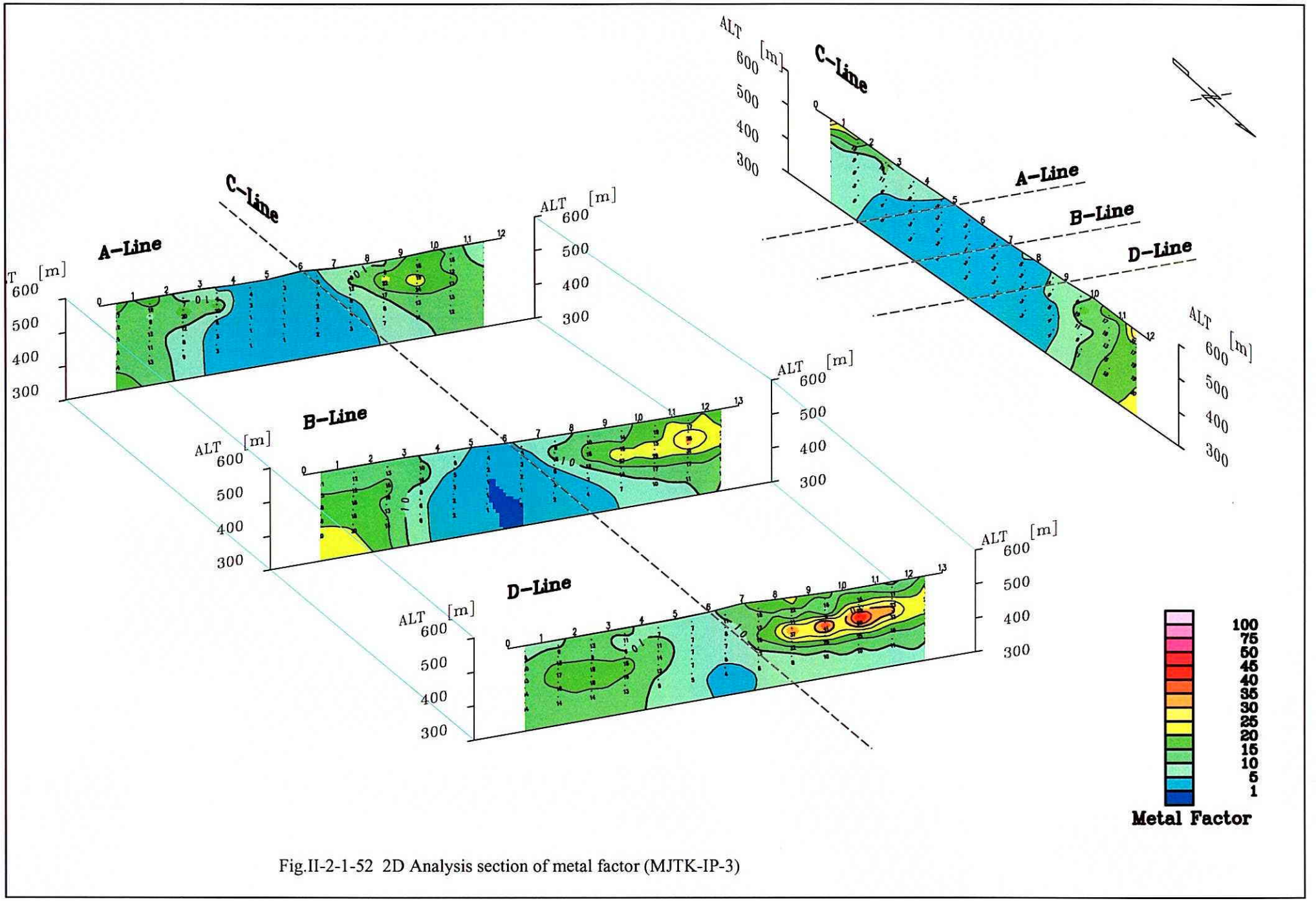

Fig.II-2-1-52 2D Analysis section of metal factor (MJTK-IP-3)

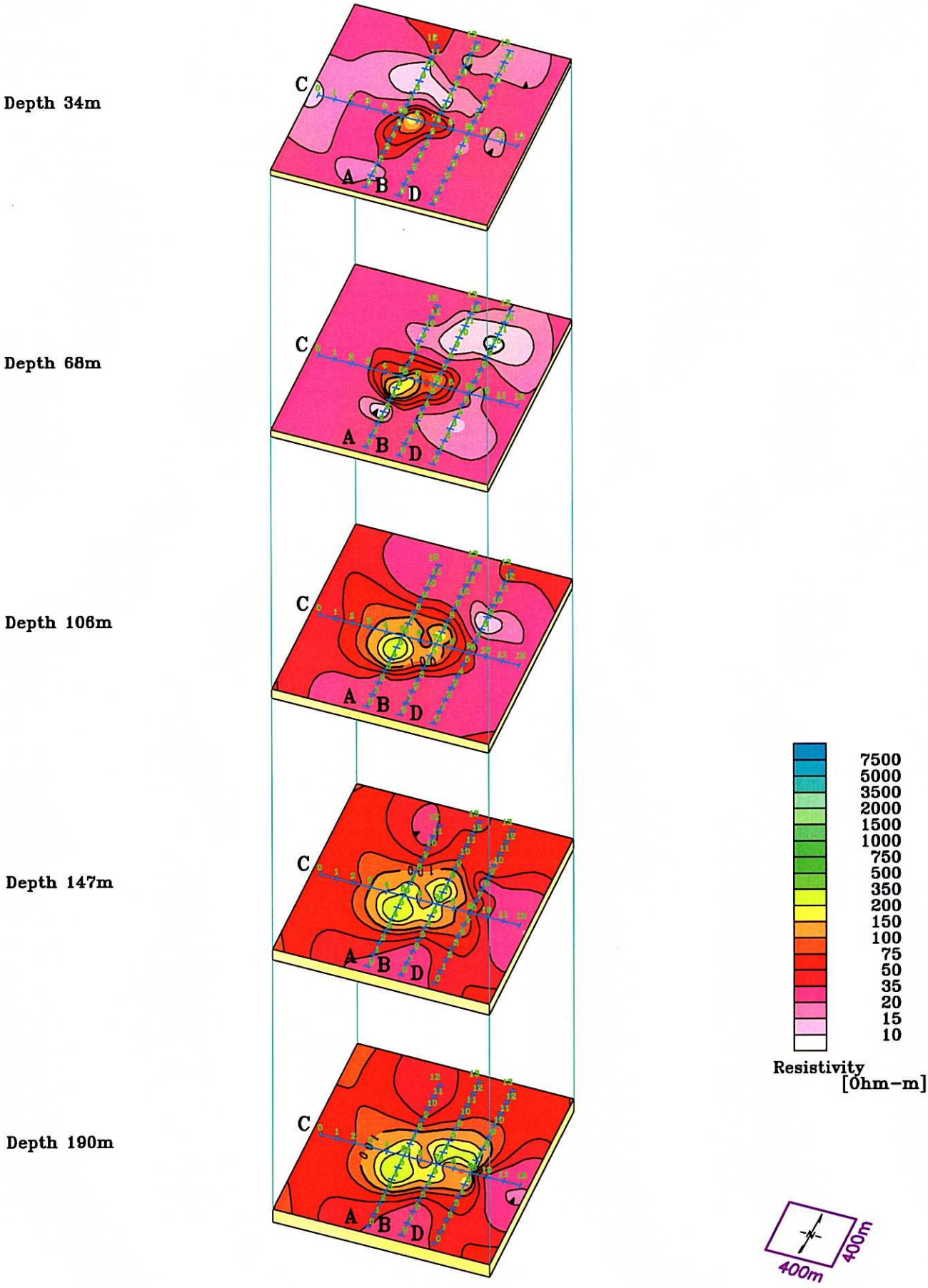

Fig.II-2-1-53 2D Analysis plane map of resistivity (MJTK-IP-3)

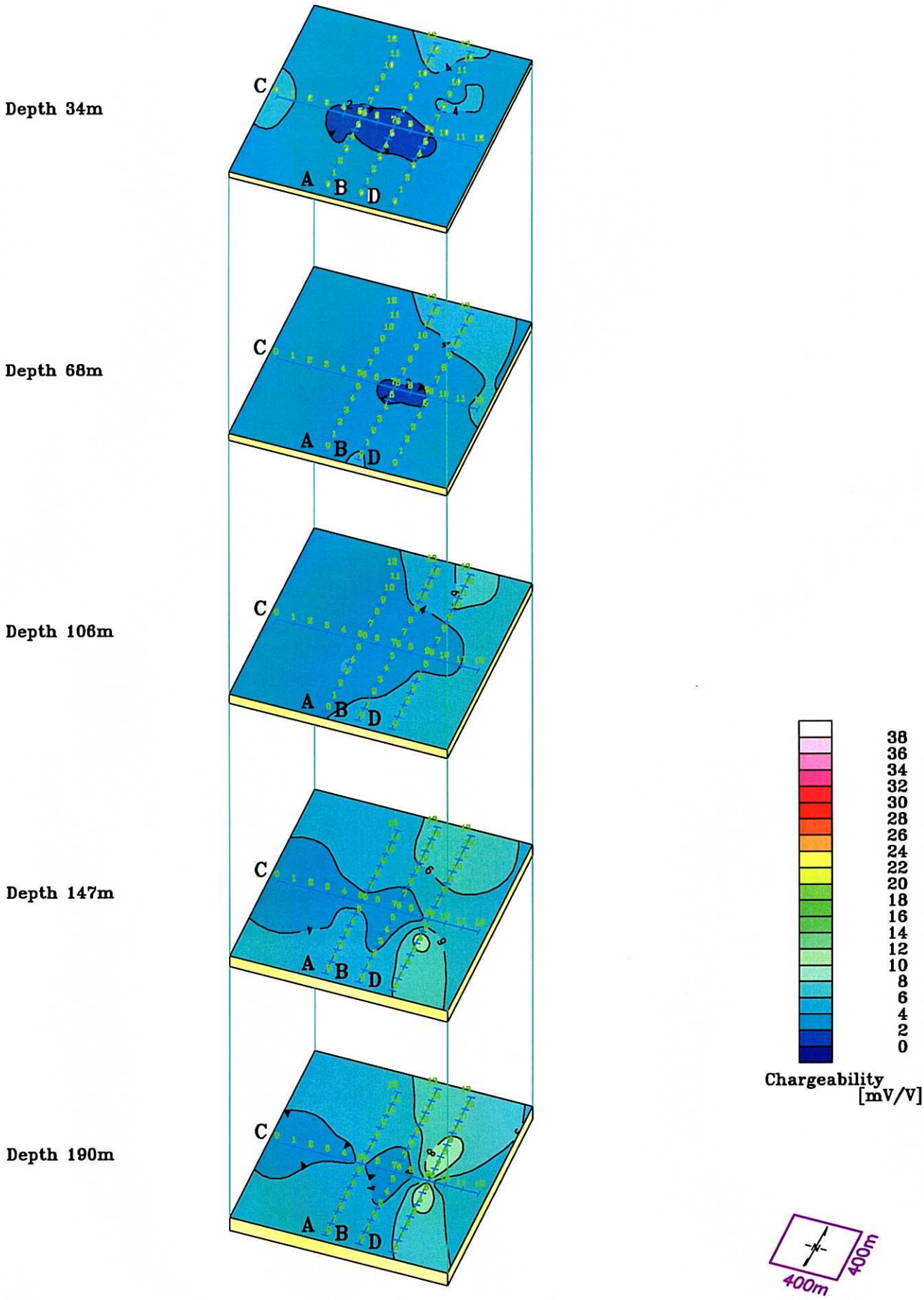

Fig.II-2-1-54 2D Analysis plane map of chargeability (MJTK-IP-3)

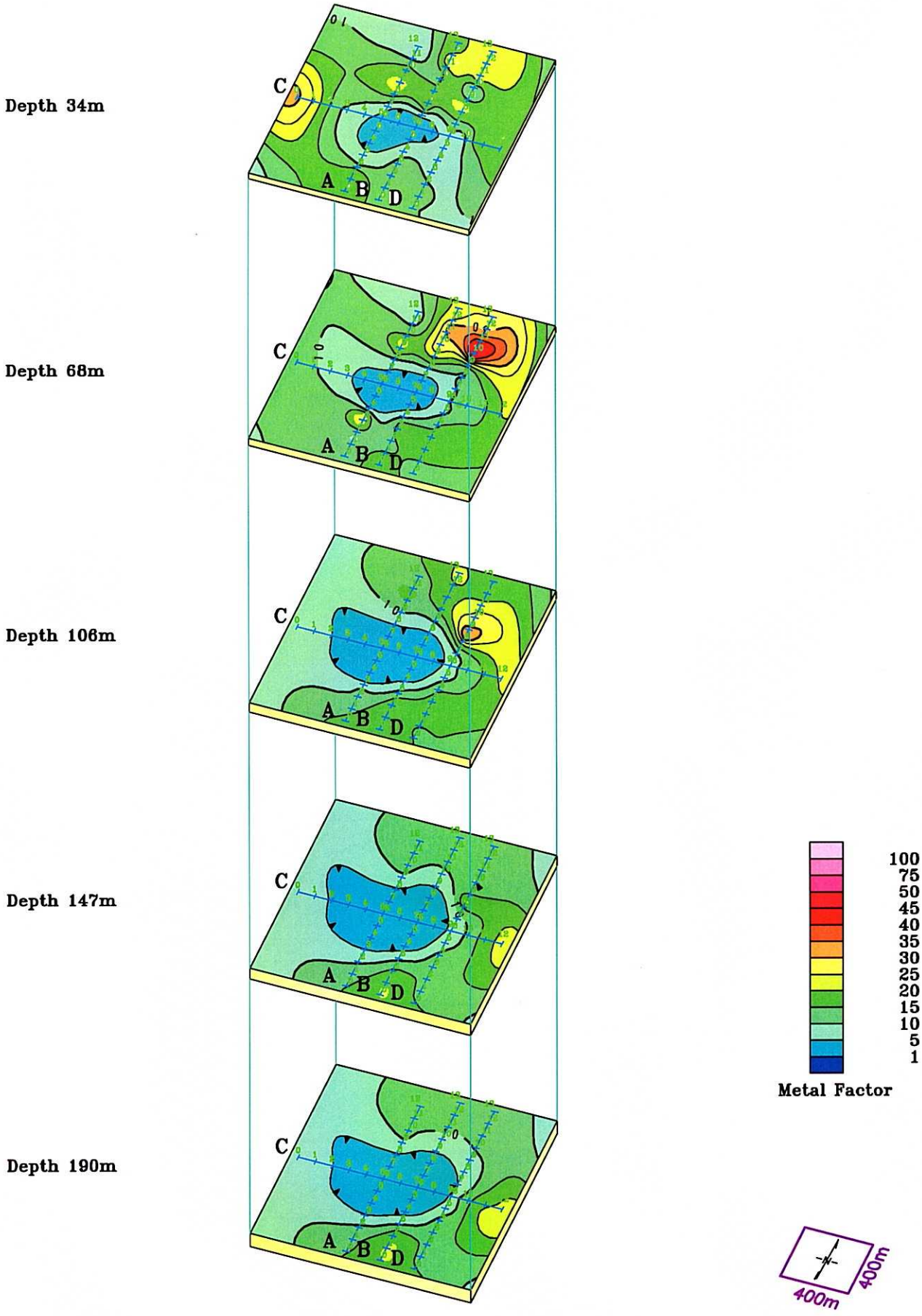

Fig.II-2-1-55 2D Analysis plane map of metal factor (MJTK-IP-3)

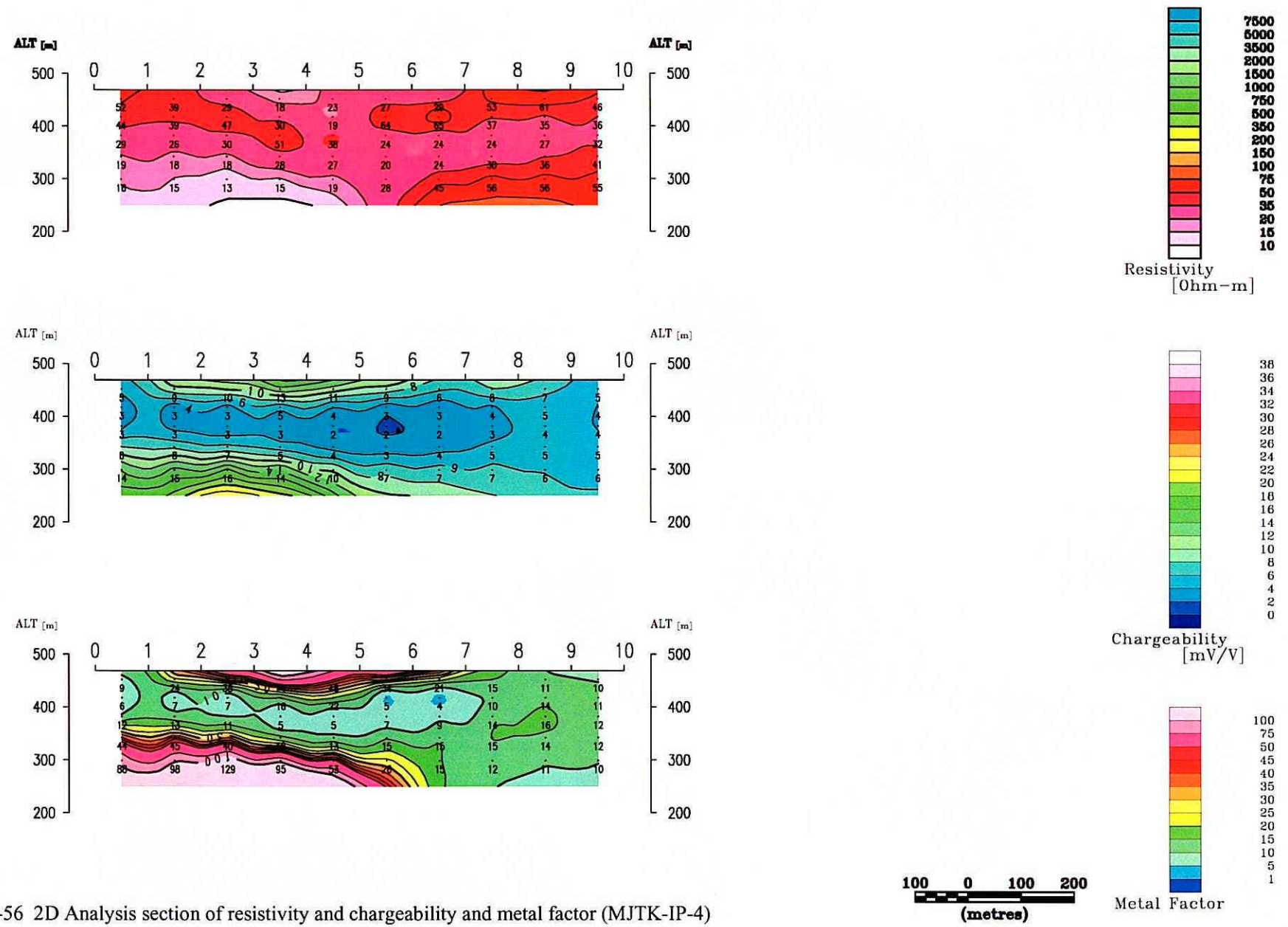

Fig.II-2-1-56 2D Analysis section of resistivity and chargeability and metal factor (MJTK-IP-4)

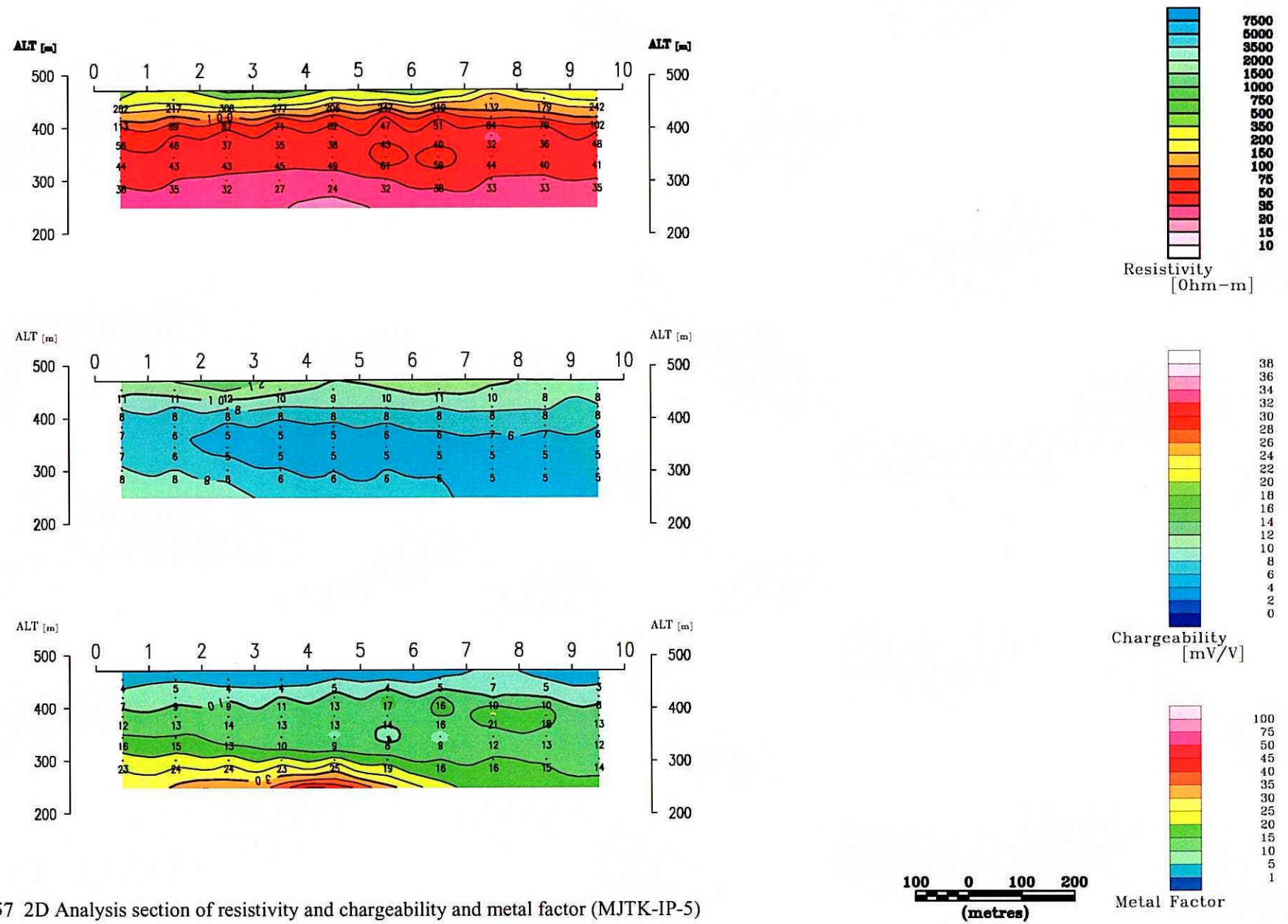

Fig.II-2-1-57 2D Analysis section of resistivity and chargeability and metal factor (MJTK-IP-5)

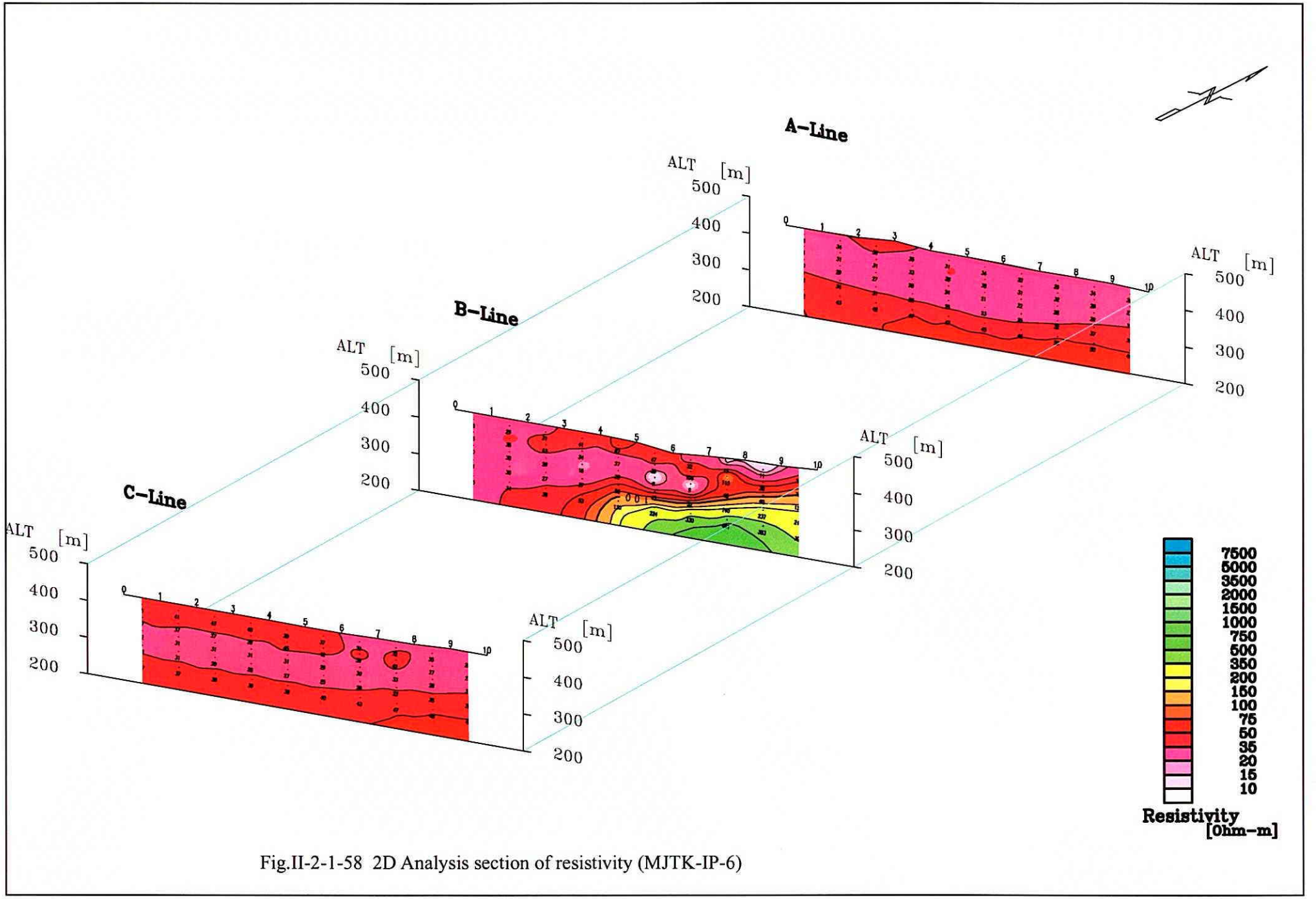

Fig.II-2-1-58 2D Analysis section of resistivity (MJTK-IP-6)

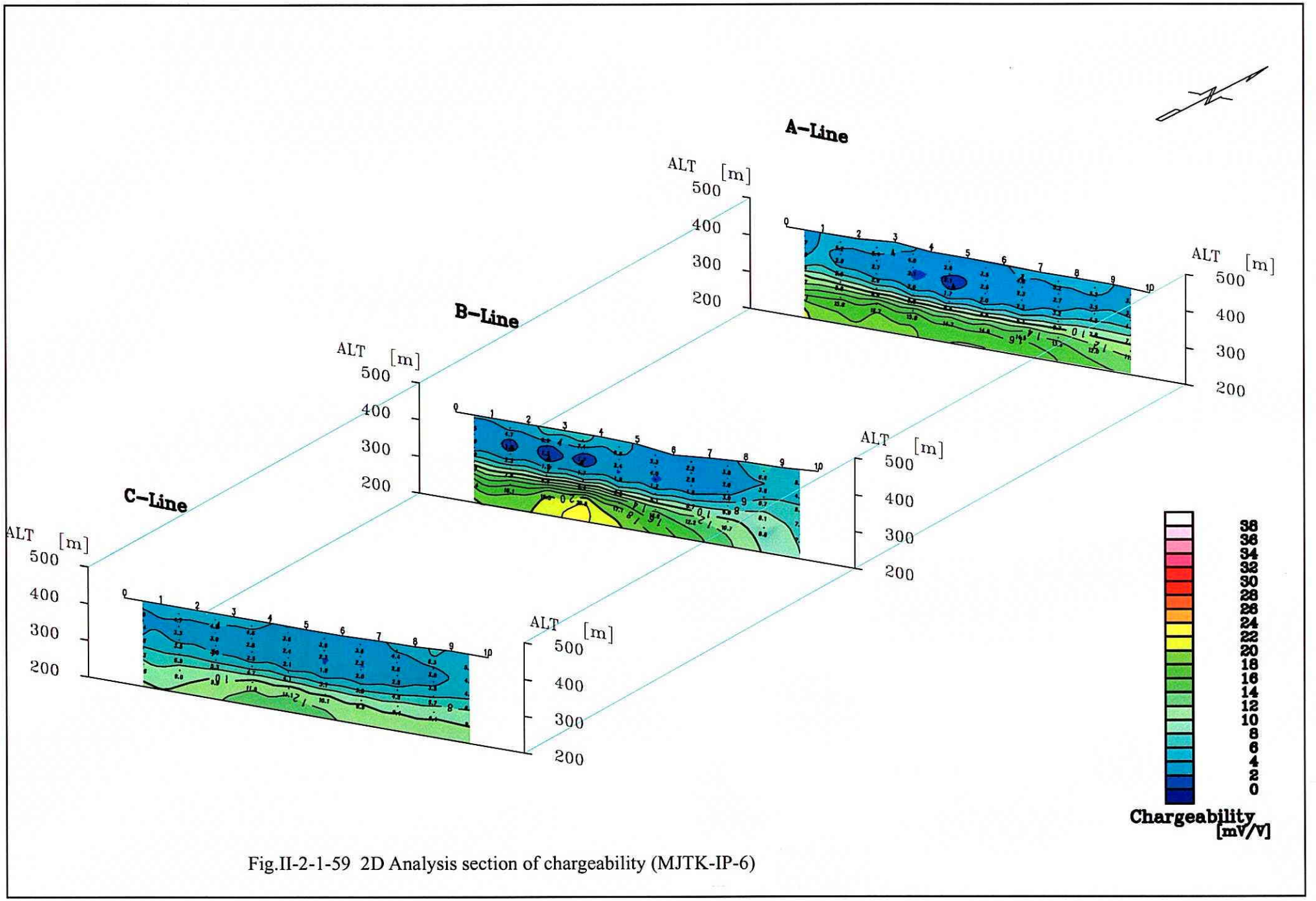

Fig.II-2-1-59 2D Analysis section of chargeability (MJTK-IP-6)

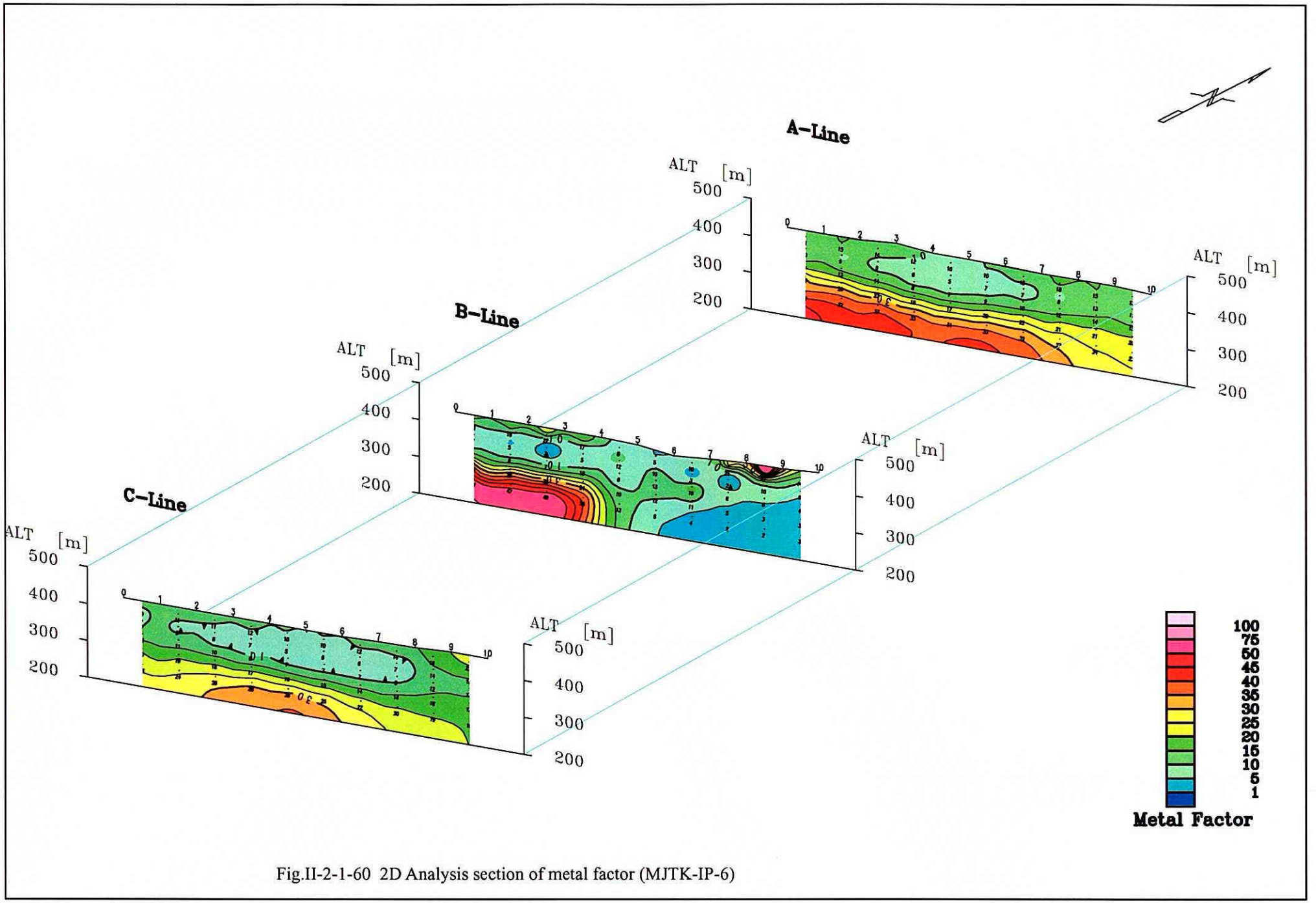

Fig.II-2-1-60 2D Analysis section of metal factor (MJTK-IP-6)

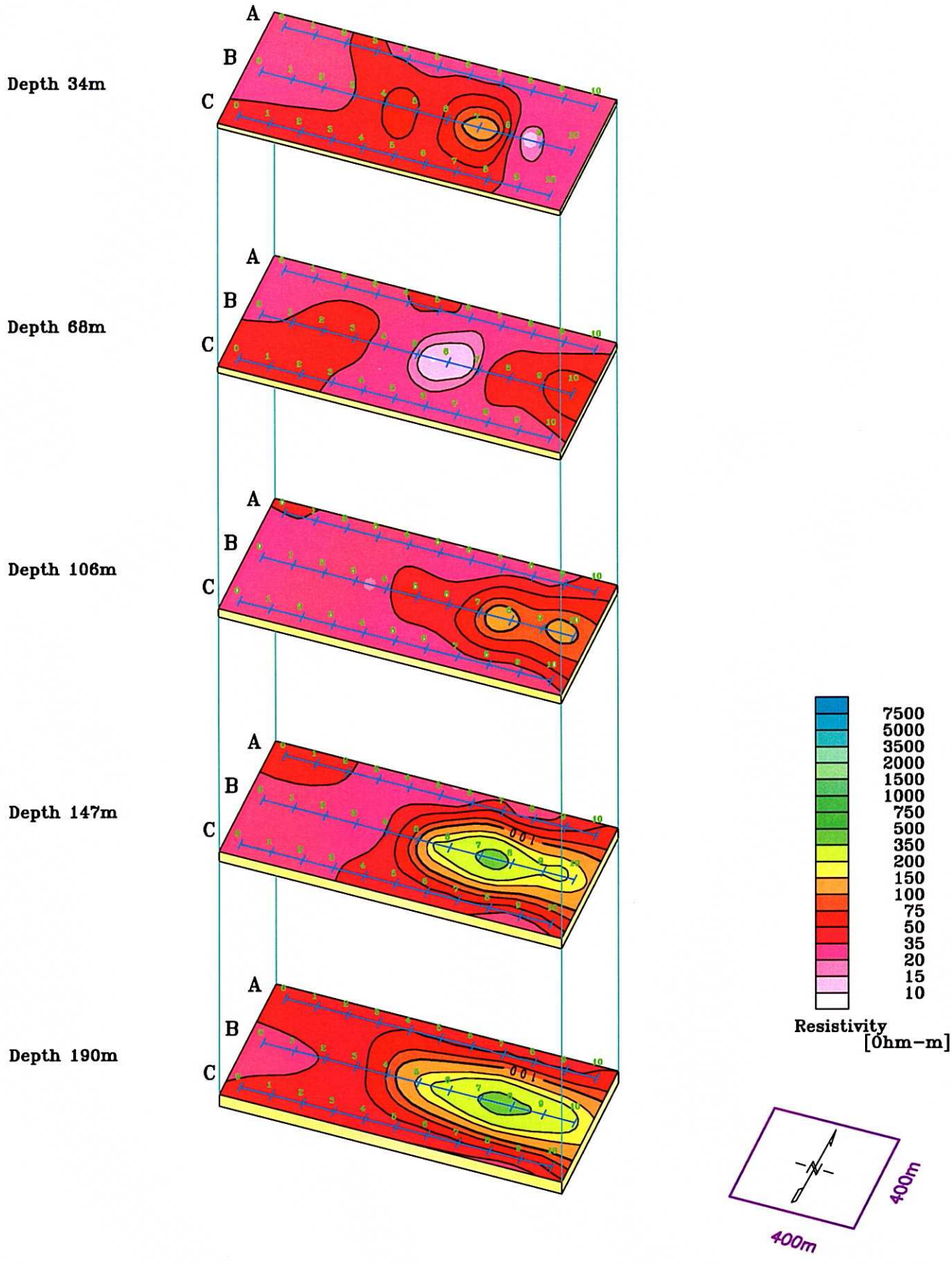

Fig.II-2-1-61 2D Analysis plane map of resistivity (MJTK-IP-6)

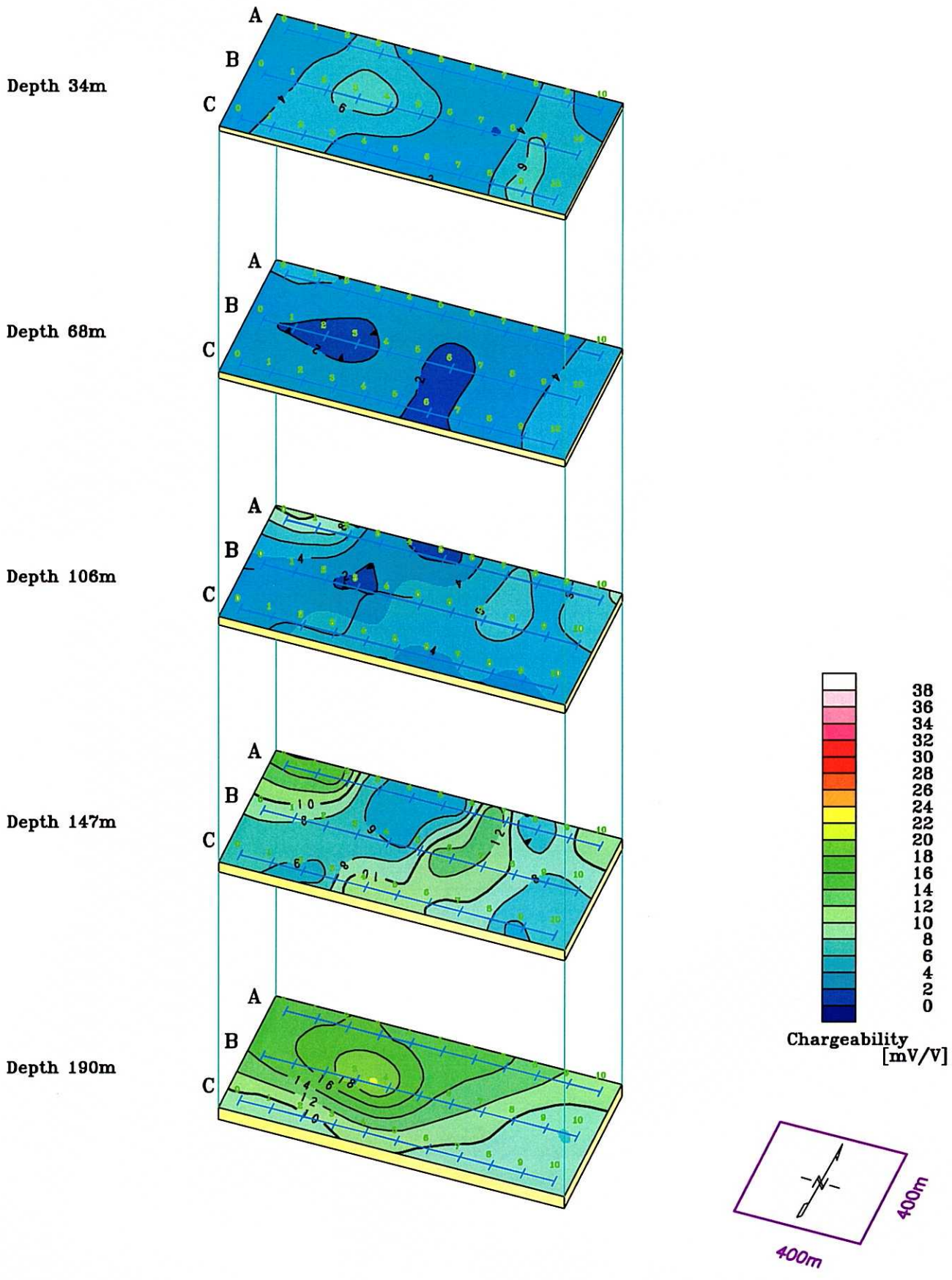

Fig.II-2-1-62 2D Analysis plane map of chargeability (MJTK-IP-6)

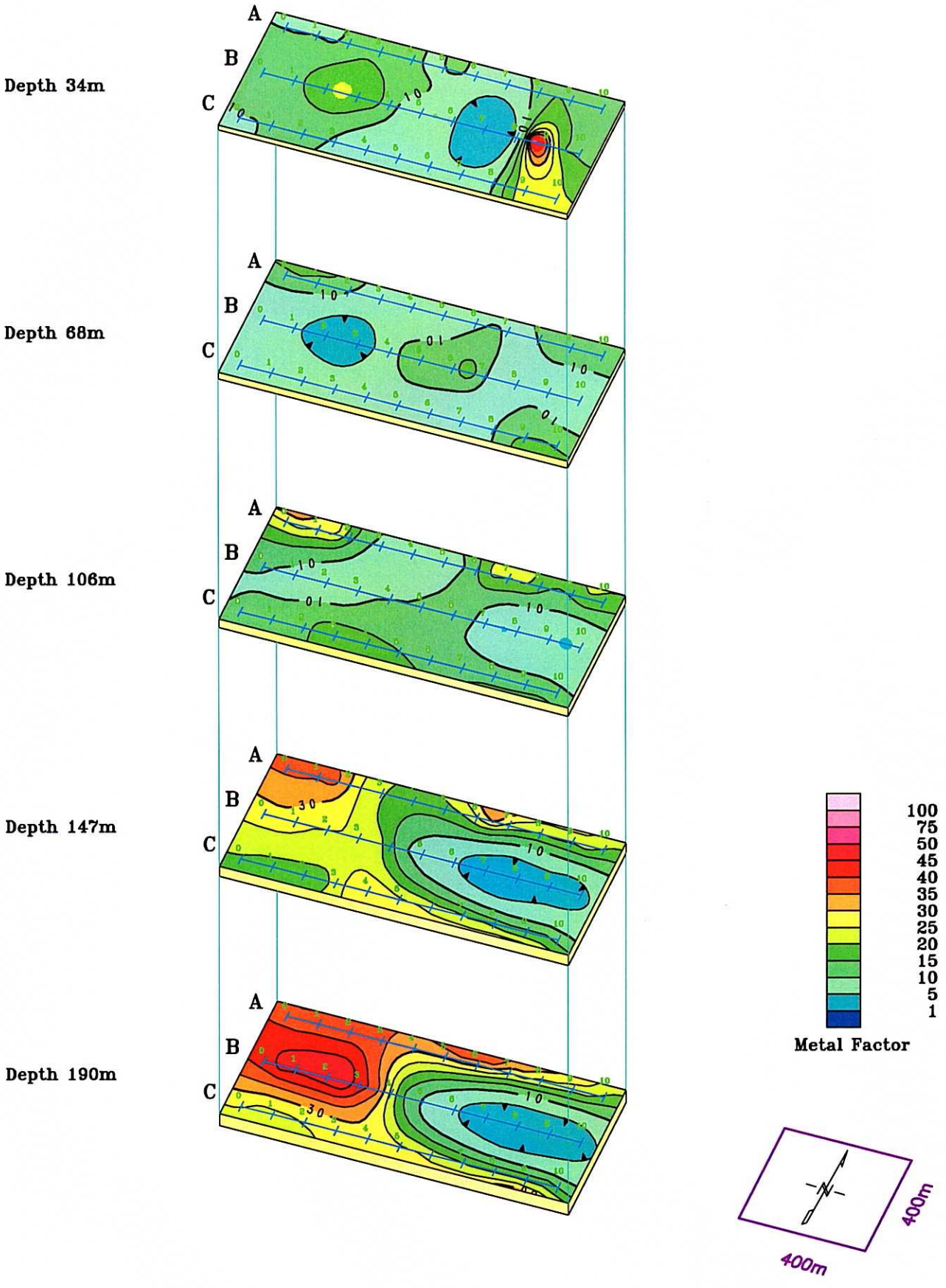

Fig.II-2-1-63 2D Analysis plane map of metal factor (MJTK-IP-6)

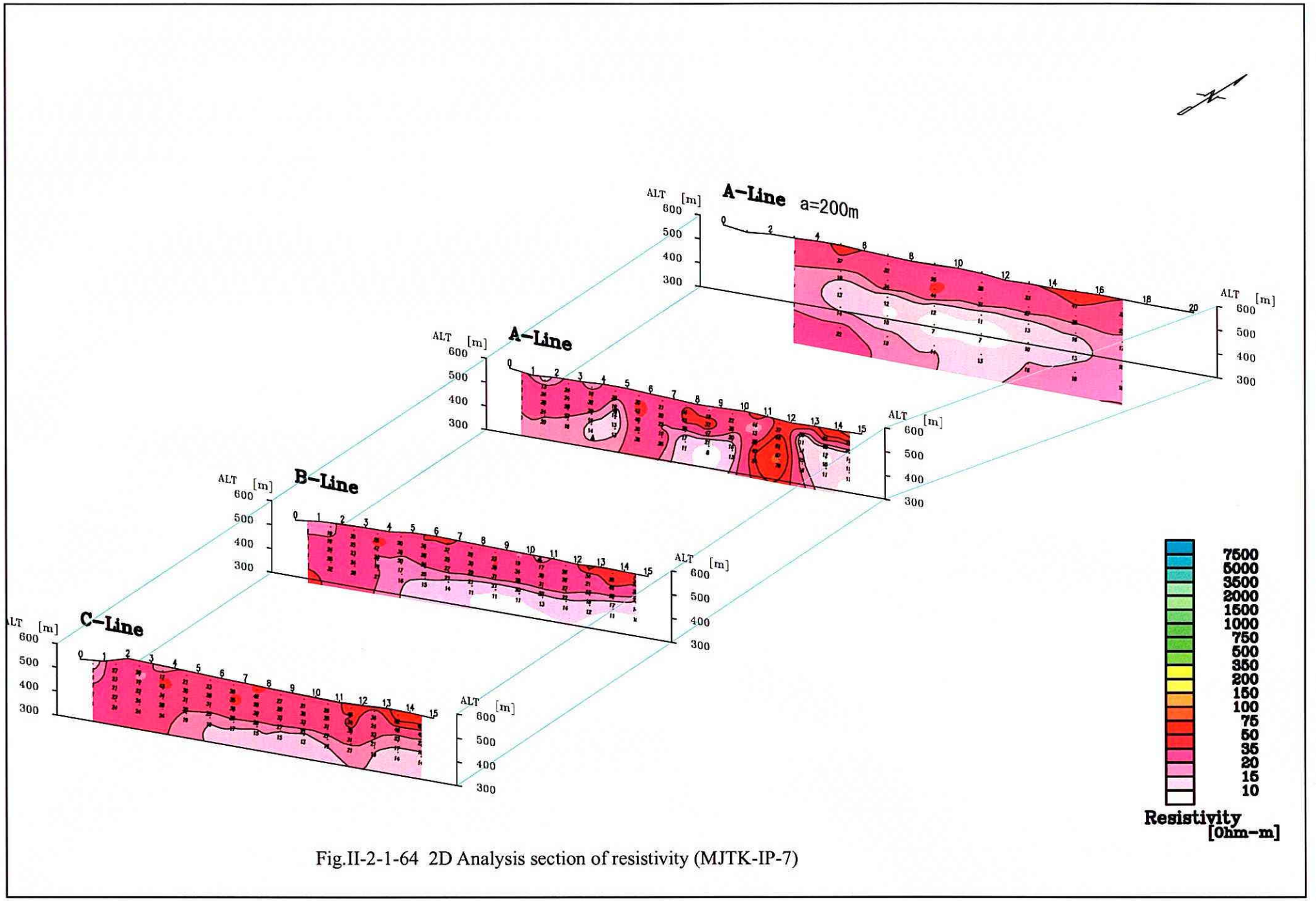

Fig.II-2-1-64 2D Analysis section of resistivity (MJTK-IP-7)

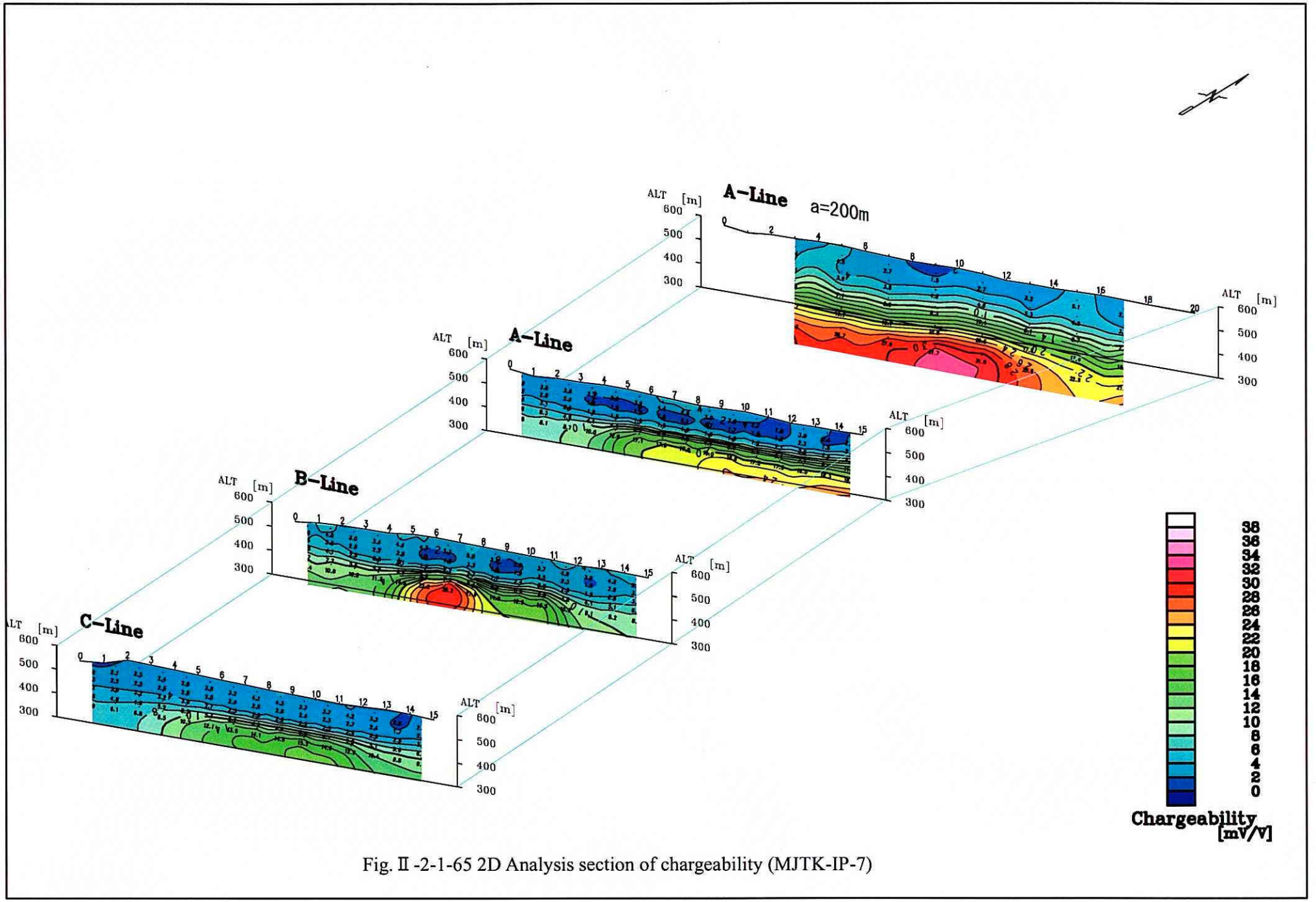

Fig. Ⅱ-2-1-65 2D Analysis section of chargeability (MJTK-IP-7)

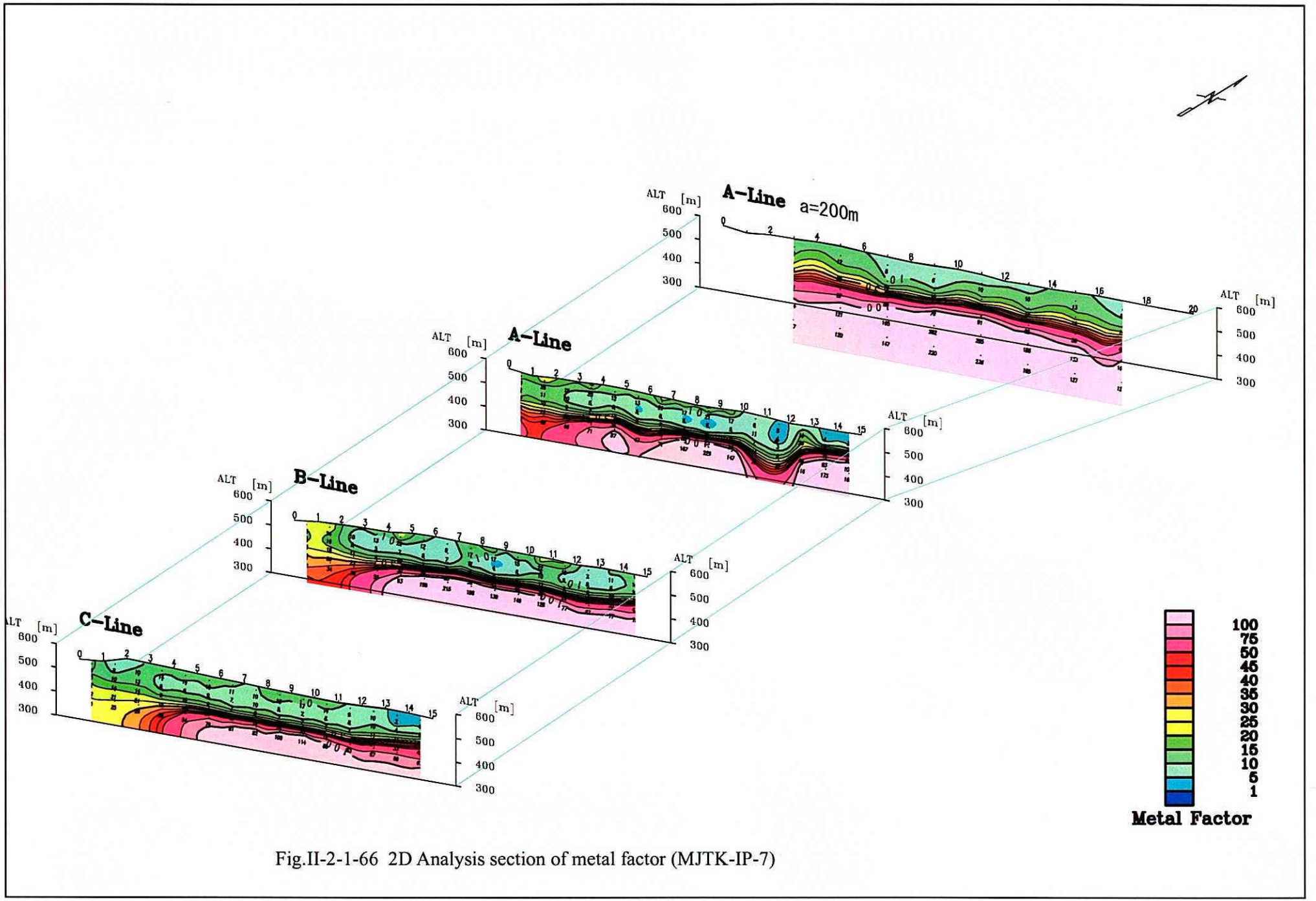

Fig.II-2-1-66 2D Analysis section of metal factor (MJTK-IP-7)

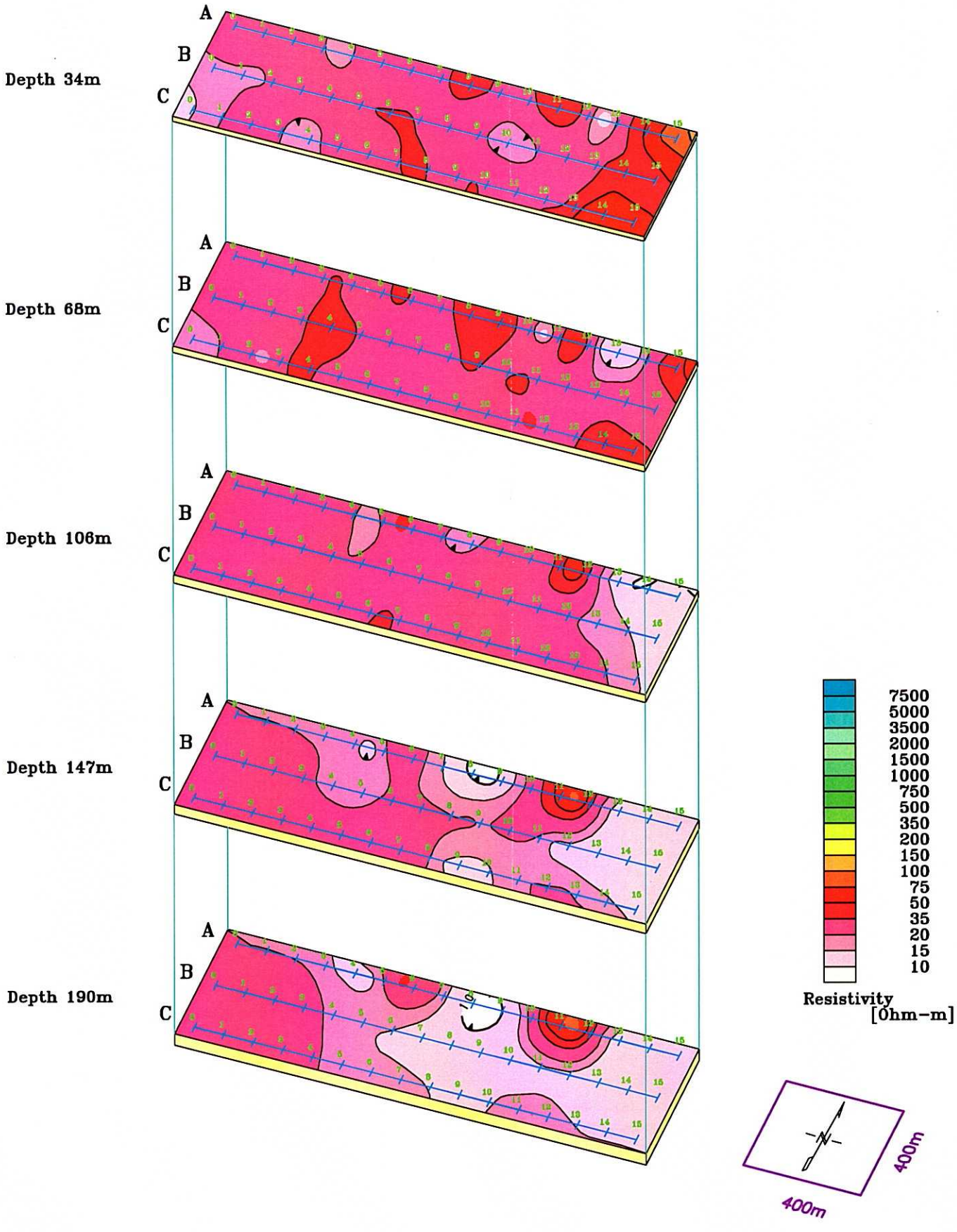

Fig.II-2-1-67 2D Analysis plane map of resistivity (MJTK-IP-7)

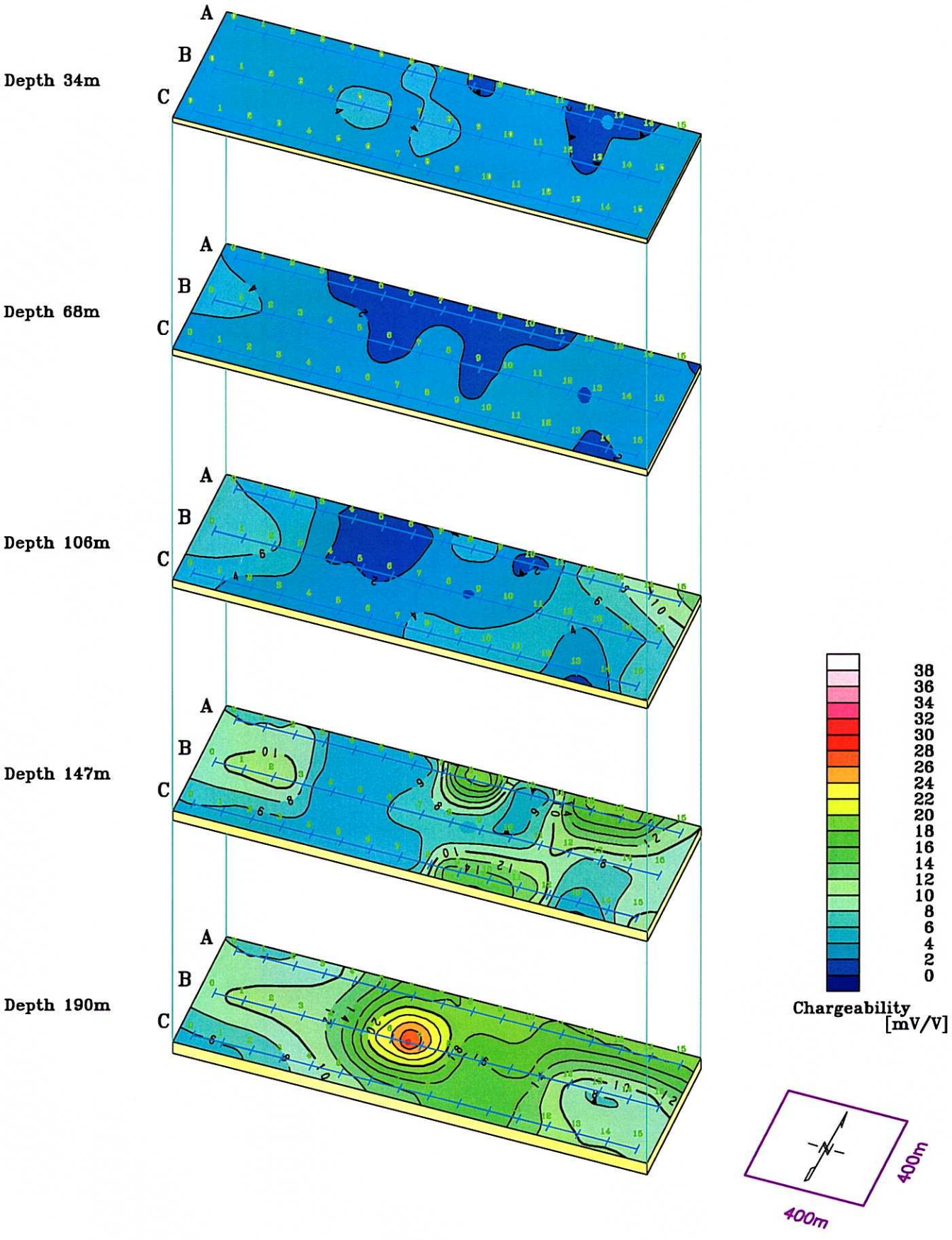

Fig.II-2-1-68 2D Analysis plane map of chargeability (MJTK-IP-7)

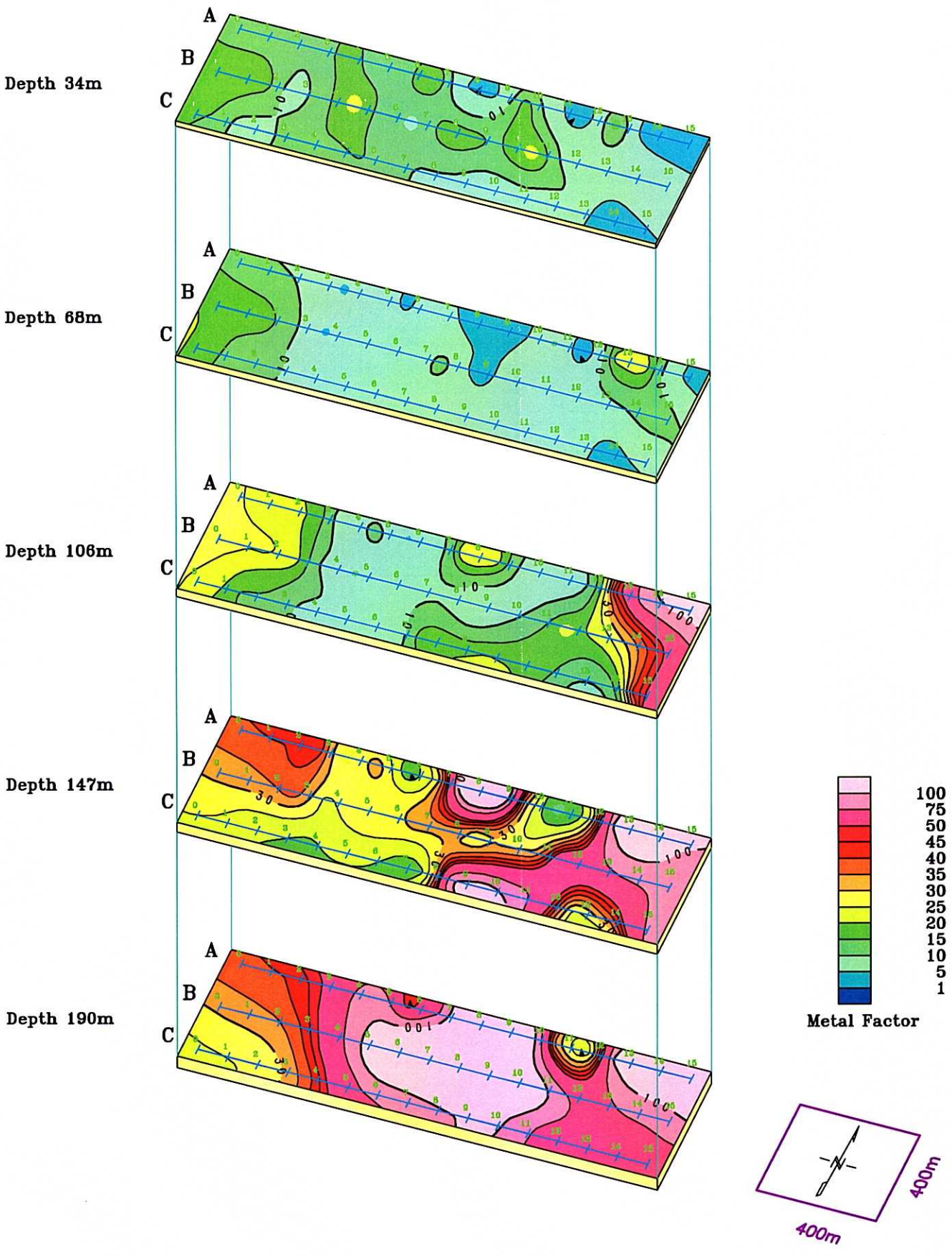

Fig.II-2-1-69 2D Analysis plane map of metal factor (MJTK-IP-7)

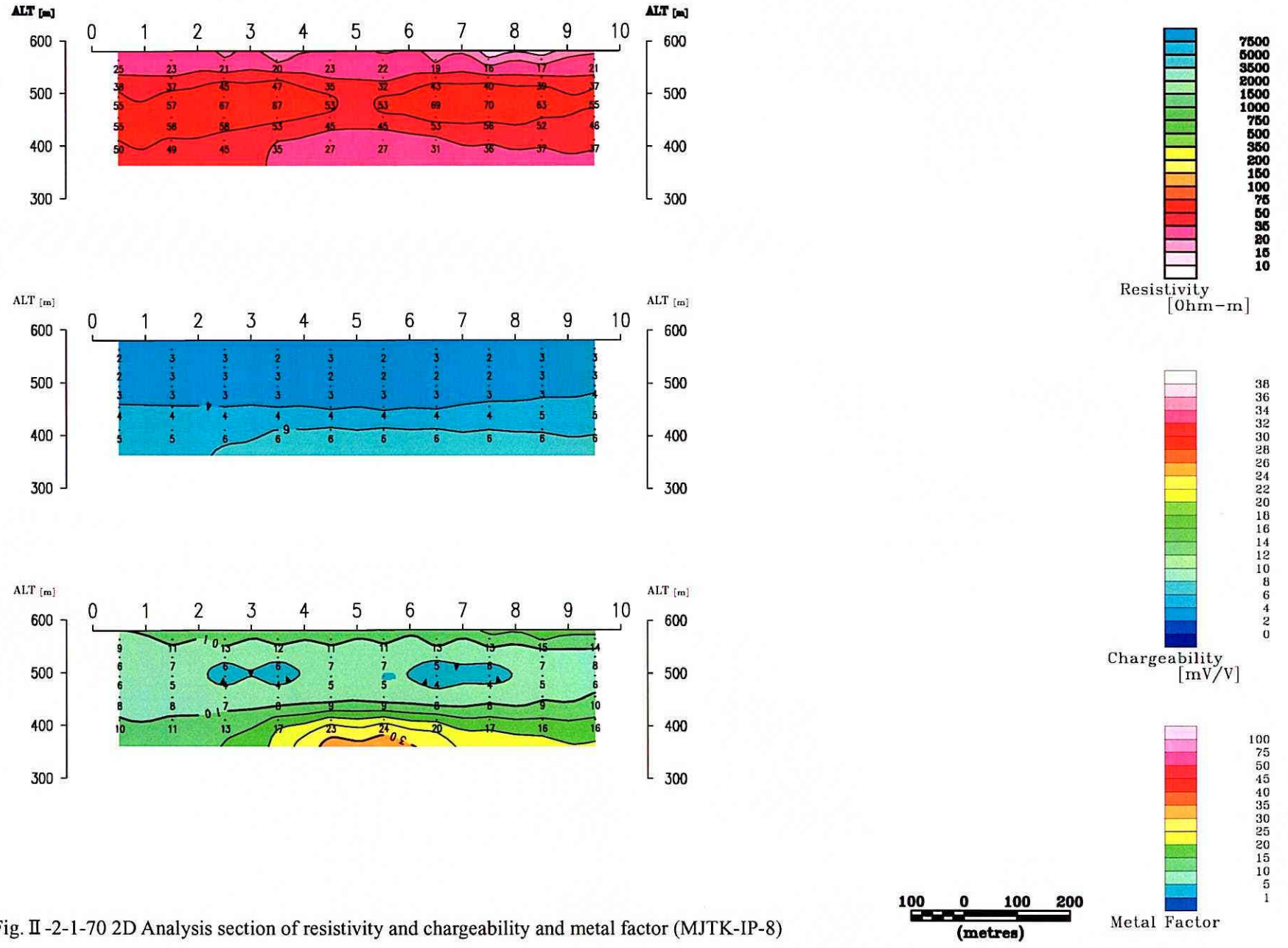

Fig. Ⅱ-2-1-70 2D Analysis section of resistivity and chargeability and metal factor (MJTK-IP-8)

2-1-6 Measurement of Physical Property

1) Method

The laboratory measurement has been performed to obtain data of the electric property of the rocks taken from the existing drilling cores and in the field. The specimens have been immersed in water, 90 Ω· m, for 48 hours, and become the supersaturated state. The 20 specimens have been measured.

The measurement of the resistivity and polarizability has been done by means of the TDIP method.

Table II-2-1-4 shows the equipment used for the measurement.

2) Result

Table II-2-5 and Figure II-2-71 show the result of the measurement of the physical property.

The resistivity of the rocks ranges from 1 to 14,000 Ω·m, and the chargeability ranges 0.2 to 761mV/V.

The pyrrhotite and sulfide minerals show below 1 Ω·m in resistivity, and over 400mV/V in chargeability.

The chargeability of the rocks is below 30mV/V except some impregnated phyllite.

The resistivity of the young sediments is below 40 Ω· m.

The Paleozoic rocks show great resistivity change. The phyllite shows higher resistivity, but is variable due to their grade of metamorphism or abundance of cracks. The weak solidity rocks show below 300 Ω· m, and some compact rocks show the highest value of 10,000 Ω· m. The igneous rocks also show high resistivity.

The argillaceous to silty rocks and rocks containing some banded structure or abundant cracks show below 10 Ω· m resistivity.

3) Summary

It is presumed that the young sediments, except gravel layers, show low resistivity, below 50 Ω· m, judging from the result of the resistivity structure analysis. This is correlated with the laboratory test result, several to several tens Ω· m.

On the other hand, the igneous and sedimentary rocks show great variety of resistivity values.

From the result of the measurement, the phyllitic rocks tend to show high resistivity, and the resistivity of the sedimentary and igneous rocks are depended upon their solidity and abundance of cracks.

The drilling core specimens have been sampled from solid parts, therefore their resistivity shows relatively high values, different from the actual resistivity in the field. It is better to take the actual

figures in the field. It is estimated that the resistivity of the Paleozoic igneous and sedimentary rocks ranges 10 to 3,000 Ω· m.

There exist some weak correlations between the low resistivity and low chargeability, and high resistivity and high chargeability.

Table Ⅱ-2-1-6 Results of physical property tests

No.	S. No.	Sample No.	Rock Name	Position				Remarks	Resistivity[Ω·m]	Mx(450-950)
1	1	090901	Andesite	IP-2	0586007	3487986	565	Paleozoic	482.8	10.46
2	2	090902	Calcareous Sandstone	IP-2	0586108	3487958		Paleozoic	4889.2	29.60
3	3	091001	Limestone	IP-7	0581008	3483574		Cenozoic	3.0	0.28
4	4	091002	Conglomerate	IP-7	0582359	3484145		Cenozoic	1.3	5.35
5	5	091301	Limestone	IP-3	0587018	3487197		Cenozoic	35.3	2.74
6	6	091401	pyrrhotite ore					Kettara, pyrrhotite ore	0.9	761.06
7	7	100301	Rhyolite					in Hajar Mine. Lower Zone.	71.0	2.63
8	8	100302	Sulfide ore					in Hajar Mine.	1.0	563.77
9	9	100303	Silt stone					in Hajar Mine. Upper Zone.	13584.2	18.30
10	10	100304	Silt stone		0581048	3471587	700	Amzough	5.1	3.31
11	11	100305	Rhyolite		0581118	3471352	706	Amzough	2253.3	3.28
12	14-1		Rhyolite		0581755	0358648	382	Draa Sfar	18.9	2.36
13	15	100402	Gabbro		0581701	3508489	357	Draa Sfar	281.4	7.87
14	17	100404	Calcareous Phyllite		0357690	3482557	577	Ghoula	8.7	3.46
15	20	100407	Sandy tuff		0576333	3482544	653		7.2	0.61
16	22	100409	Tuff-Phyllite alt		0576370	3482559	588		110.0	2.66
17	24	b	Micro-diorite					Kouadra.S3 302.30m	4847.7	5.14
18	25	c	Sandy Phyllite					Kouadra.S10 262.30m	1215.3	79.83
19	26	d	Sandy Phyllite					Kouadra.S10 361.50m	14212.1	7.34
20	29	090901	Andesite	IP-2	0586007	3487986	565	Paleozoic	3544.0	14.64

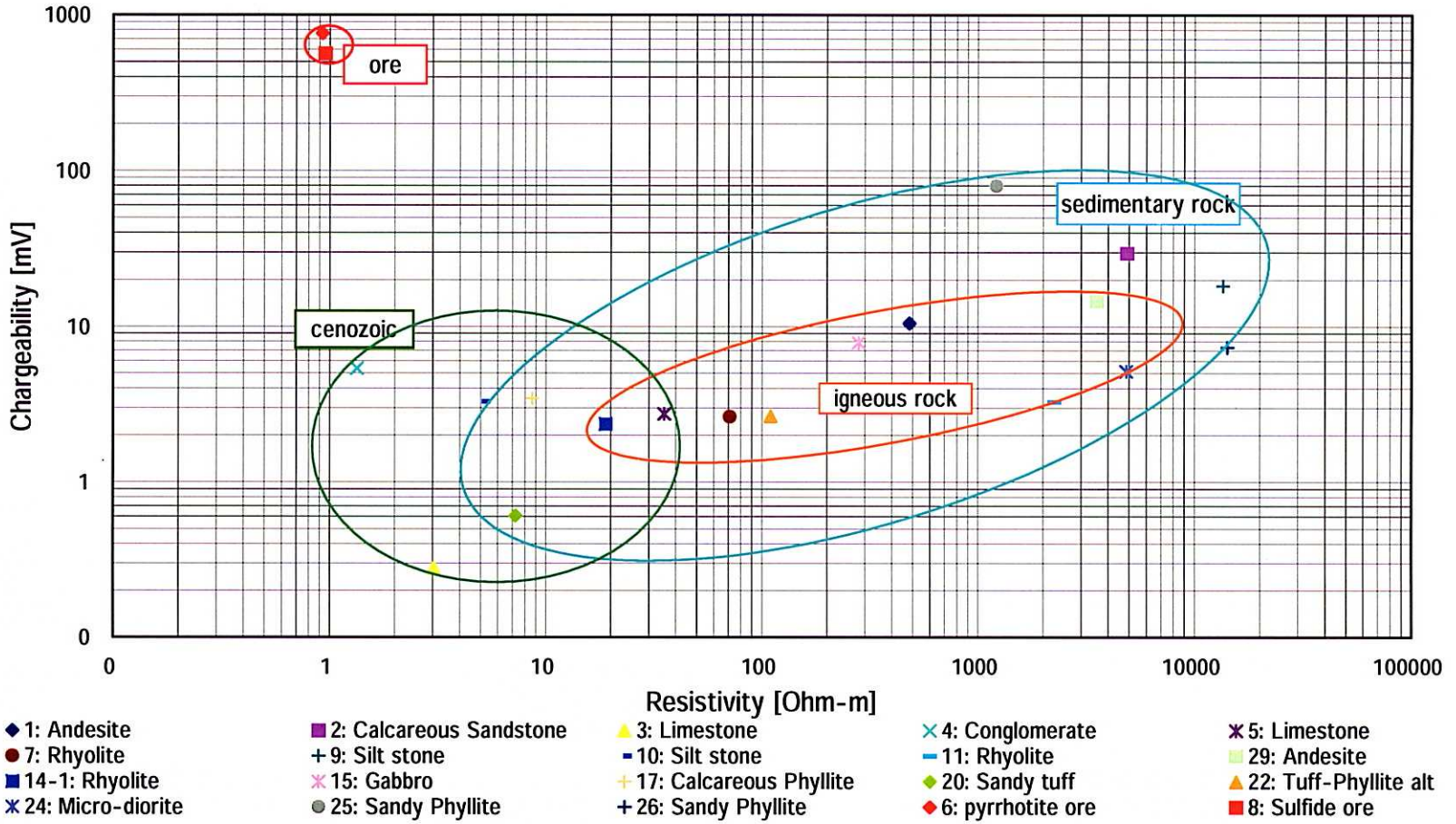

Fig.II-2-1-71 Relation between resistivity and chargeability for different types of rock

2-1-7 Discussion

The results of the analysis of the survey have revealed good correlation to the airborne magnetic and electromagnetic survey results. The conductivity distribution is well correlated to the distribution of the young sediments. Judging from the resistivity structure analysis and laboratory test result of the physical property, the resistivity of the young sediments is below 50 Ω· m, and their distribution pattern is of the horizontal stratigraphic structure.

The conductivity obtained by the airborne electromagnetic survey has revealed some local anomalies in the MJTK-IP-4 and MJTK-IP-8 districts. The resistivity distribution in the above-mentioned districts, however, is similar to those of the other districts. Furthermore, no chargeability anomaly exists in the districts.

The MJTK-IP-1, 2, 3, 4, 5, and 6 districts were been selected based on the airborne magnetic anomalies, and all laboratory test results on these districts are well corresponded with the airborne survey results for each district.

In MJTK-1 district, a weak chargeability zone is analyzed. The chargeability zone is distributed surrounding a high resistivity zone centering depth of 150 meters, around No.8 of the survey line C. There are two systems, north to south system through No.5 of the survey lines E, A, B, C, and D, and northwest to southeast system through No.14 of the survey line B.

On the other hand, the resistivity structure is characterized by a swelled high resistivity zone, over 200 Ω· m, around No.7 of the survey line C at the depth of 150 meters, and extending to the depth. The central anomaly among the three magnetic anomalies detected by the airborne survey is corresponded with the high resistivity zone.

It is reasonable to set that the existing ore deposits are characterized by stratiform and vertical extension. If it is so, some continuous chargeability zones should be noticed.

In the MJTK-IP-2 district, the high resistivity zone distributed in a broad area centering the summit, detected the by the test, is well corresponded with the relatively weak airborne magnetic anomaly. The high resistivity zone on the summit is in the andesite and calcareous siltstone distributed zone. It is resumed that the andesite extends to the north in the deep high resistivity zone. It is judged that the airborne magnetic anomaly reflects the andesite.

The deep part underneath the summit is of presumably low resistivity structure, several tens Ω· m. It probably reflects abundant cracks.

The compact andesite and siltstone show high resistivity in the laboratory test, but it varies due to cracks.

In MJTK-IP-3, the dome-shape high resistivity zone and low chargeability zone detected by the test is well corresponded with the airborne magnetic anomaly. However, it is judged that this anomaly is not related to mineralization, because the IP effect is too low.

The MLTK-IP-5 district shows a local airborne anomaly. The analyzed result of the test indicates a monotone horizontal stratigraphic structure in the resistivity. It is judged that the local anomaly reflects crushing factory there. The resistivity structure shows a high resistivity zone, about 200 Ω· m, in shallow part, corresponding to the surface gravel distribution. The deep part is of low resistivity and low chargeability, and no anomaly exists.

The weak airborne magnetic anomaly in MJTK-IP-6 more widely spreads over the district compared with other districts. Both the resistivity structure and chargeability structure in this district tends to show higher in the central district, deep part. It is thought that these structures reflect the Paleozoic rock facies in the deep part, however, no chargeability anomaly exists there. The Laboratory test result shows several hundreds Ω· m in resistivity, and 20mV/V in chargeability, being reasonable figures.

The MJTK-IP-7 district is of generally high conductivity zone, and no significant change is seen in the resistivity structure obtained from the resistivity structure analysis down to the depth of 150 meters, showing 25 Ω· m. In the resistivity structure analysis by the 200 meters electrode interval, the resistivity in the deeper part shows lower values, below 10 Ω· m. In this district, some change appears in the deep part chargeability, but no change appears in the resistivity, therefore the thickness of the young sediments is unknown. The chargeability tends to show slightly high in the deep part, but no anomaly can be seen.

The summary of this discussion is as follows.

- The resistivity of Paleozoic rocks varies from several tens to several thousands Ω· m, and no characteristic point to correlate with the upper layer or lower layer existence.
- The chargeability of rocks tends to show slightly higher to the high resistivity.
- Two chargeability zones analyzed are of weak value.
- The west chargeability zone is roughly corresponded with the high resistivity zone, over 100 Ω· m.
- The central anomaly among three airborne magnetic anomalies corresponds to the high resistivity zone, presumably being affected from some igneous body. The west airborne anomaly is not correlated with any valuable anomaly due to the end effect of the survey line.

Generally, rocks tend to show higher chargeability for higher resistivity, therefore, it is necessary to be careful for the high chargeability in high resistivity.

It is worth to emphasize to say that the northwest to southeast extending weak chargeability zone at No.14 of the survey line B should be noticed.

The existing ore deposits around the survey area commonly contain pyrrhotite, chalcopyrite, pyrite, and arsenopyrite, therefore, both of magnetic and IP effect should be considered for the exploration guide.

2-2 Electromagnetic Prospecting TEM Method

2-2-1 Object

The electromagnetic prospecting TEM method, hereafter TEM method, has been applied to make clear the detail resistivity structure and to extract some potential zones for mineral deposits in the IP anomalies detected by the proceeding geophysical survey. This survey program has been performed with special emphasis on estimation of the thickness of the sedimentary formations and to know areas of IP anomaly zones.

2-2-2 Location and Performed Survey

The last year's airborne geophysical survey program revealed some geophysical anomaly zones. Based on the result, eight favorable target districts for ground IP prospecting, MJTK-IP-1 to MJTK-IP-8, were selected for the ground follow up IP prospecting survey program. Those extracted three zones, the TEM method program has examined MJTK-1, MJTK-6, and MJTK-7.

Figures II-2-2-1 to II-2-2-3 show the TEM examination points in the districts. Table II-2-2-1 shows the works done for the survey. Total 139 points have been tested.

In the MJTK-IP-1 district, one survey line extending east to west and nine lines extending north to south have been measured by the TEM. The measuring interval is 50 meters for the east to west line, and 100 meters for the north to south lines. Total 104 points have been measured.

In the MJTK-IP-6 district, one east to west extending survey line has been measured. The measuring interval is 100 meters. The total nine points have been measured in total.

In the MJTK-IP-7 district, one survey line extending east to west and one line extending north to south have been measured. The measuring interval is 50 meters for the east to west extending line, and 100 meters interval for the north to south extending line. Totally 29 points have been measured.

Table II-2-2-1 Detail Specification of TEM Survey

Area name	Number of stations	Length of survey lines	Spacing (m)
MJTK-IP-1	104	N-S 9 lines 4050m E-W 1 line 2000m	50 100
MJTK-IP-6	9	E-W 1 line 800m	100
MJTK-IP-7	26	N-S 1 line 400m E-W 1 line 1800m	50 100
Total	139	9050m	

2-2-3 Survey Method

The measuring equipment applied is of Genics, Canada. The data-recording instrument POTEM(D) equips setting mechanism of some measuring ranges to record magnetic field changing rate after transmitting current interruption. The target depth range for the survey is from the surface to 300 meters, therefore, the transmitter TEM47 for shallow prospecting and TEM57 for deep prospecting have been used. The measurement ranges are 0.00613 to 0.06959 ms (U mode), 0.08813 to 6.978 ms (H mode), and 0.8813 to 69.78 ms (L mode).

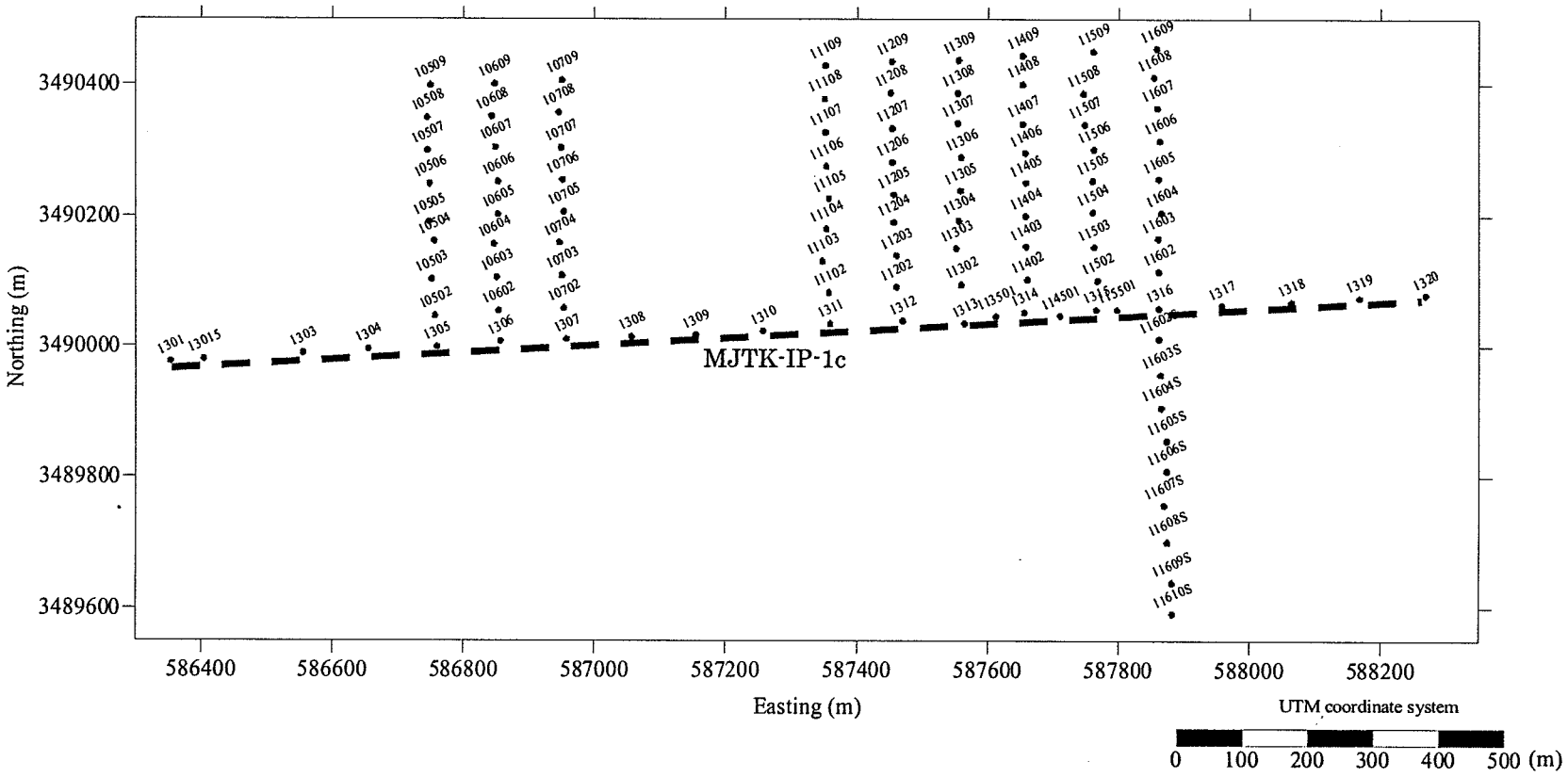

Fig. II -2-2-1 Observed points of TEM method at MJTK-IP-1 area

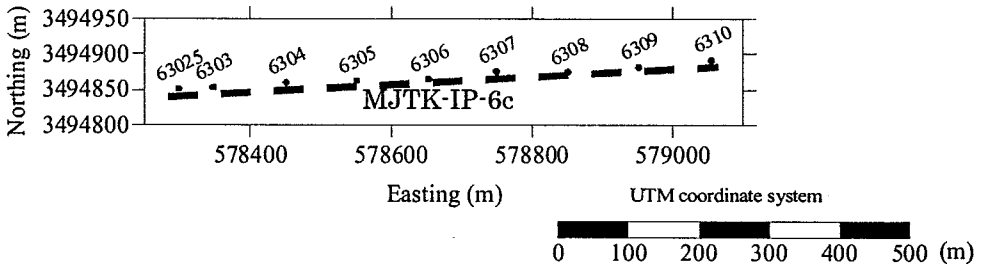

Fig. II -2-2-2 Observed points of TEM method at MJTK-IP-6

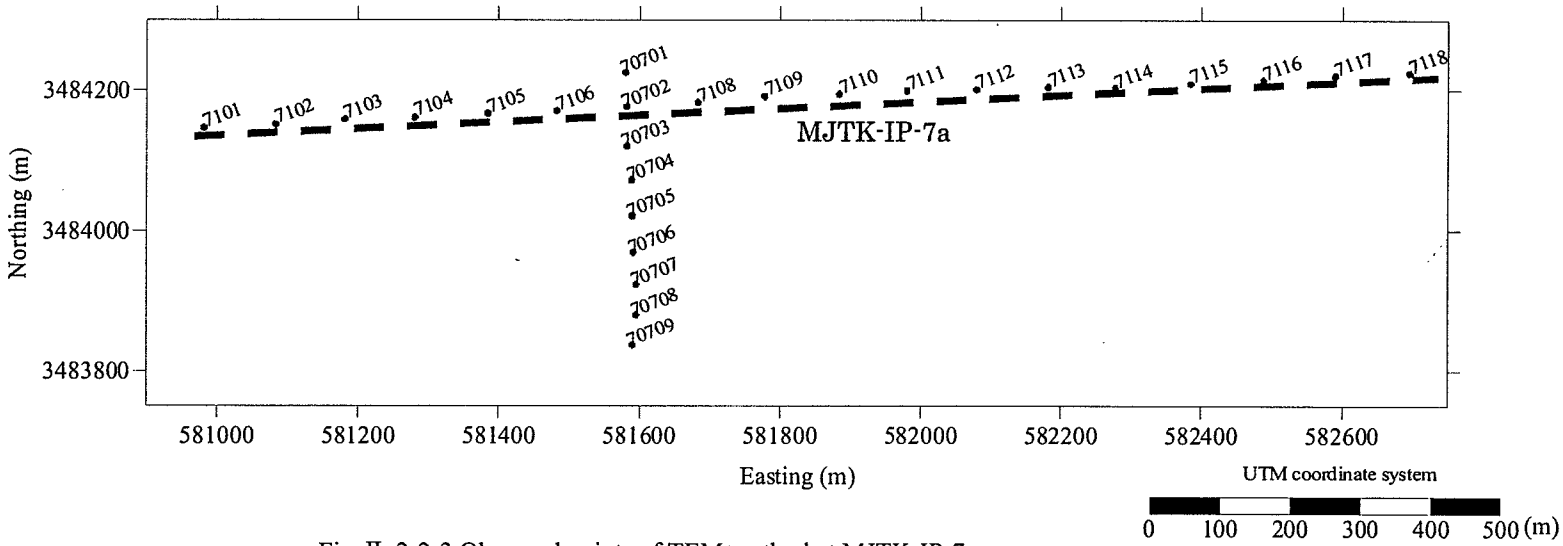

Fig. II -2-2-3 Observed points of TEM method at MJTK-IP-7 area

Transmitting loops, 100 x 100 meters, have been set for the measuring, and the transmitting current 2 amperes in TEM47 and 10 amperes in TEM57 have been remitted. The receiving coil has been set at the center of the loop. Multiple measuring method has been applied for each measuring point, and the repeatability of the measuring has been confirmed. It has been endeavored to obtain good data regarding the signal to noise ratio, S/N.

Figure II-2-2-4 shows the schematic diagram of TEM method by using central loop configuration.

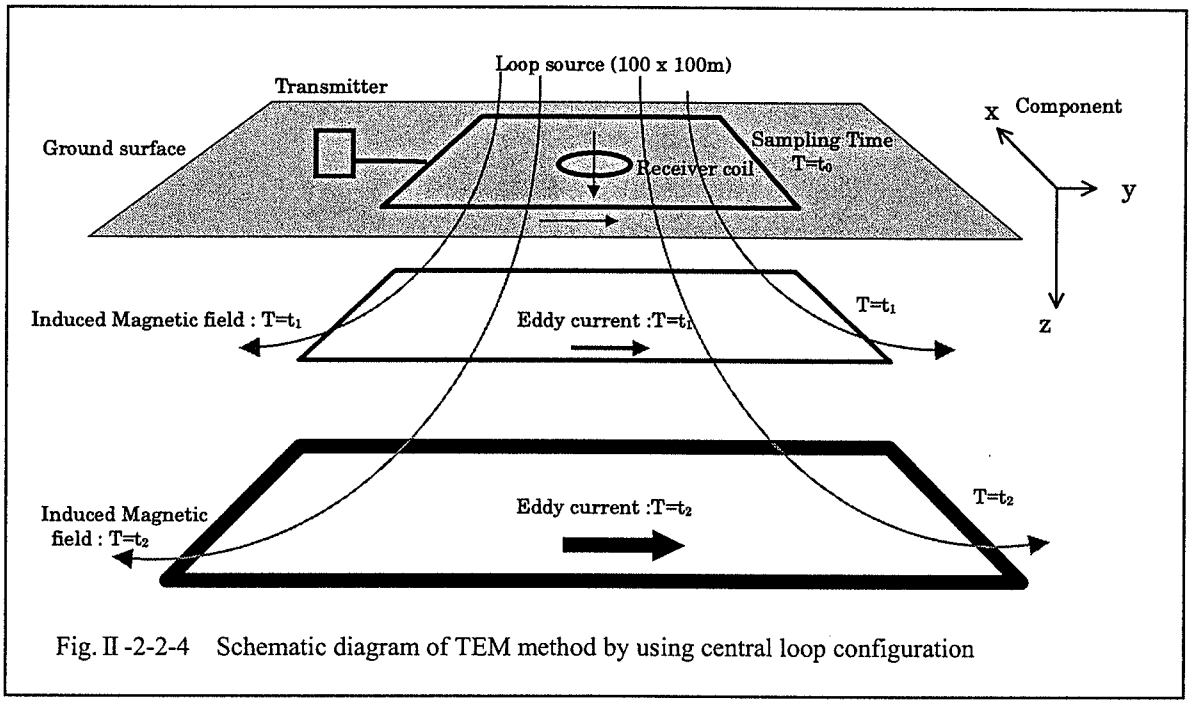

Fig. II -2-2-4 Schematic diagram of TEM method by using central loop configuration

2-2-4 Analysis Method

The measured voltage Vo (mV) by PROTEM(D) is able to convert to magnetic field change rate dB/dt (nV/m3) as follows.

$$\frac{dB}{dt} = \frac{V_0 \cdot 19200}{E \cdot 2^n} \qquad (2\text{-}2\text{-}1)$$

Where

E (m2): effective area of receiving coil 2^n: amplifier gain

The magnetic field change rate can be representing the apparent resistivity of time function $\rho_a\ (t)$ ($\Omega \cdot$m) .

$$\rho_a(t) \cong \frac{\mu}{4\,p\,t_c}\left(\frac{2\,\mu M}{5\,t_c\,dB/dt}\right)^{2/3} \qquad (2\text{-}2\text{-}2)$$

Where

μ : magnetic permeability (4 π x 10-7 H/m)

tc (msec): time after transmitting current interruption

M: moment of transmitter, area of transmitting loop (m^2) x transmitting current (A)

The analysis has been performed by means of the one dimensional multi-layers structure analysis using the apparent resistivity value. TEMIXXL of INTEREX has been used for the analysis.

2-2-5 Survey Result and Result of Analysis

Appendix shows cross section of a measurement results.

Tables II-2-2-2 to II2-2-4 show the summary of the one-dimensional analysis for each district. The resistivity structure cross-sections have been created as the result. Figure II-2-2-7 and Figure II-2-2-8 shows that of MJTK-IP-1, Figure II-2-2-9 shows that of MJTK-IP-9, and Figure II-2-2-10 shows that of MJTK-IP-7IP-7. The detail description for each district is as follows.

Table II-2-2-2 Classification of resistivity values

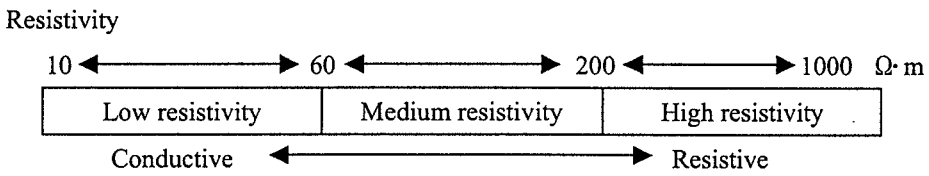

2-2-5-1 MJTK-IP-1 district

The three survey lines, MJTK-IP-1a, MJTK-IP-1b, and MJTK-IP-1c were previously measured by the ground IP method. The TEM survey has been performed on the east to west extending survey line MJTK-IP-1c, where the clear IP anomaly exists. Also, the measurement has been performed along the nine survey lines crossing the MJTK-IP-1c line at the right angle.

The wave pattern for the IP effect has been obtained from the measurement (Figure II-2-2-5). In the central loop configuration in the TEM method, the measuring voltage wave pattern decays by and by, and reaches the noise level. However, some reverse polarity phenomenon in late time been observed in this district, and the apparent resistivity value shows negative during L mode measuring as seen in Figure II-2-2-5. It is known that this kind reverse phenomenon in the central configuration measuring is caused by the IP effect (Flis et al., 1989).

In case of considering polarity rocks affected the vortex current underneath the transmitting loop, it is considered on the IP effect. As shown in Figure II-2-2-6, the ion is electrically in equilibrium in the pre-transmission (a) state. The ion is removed by the vortex current in the (b) state, and new current is introduced in the same direction of the vortex current. This is called the polarization current. The ion ceases its move in the state (c), the polarization conductor is in the state of full charged. In the state (d), the charged ion introduces the polarization current in the reverse direction in the process back to the equilibrium state. Accordingly, if the polarization in the underground is satisfactory strong, the magnetic field due to the polarization exceeds the magnetic field due to the vortex current, because the polarization current exceeds the vortex current. The polarity of the magnetic field, eventually, is reversed.

In this district, points seen such measuring voltage wave-pattern have been marked as the IP anomaly zone.

Because the IP effect is produced by the two-dimensional and three-dimensional structure, the one-dimensional structure analysis is impossible to perform, after the time of the polarity reverse phenomenon of the measuring voltage seen. Therefore, the one-dimensional structure analysis has been applied for the data in the time zone before the reverse phenomenon appears, regarding data observed the polarity reverse phenomenon.

It is apparently said that the resistivity structure is of horizontal stratiform, judging from the result of the one-dimensional structure analysis. The resistivity layers can be divided into three layers, Layer 1, Layer 2, and Layer 3 from the top, as shown in Table II-2-2-3. The resistivity figures and thickness of layers for each layer are shown in the average figures of the analyzed values. The resistivity value of Layer 1 is low as 17 Ω· m, and about 70 meters thick. The resistivity value of Layer 2 is medium as 169 Ω· m, and about 70 meters thick. The resistivity of Layer 3 is high as 414 Ω· m.

The high resistivity analyzed zone adequate to Layer 2 and Layer 3 is corresponded to the time zone right before measurement start. Mixed existence of high resistivity zones in Layer 2 and Layer 3 means that the depth of the IP effect appearance points different from each point.

The cross sections for the resistivity structure for each survey line have drawn to present the above-mentioned layer structure (Figure II-2-2-8). The resistivity values in the cross-sections are classified in the log scale. The warm color represents low resistivity, and cold color represents high resistivity.

The characteristic of the resistivity structure in the area is as follows.

1) Layer 1 from the surface to 450 meters depth is all in the low resistivity zone.
2) Layer 1 is thin in the west, and thicker to the west. No significant change from north to south is noticed, due to its short length.

3) The high resistivity layer affected by the IP effect is noted underneath the low resistivity Layer 1.

4) In the north to south survey line in Figure II-2-2-7, no high resistivity zone indicating IP effect is recognized to the north side from the cross point with the IP survey line IP1-b. There exists all in the low resistivity zone.

Table II-2-2-3 The results of TEM survey at area MJTK-IP-1.

	Resistivity(Ω·m)	Thickness(m)
Layer 1	17	74
Layer 2	169	71
Layer 3	414	

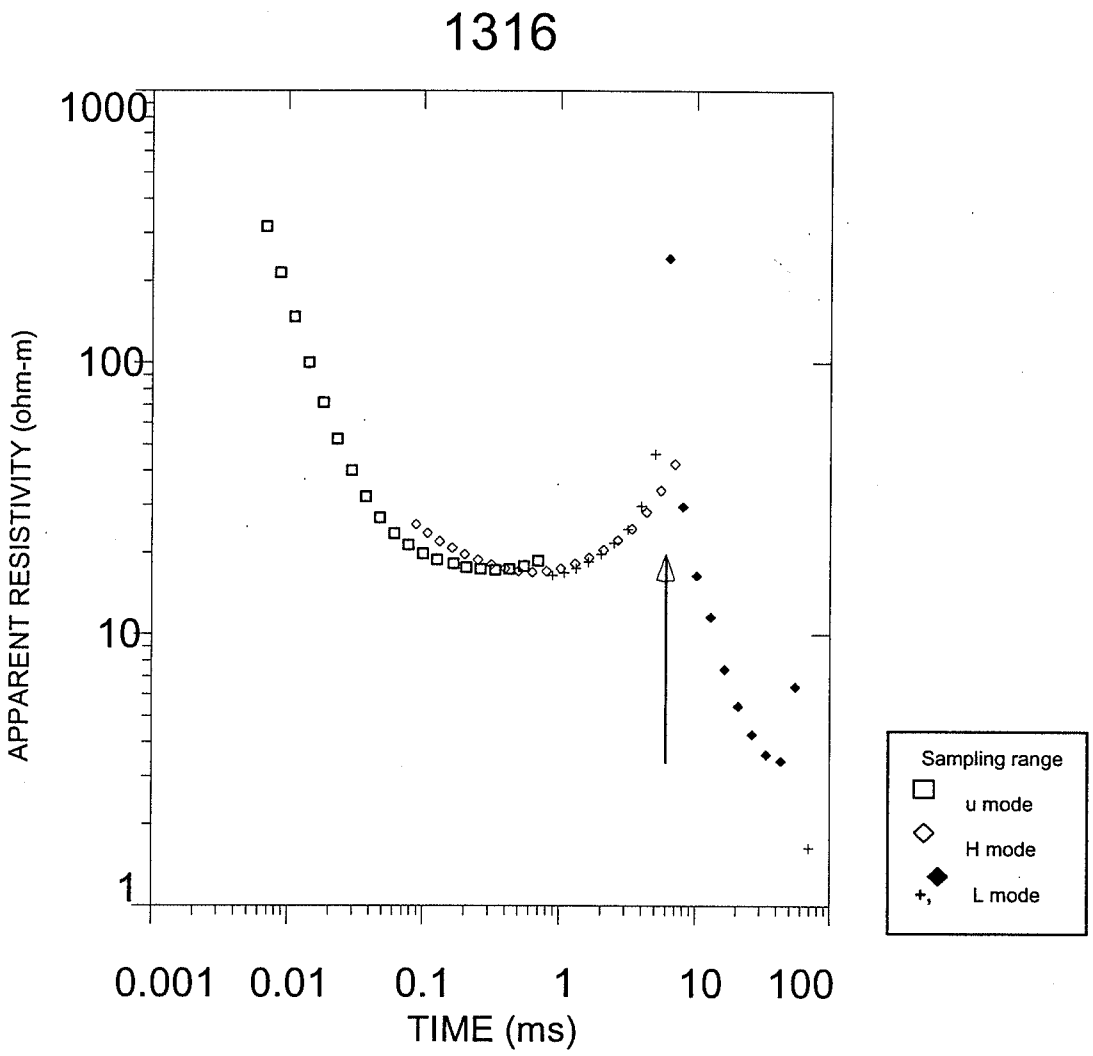

Fig. II-2-2-5 Typical transient curves in the MJTK-IP-1 area

The polarity of apparent resistivity is changing at arrow mark position.

The "+" marked data between the L mode curve shows the positive values and the "◆" marked data shows the negative value.

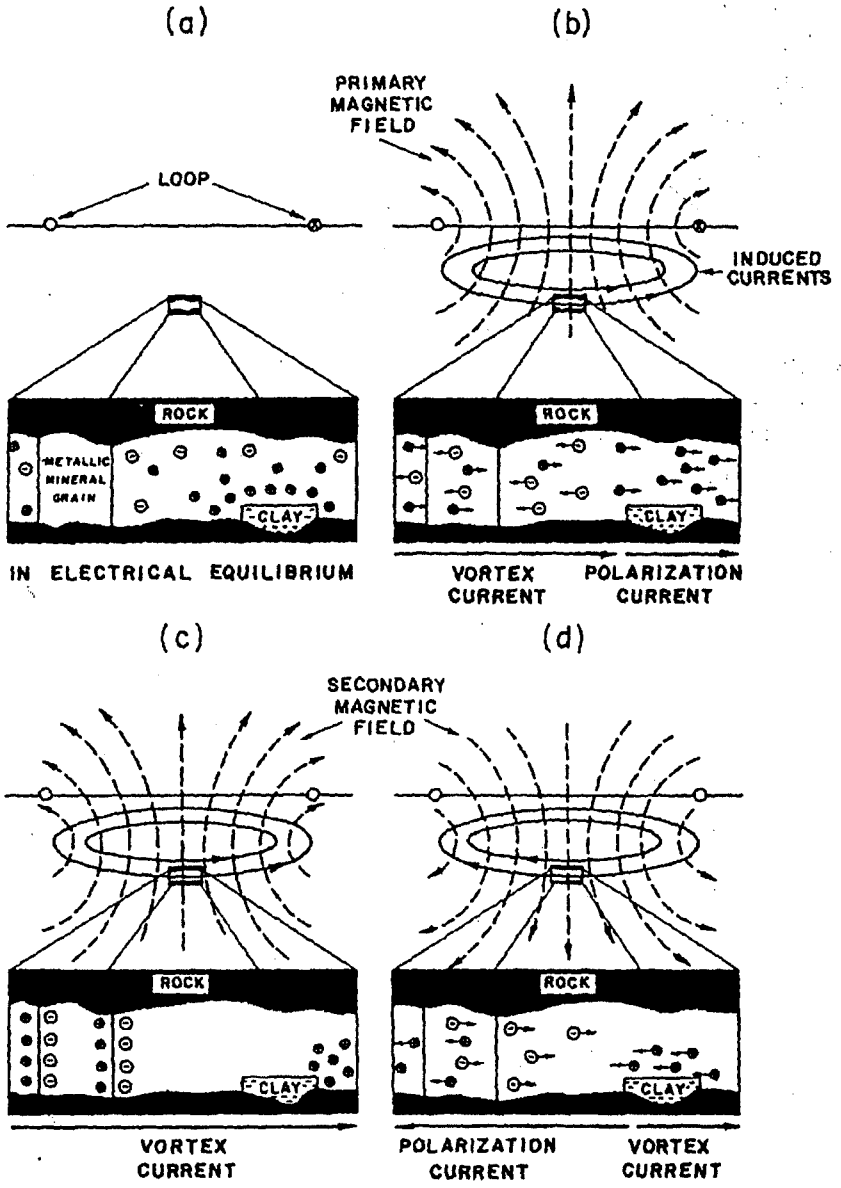

Fig. II-2-2-6 Schematic diagram of ionic movement in a volume of polarizable rock beneath a TEM transmitter loop.

(a) Before transmitter turnoff, ions are in electrical equilibrium with any metallic mineral grains and negatively charged crays present. (b) During turnoff and for a short time thereafter, cations, driven in the same direction as the vortex current, constitute a positive polarization current. (c) At some intermediate time the ions attain a fully charged state and the polarization current is zero. (d) At later times, the decaying vortex current can no longer support this charge state ; the ions drift back to their original positions producing a negative polarization current. (After Flis et al., 1989)

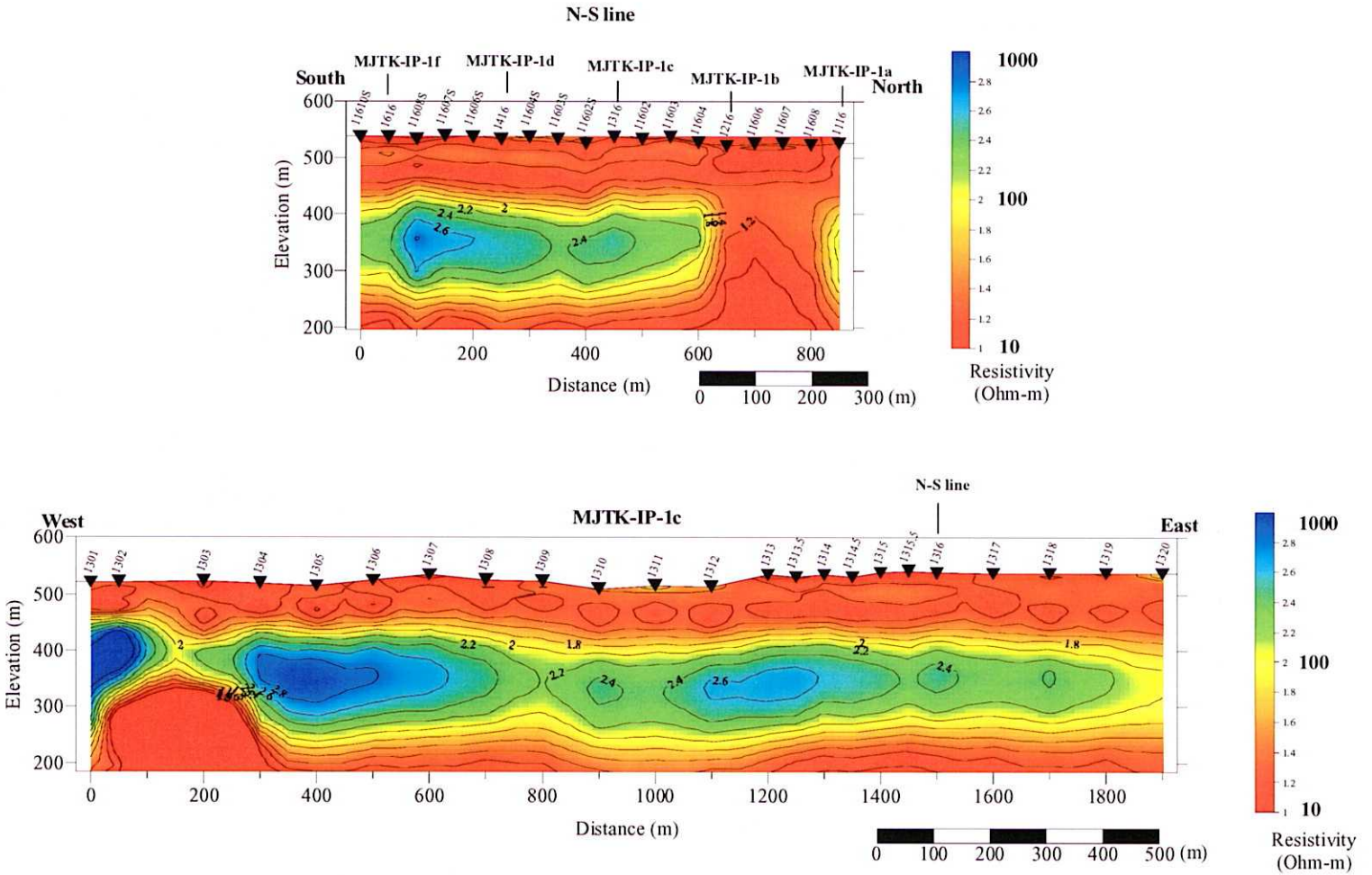

Fig. Ⅱ-2-2-7 Resistivity structure cross sections at MJTK-IP-1 area

Upper part is along the N-S direction line and lower part is along the E-W direction line MJTK-IP-1c. Each section is crossing at station 1316.

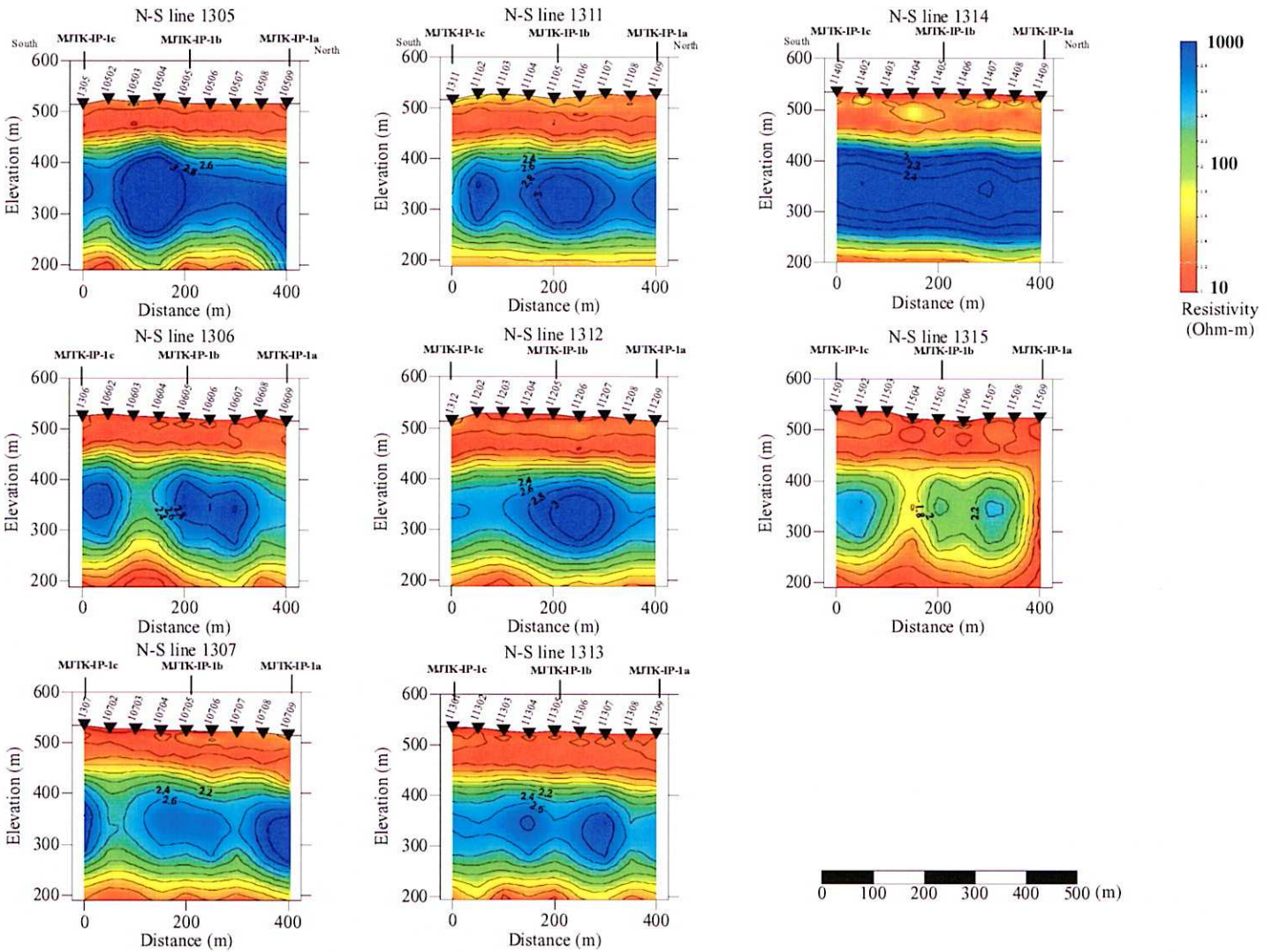

Fig. Ⅱ-2-2-8 Resistivity structure cross sections along the N-S direction line at MJTK-IP-1 area

Each sections are crossing at line MJTK-IP-1a, MJTK-IP-1b and MJTK-IP-1c.

2-2-5-2 MJTK-IP-6 district

It is known that no IP anomaly is detected from the prospecting survey result in the district. The district is underlain by the thick young sediments, accordingly low resistivity zone is expected there. The TEM survey has been performed on the IP method survey line IP-6-c.

The resistivity structure of each measuring point is well coincident, comparing each depth of the resistivity structure obtained from the one-dimensional structure analysis, and it continuously extends horizontally. Based on the analyzed depth and analyzed resistivity values, the resistivity structures in this district have been classify into four layers, Layer 1 to Layer 4, from the top as shown in Table II-2-2-4. The figures of the resistivity and thickness of the layers are the average values of each category.

The resistivity values of Layer 1 to Layer 3 are low as below 40 Ω·m, and the thickness of the layers is about 200 meters. The resistivity value of Layer 4 is medium as 82 Ω·m.

Figure II-2-2-9 shows the resistivity structure cross-section to present the layer structure. The resistivity values in the cross-section are classified in the log scale. The warm color in the resistivity classification represents the low resistivity, and the cool color for the high resistivity.

The characteristic of the resistivity structure in the district is as follows.

1) The resistivity structure is of stratified.
2) If Layer 1, 2, and 3 are treated as one resistivity layer, the layer is total 200 meters thick, and no significant change in the resistivity and thickness is noticed in the direction of the survey line.
3) Medium resistivity Layer 4 is underlies the low resistivity layer, and this is said as the resistivity basement in this district.
4) Within low resistivity Layer1, 2, and 3, Layer 2 shows slightly high resistivity.

Table II-2-2-4 Results of TEM survey in MJTK-IP-6

	Resistivity(Ω·m)	Thickness(m)
Layer 1	28	53
Layer 2	40	51
Layer 3	30	100
Layer 4	82	

2-2-5-3 MJTK-IP-7 district

It is known that no IP anomaly exists in the district from the preceding survey. However, the TEM survey has been performed to clarify its resistivity structure, because some anomalous zones were detected in the last year's airborne geophysical survey, and no artificial construction causing IP anomaly is seen in the district. The TEM survey has been performed on the IP survey line IP-7-a. Also as a supplementary survey, a north to south extending survey line has been set crossing with the IP-7-a line at the right angles.

It has been clarified that the resistivity structure in the district is of low to medium, from the one-dimensional structure analysis. Almost all part is of low resistivity. However, some structural change in the part between 400 and 500 meters deep is seen. Therefore, the layers have been classified into five resistivity layers, Layer 1, 2, 3, 4, and 5, based on the analyzed depth and analyzed resistivity value. The average resistivity values for all layers are low as below 40 Ω· m.

The resistivity structure cross-sections have been created to present the above-mentioned layer structure. Figure II-2-2-10 shows the cross sections. The resistivity values in the cross sections are classified in the log scale. The warm color represents low resistivity, and the cool color represents high resistivity.

The characteristic of the resistivity structure in the district is as follows.

1) All resistivity values within the analyzable depth show low resistivity.
2) No IP effect is obtained in the measuring data.
3) No low resistivity structure is detected to explain the airborne geophysical anomaly.

Table II-2-2-5 Result of TEM survey in MJTK-IP-7

	Resistivity(Ω·m)	Thickness(m)
Layer 1	42	14
Layer 2	26	24
Layer 3	33	66
Layer 4	23	182
Layer 5	27	

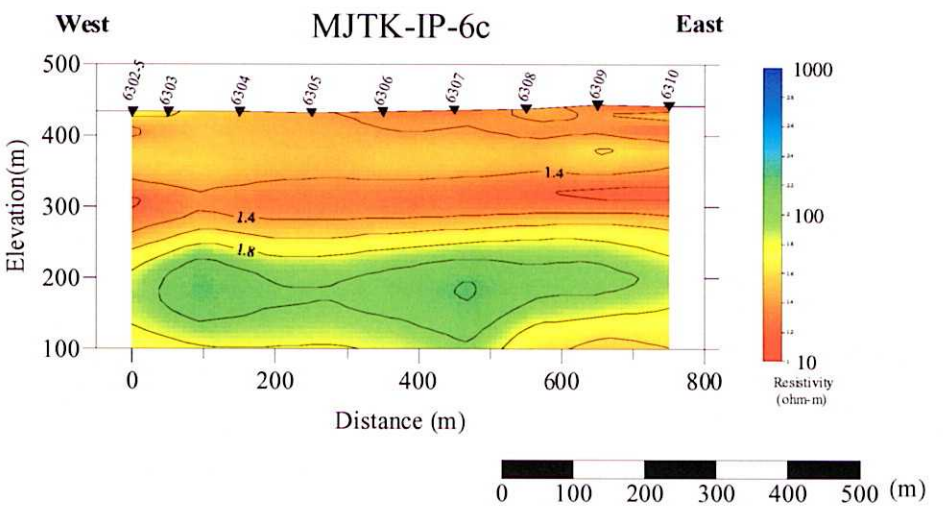

Fig. Ⅱ -2-2-9 Resistivity structure cross section along the E-W direction line MJTK-IP-6c at MJTK-IP-6 area

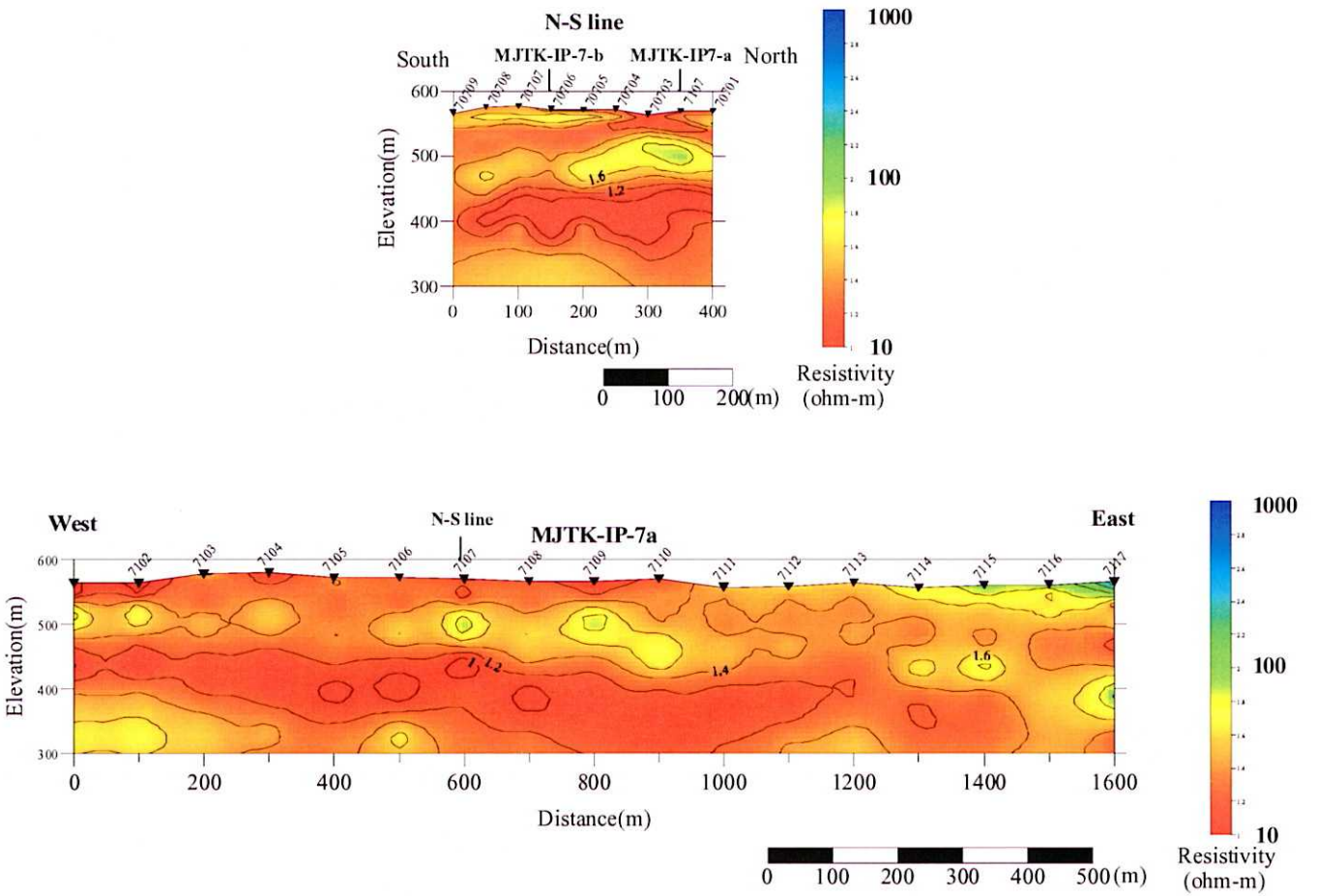

Fig. Ⅱ-2-2-10 Resistivity structure cross sections at MJTK-IP-7 area

Upper part is along the N-S direction line and lower part is along the E-W direction line MJTK-IP-7a. Each section is crossing at station 7107.

2-2-6 Discussion

The summary of the TEM survey result is as follows.

1) The IP effect data is obtained in the MJTK-IP-1 district, and it is significant where the IP anomaly detected in the preceding IP survey.
2) The high resistivity basement is noticed in the MJTK-IP-6 district, and it shows the horizontal stratiform structure.
3) All survey lines show low resistivity structure, and it is impossible to explain the airborne geophysical anomaly.

The MJTK-IP-1 district is the only one where the low resistivity structure has been detected in the area. Accordingly, MJTK-IP-1 has been concentrated for the analytical consideration.

The IP anomalies in the district have been detected in the measuring points between 1305 and 1308 and 1311 and 1315, and those tend to extend north to south. On the analytical result of the IP effect, the planes at the levels of 500, 450, 400, and 350 meters have been made based on the TEM analytical result. Based on the resistivity distribution of the level planes, the domains of IP effect influence has been considered.

Figures II-2-2-11 to II-2-2-14 show the resistivity distribution for each level. The resistivity values in the planes are classified in the log scale. The warm color represents low resistivity, and cool color represents high resistivity.

In the 500 meters level plane, the low resistivity zone widely spreads over the whole area. The lowest resistivity value, 10 to 15 Ω· m, is plotted in the zone between 11605 and 11608 on the survey line, to the north from the cross point with IP1-c. No IP effect is shown in this basic plane.

In the 450 meters level plane, the high resistivity zone affected some IP effect is in the area between 1305 and 1308 of the northern extension line, 200 meters from the cross point with MJTK-IP-1c. On the east side, the low resistivity zone similar to that of the 500 meters level plane is distributed. The anomaly at the point 1304 is eliminated from the target due to possible affect from the teransmitter line.

In the 400 meters level plane, the high resistivity zone is newly analyzed in the zone 200 to 300 meters north from the zone between 1311 and 1312 of the survey line MJTK-IP-1c, and it indicates that the resistivity structure causing the IP effect in the central survey line is in the deeper part than that of on the west side.

In the 350 meters level plane, the high resistivity zone is analyzed in the area from the central

survey line to the southeast, and it indicates that the resistivity structure causing the IP effect is deeper than that of on the east side.

Comparing the above-mentioned result and the resistivity structure cross-section, the depth to start the affection by the IP effect tends to get deeper to the east, and this is corresponded with the tendency of the bottom plane of the low resistivity layer. Accordingly, it is presumed that the resistivity structure causing the IP effect is distributed in the bottom lower part of the low resistivity layer.

This structure tends to extend northwest to southeast, but it is unable to confirm due to the limit of TEM measuring area.

From the result of the TEM survey in the IP1 district, the resistivity structure is summarized as follows.

1) The IP effect has been confirmed in the IP anomaly zone detected by the IP method survey.
2) The structure casing IP effect is in the lower part of the low resistivity layer, and its depth tends to get deeper from west to east.
3) The low resistivity layer is 140 meters thick in average. It is presumed that the structure causing IP effect is situated below 140 meters.

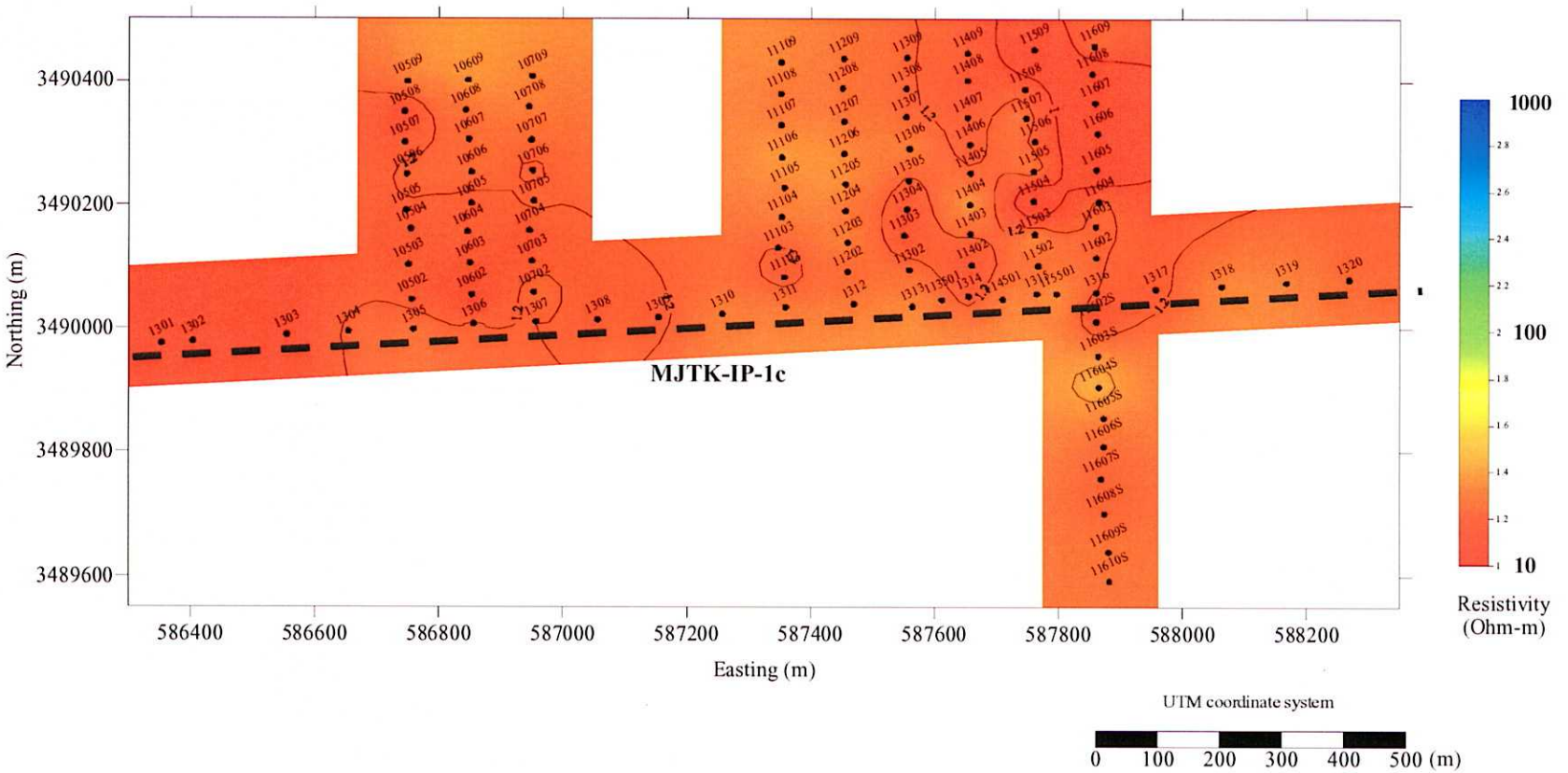

Fig. Ⅱ-2-2-11 Resistivity distribution at level 500m

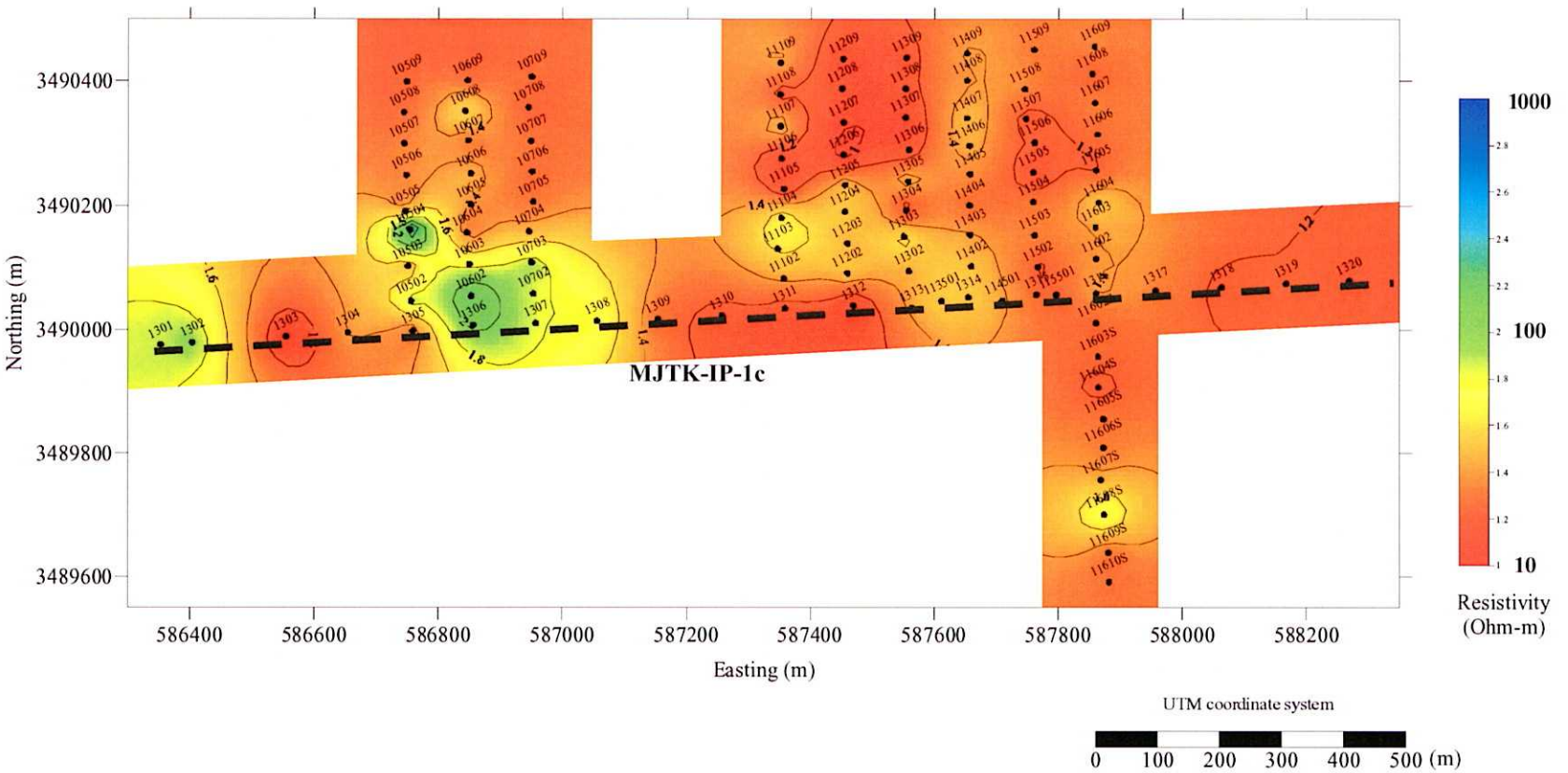

Fig. Ⅱ-2-2-12 Resistivity distribution at level 450m

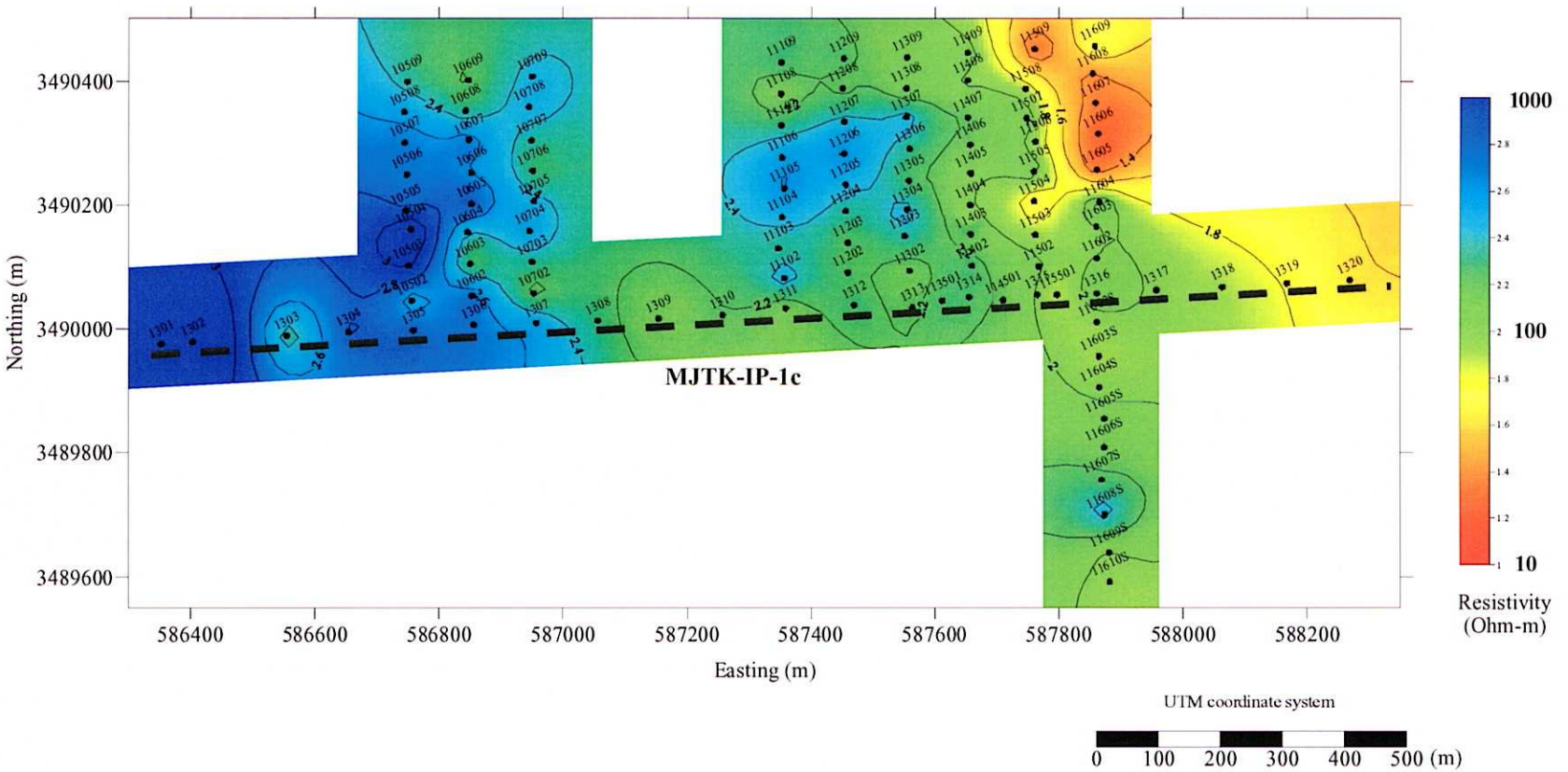

Fig. Ⅱ-2-2-13 Resistivity distribution at level 400m

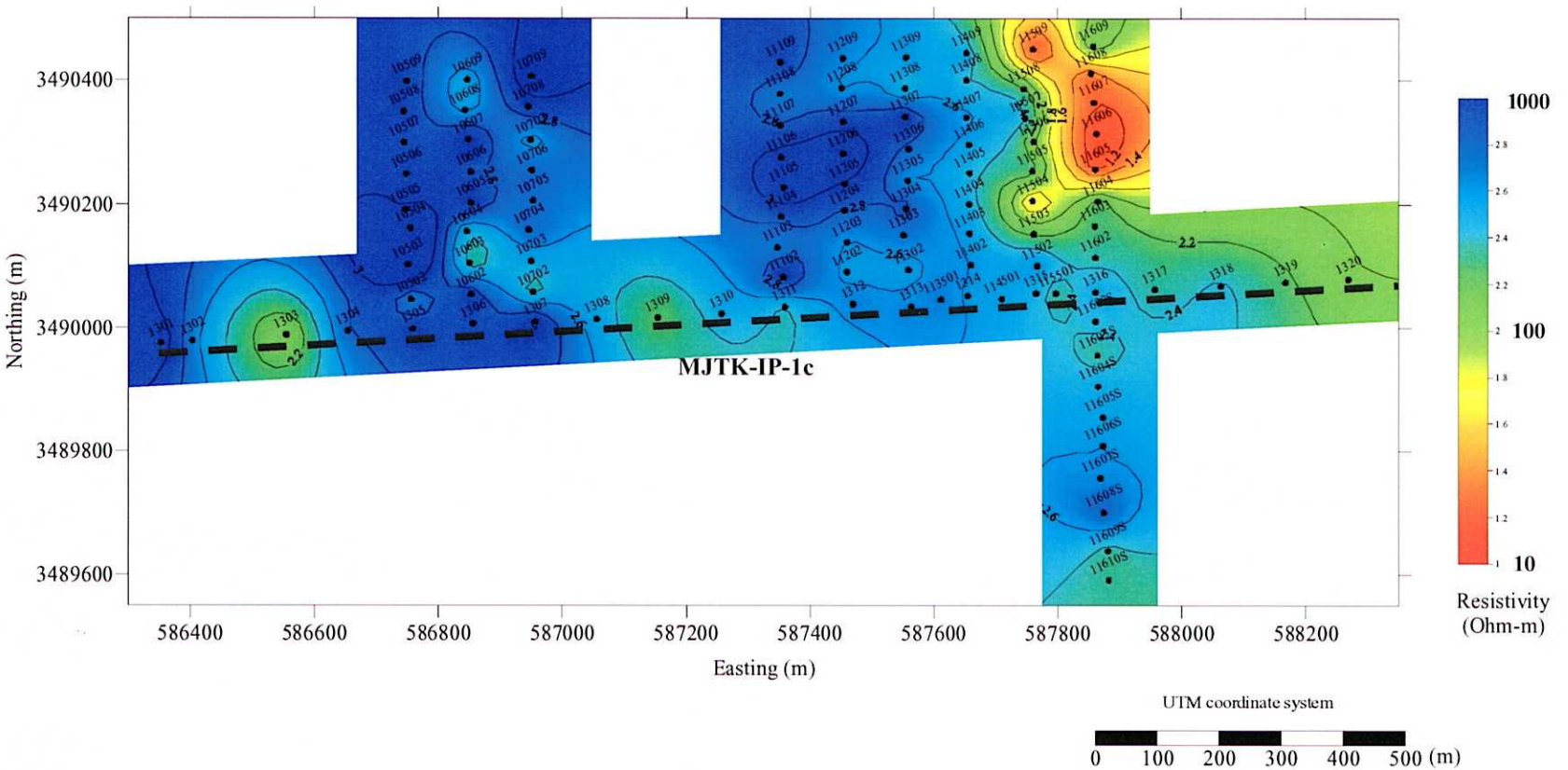

Fig. Ⅱ-2-2-14 Resistivity distribution at level 350m

2-3 Conclusion

2-3-1 Conclusion of Result and Phase I

The integrated interpretation of the survey results for each district in this year and the airborne geophysical survey conducted last year as follows.

- MJTK-IP-1 district

The last year's airborne survey revealed a magnetic anomaly in this district. This year's electric and electromagnetic survey has revealed IP anomalies. The IP anomalies are distributed in the north eastern district, and it is expected that some metal mineral exist there.

- MJTK-IP-2 district

The last year's airborne survey revealed a magnetic anomaly in this district. The electric prospecting in this year has revealed a high resistivity and high IP anomaly zone. The resistivity and chargeability are reasonably high, therefore, the airborne magnetic anomaly possibly indicates some igneous body.

- MJTK-IP-3 district

The last year's airborne survey revealed a magnetic anomaly in this district. This year's electric prospecting has revealed a dome-shape high resistivity and low IP anomaly zone corresponding with the airborne magnetic anomaly. The district is situated near the MJTK-2 district, consequently, it is presumed that the young sediments are relatively thin. The airborne magnetic anomaly possibly corresponded with some igneous body as well as that of MJTK-2 district.

- MJTK-IP-4 district

The last year's airborne survey revealed an anomaly on conductivity in this district. No IP anomaly has been detected in this year's electric prospecting. It has made clear that some artificial material buried in the vineyard made caused the conductive anomaly.

- MJTK-IP-5 district

The last year's airborne survey revealed a magnetic anomaly in this district. No IP anomaly has been detected in this year's electric prospecting. It has been clarified that some gravel mining facility along a river has caused the airborne magnetic anomaly.

- MJTK-IP-6 district

The last year's airborne survey revealed a weak magnetic anomaly in this district. No IP anomaly has been detected in this year's electric prospecting. It is possible that the airborne magnetic anomaly reflects something in the deep part.

- MJTK-IP-7 district

The last year's airborne survey revealed a weak anomaly of conductivity and magnetism in this district. No significant IP anomaly has been detected in this year's electric prospecting. It is presumed that the young sediments lies very thickly.

- MJTK-IP-8 district

The last year's airborne survey revealed a conductivity anomaly in this district. No IP anomaly has been detected in this year's electric prospecting. It has been made clear that some artificial material buried in the vineyard has caused the anomaly.

2-3-2 Supplemental Survey by BRPM

BRPM has conducted a follow-up ground magnetic and gravity survey program for the target zone in the MJTK-IP-1 district obtained by this year's survey program. Figures III-1-1 to III-1-3 show the result of the follow-up program.

The gravity map is the result of the primary residual difference. The maximum one-milligal positive anomaly has been detected from No.9 to No.10 of the survey line C.

In the ground magnetic survey, relatively high anomaly zones have been detected on the survey lines C, D, and E, and contractively negative anomalies on the survey line A and B. The high magnetic anomaly zones are roughly divided in three parts, and corresponded with the airborne magnetic anomaly zones. These anomaly zones are low in the west side, high in the central part, and slightly high in the east side. The paired positive and negative magnetic anomaly zone in the central part is roughly correlated with the high gravity anomaly zone, consequently it is presumed that the anomaly reflects some magnetic rock surrounding the rim of the high gravity anomaly. The presumed magnetic rock body occupies an area approximately 500 meters square. The east side and west side magnetic anomaly zones are correlated with slightly low gravity zones.

1-2 Summary of Survey Result

Figures III-1-4 and III-1-5 show the IP effect distribution by the TEM survey. The strength of the IP effect of the gate 41 (0.881 msec) to gate 60 (69.8 msec) is shown on the planes. The IP effect is negative, shown in blue.

In the survey area, some IP anomaly appears near the boundary between the young sediments and Paleozoic terrain. The interpreted depth of the resistivity structure contains some error due to the IP effect.

Not all the survey lines have been measured by the TEM method, therefore, the correlation with the electric IP survey is not comprehensive.

No IP effect appears in relatively large area around No.7 of the survey line C, and the area is roughly corresponded with the gravity, magnetism, and high resistivity zone.

Relatively intense IP effects appear near No.4 of the survey line C, and No.11, 14, 15 of the survey line B and C, roughly corresponding with the chargeability anomaly zone.

Figures III-1-6 and III-1-7 show the integrated interpretation maps of the all survey results and the result of the supplemental survey by BRPM. The resistivity and metal factor maps have been overlaid by the gravity primary residual difference and magnetic distribution, on the depth 150 meters and 190 meters levels in the MJTK-IP-1 district.

* Relation between IP and TEM

The electromagnetic prospecting TEM method has not covered the all area of the Electric IP method, however, the chargeability anomaly zone is well correlated with the IP effect zone of the electromagnetic TEM method.

* Resistivity and Chargeability

The chargeability anomaly zone extends along the rim of the high resistivity zone. The N-S and NW-SE trending chargeability anomaly zone is distinguished at the depth.

The high resistivity zone of the resistivity analysis is of the swell resistivity structure from the surrounding area.

* Resistivity and Gravity

The high resistivity distribution at the depth of 147 meters and 190 meters in the MJTK-IP-1 district has been made clear in an area extending to the north to south and east to west with about 600 meters wide, and further extends to the deeper part. The high resistivity distribution is well corresponded with the high gravity anomaly distribution.

* Magnetism, Gravity, and Chargeability

The positive magnetic anomaly zones are seen in the No.1 and 8 of the IP survey lines C and D, and No.15 of the survey line D and F on the ground magnetic map. The anomaly around No.8 of the survey line C and D among these magnetic anomalies accompanies a distinct and contractively negative anomaly in the north side, and the high gravity anomaly exists in between those.

The high gravity anomaly zone is corresponded with the magnetic anomaly zone, high resistivity zone, and low chargeability zone, and it is possible that the gravity anomaly well reflects a high-density rock body. However, the high resistivity zone gently swell, based on the resistivity structure analysis, it is also possible that the gravity anomaly reflects a composite body of igneous rocks and sedimentary rocks.

The clear correlation is noticed among the high resistivity, low chargeability, and gravity anomaly zone, and also partly between chargeability anomaly zone and magnetic anomaly zone. The magnetism changes in narrow range, accordingly, it is thought that the anomaly corresponds to some weak magnetic minerals.

It is thought that the cause of the two chargeability anomaly zones trending north to south and the IP effect zone of the TEM survey distributing both sides of the gravity anomaly zone as follows.

* The west side chargeability anomaly zone is distributed in the high resistivity zone, and the magnetic anomaly zone is distributed the relatively high to low magnetic zone. Therefore, it is supposed that the anomaly zone reflects a weak mineralized zone.

* The east side chargeability anomaly zone is corresponded with low resistivity zone, below 100

Ω・m, and relatively high magnetic anomaly zone. Therefore, it is thought that some magnetic massive sulfide ore deposit exists in this zone.

Table III-1-1 shows the result of the geophysical surveys.

Table II-2-3-1 Result of geophysical survey

Location	Survey lines B and C, near No.9	Cause
IP	High resistivity, low chargeability, gentle swell of resistivity	Igneous rock
TEM	Relatively extensive no IP effect area	
Gravity	About one mgal high gravity anomaly	
Magnetism	Relatively weak positive and negative paired anomaly	

Location	Survey lines E, A, B, C, and D, near No.5	Cause
IP	70 to 300Ω・m chargeability anomaly	High resistivity and high chargeability rock?
TEM	Relatively extensive IP effect	
Gravity	Rim of high gravity anomaly zone	
Magnetism	Relatively high to low magnetic zone	

Location	Survey lines E, A, B, and C, No.10 to No.14	Cause
IP	Low resistivity, chargeability anomaly zone	Mineralized zone?
TEM	Relatively extensive IP effect	
Gravity	Rim of high gravity anomaly zone	
Magnetism	Relatively weak magnetic anomaly zone	

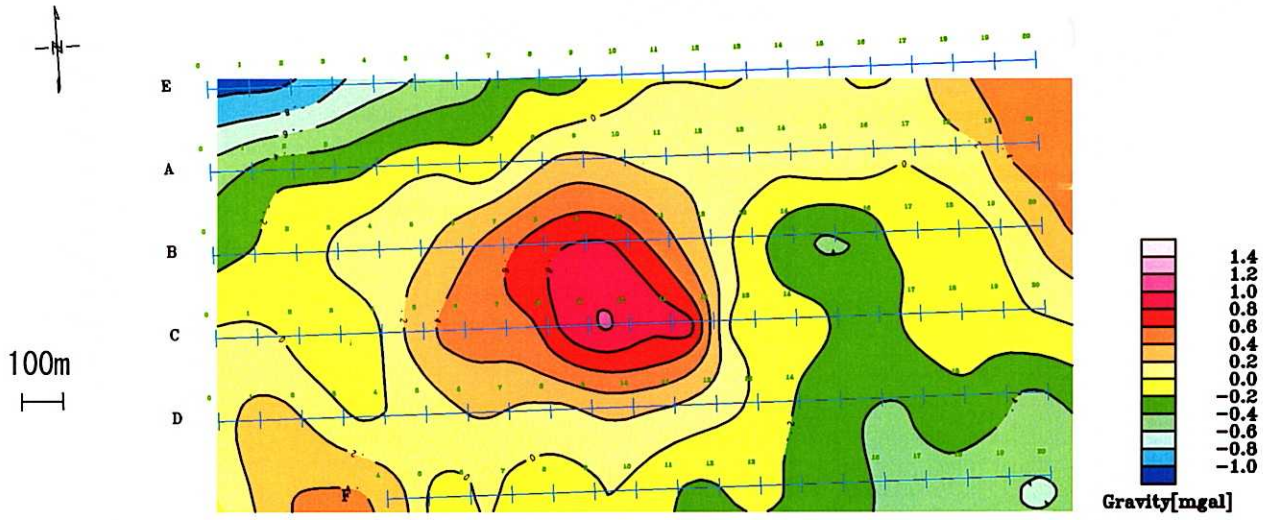

Fig.II-2-3-1 Plane map of Gravity by BRPM

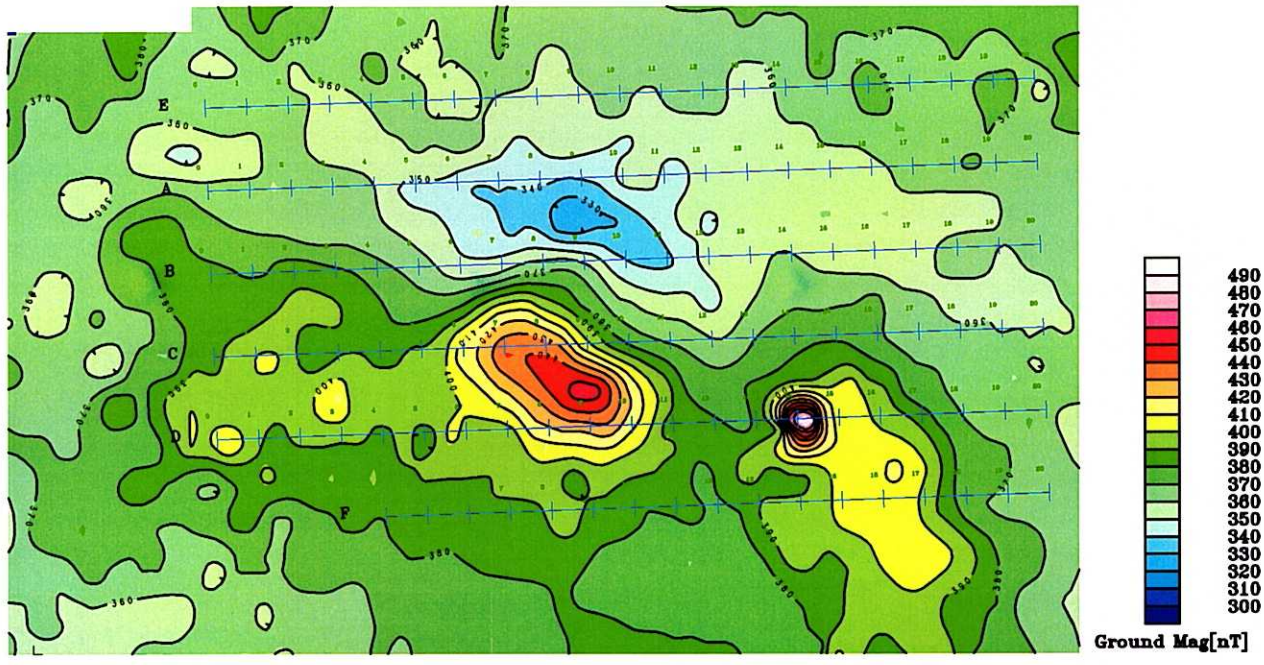

Fig.II-2-3-2 Plane map of Ground MAG by BRPM

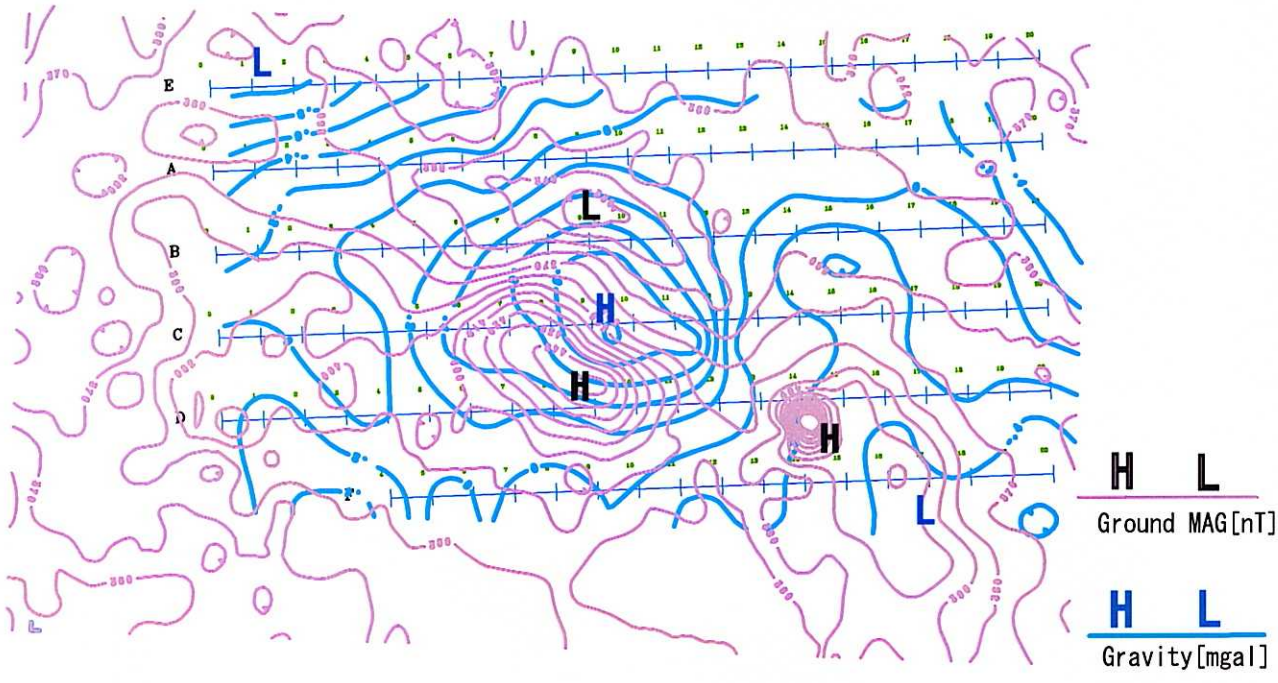

Fig.II-2-3-3 Plane map of Ground MAG and Gravity by BRPM

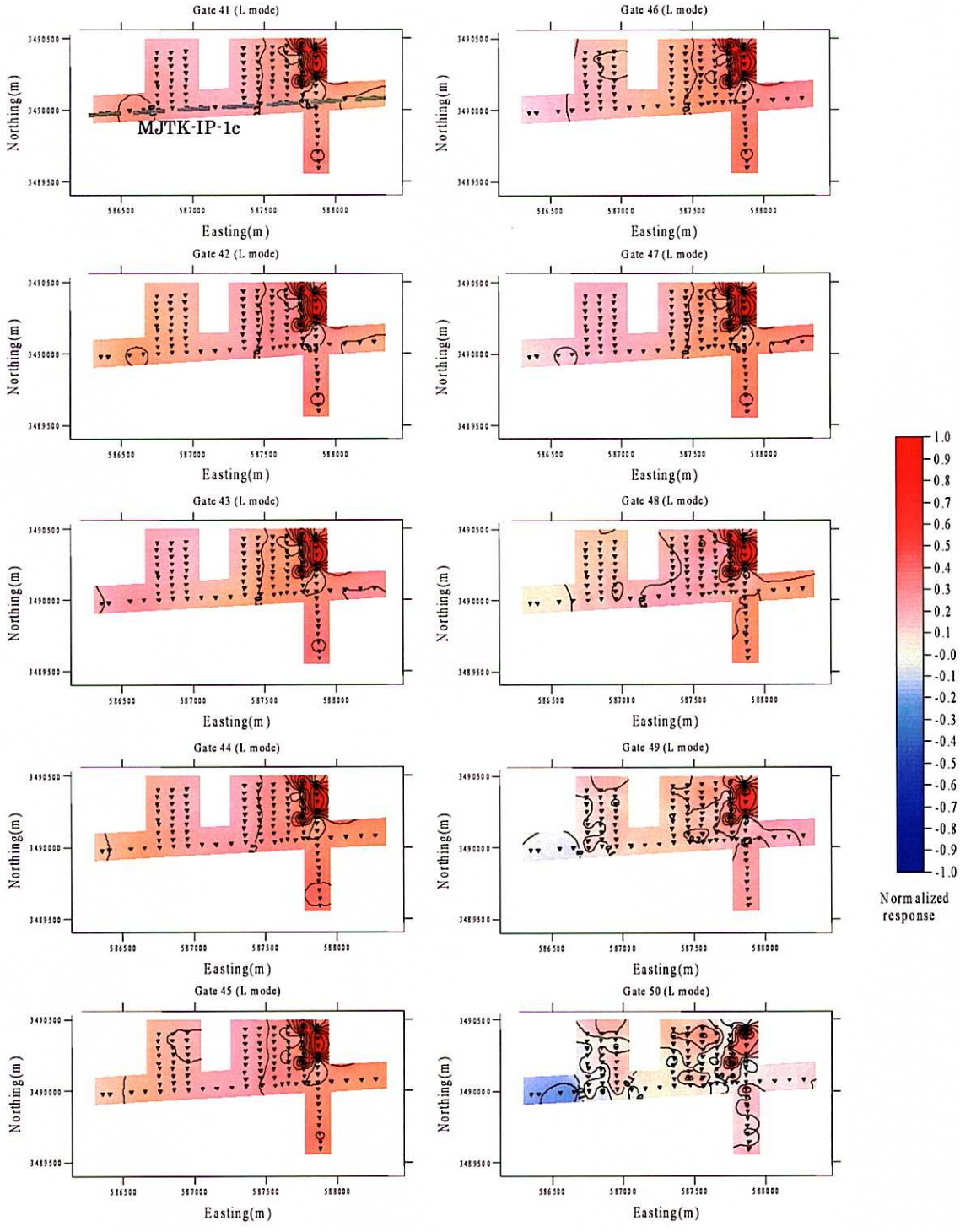

Fig. II-2-3-4 Normalized response maps of L mode (from Gate41 to Gate50)

Observed data was normalized by maximum value of each gate. Red shows the positive value and blue shows the negative value.

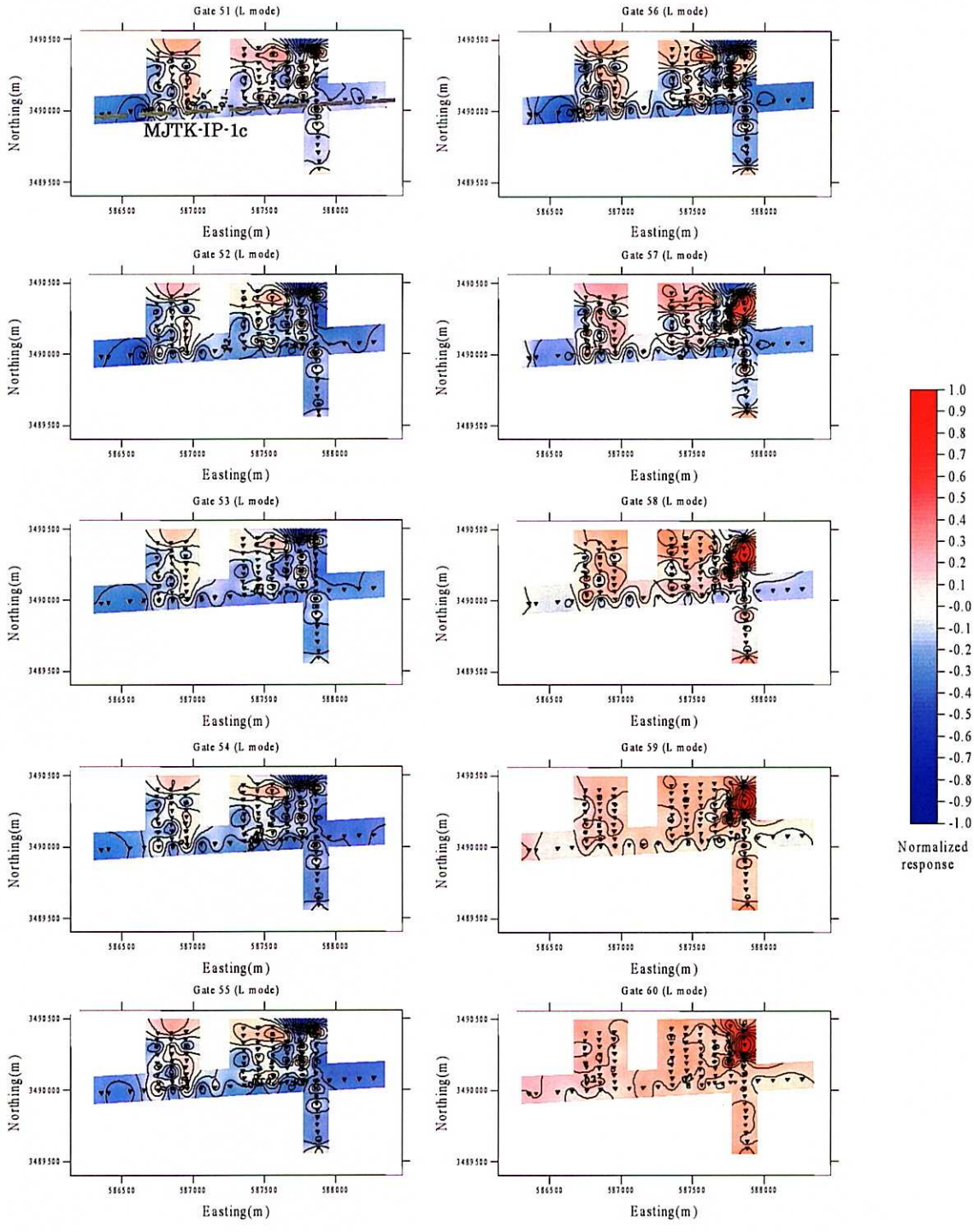

Fig. II-2-3-5 Normalized response maps of L mode (from Gate51 to Gate60)

Observed data was normalized by maximum value of each gate. Red shows the positive value and blue shows the negative value.

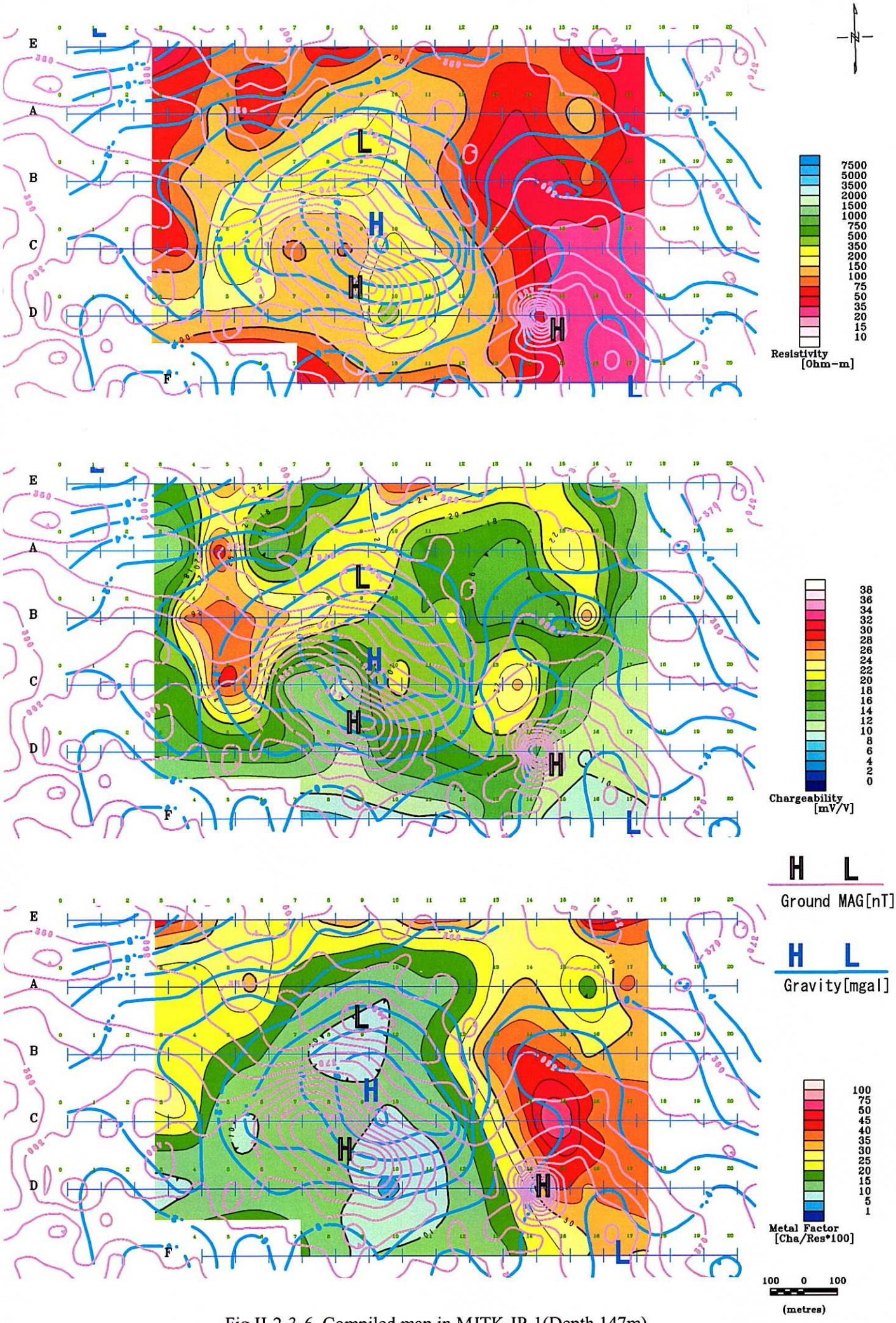

Fig.II-2-3-6 Compiled map in MJTK-IP-1(Depth 147m)

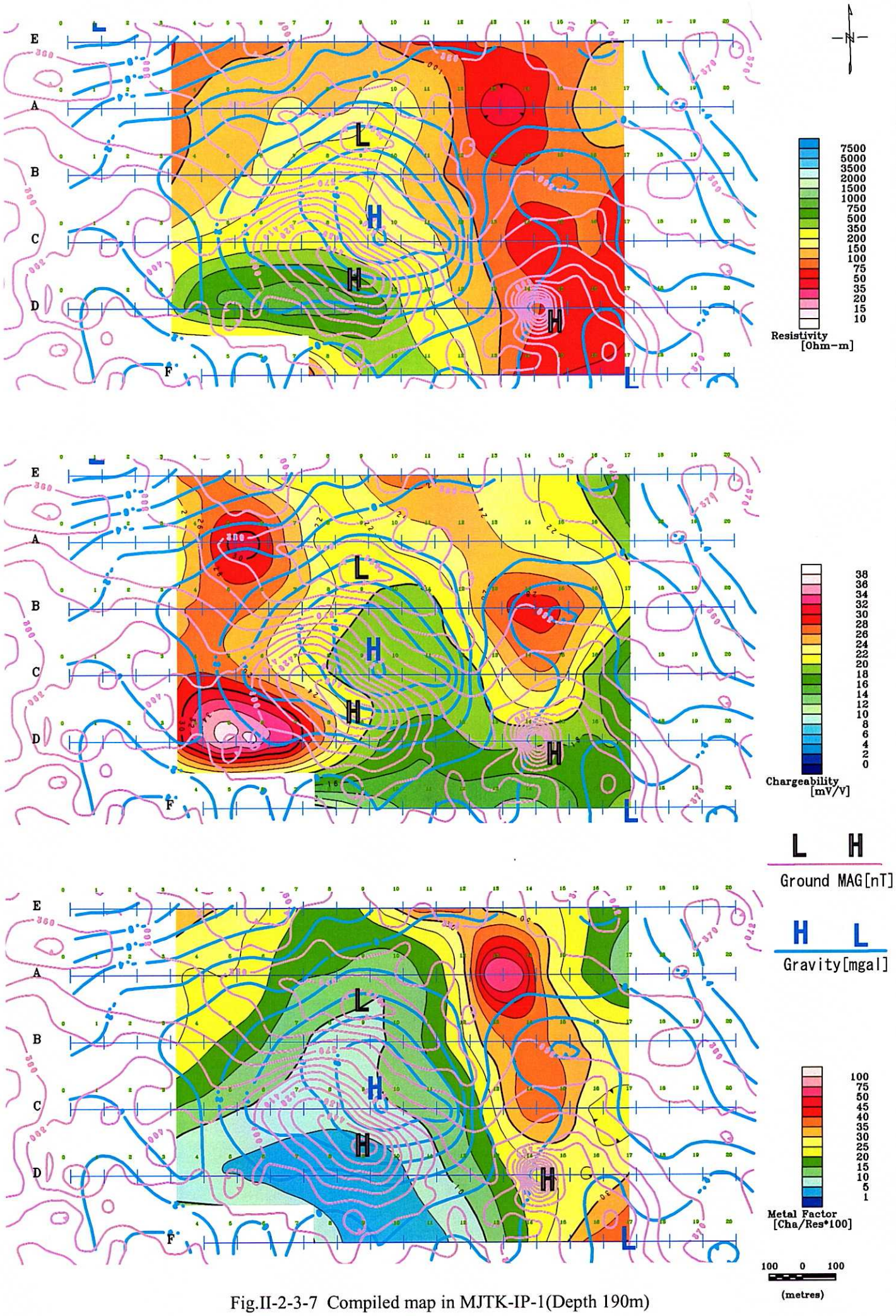

Fig.II-2-3-7 Compiled map in MJTK-IP-1(Depth 190m)

2-4 Recommendation for Further Prospecting

2-4-1 This year's Survey

The premise of the possibility "Case 1" and "Case 2" mentioned in the preceding section is put on the existence of some ore deposit, however, it is unable to say whether it is right.

Accordingly, it is recommended to conduct some drilling program to obtain the exact geological information and to know the state of mineralization.

Table II-2-4-1 Proposed drilling

MJTK-1	
Location	No. 14 point of IP survey line B
Direction	Vertical
Main Object	IP anomaly (high chargeability) and low resistivity zone noted in the east wing of the supposed rhyolite body in "Case 1". Potential for sulfide ore deposit or mineralized zone.
MJTK-2	
Location	No.8 point of TP survey line C
Direction	To the south, dip 70 degree
Main object	Intense magnetic and gravity anomaly in the north wing of the supposed rhyolite body in "Case 2"

Figure II-2-4-1 shows the proposed drill holes on the model drawing.

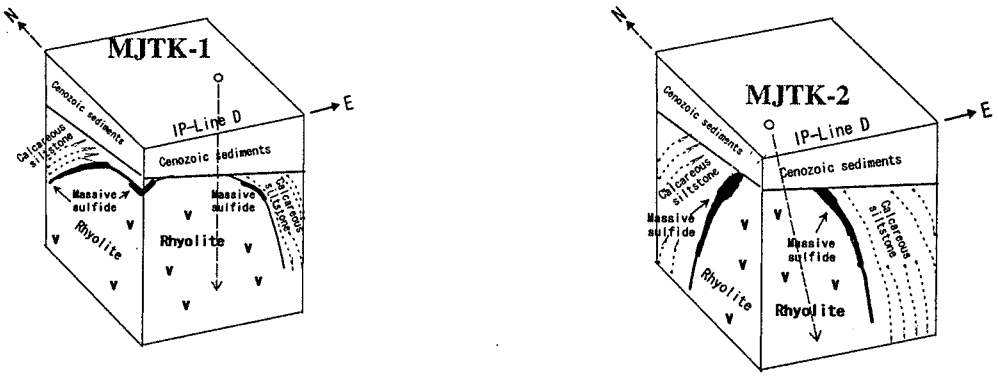

Fig.II-2-4-1 Proposed drilling

It is expected that MJTK-1 can reach some mineralized zone correlated with the high IP anomaly and the footwall rhyolite, after the young sediments and Paleozoic muddy rock.

MJTK-2 can expect to reach some ore body correlated with the magnetic and gravity anomaly, after the young sediments and Paleozoic muddy and calcareous siltstone.

2-4-2 Third year's Survey

It depends upon the drilling survey result, however, some follow up survey for the extension trend to the southwest and east of the MJTK-IP-1 district is recommended.

Based on the airborne magnetic and electromagnetic survey result, some prospecting survey programs for other districts are recommended, considering following points.

* Large-scale, simple magnetic anomaly zones possibly indicate some igneous bodies in many cases. Small-scale magnetic anomalies should be noticed for mineral prospecting purpose.
* Some contrastive positive and negative magnetic anomaly or irregular pattern anomaly should be extracted for further exploration. This type of magnetic anomaly is common for stratiform steep dipping magnetic mineral ore body.

It is possible that magnetic or conductivity anomaly is caused by some artificial material. The target area for ground prospecting should be inspected in site before actual survey start. In some district, the ground magnetic or gravity survey should be proceeded before the electric (IP method) or electromagnetic survey start, considering actual situation of the target area.